The Tropical Atlantic SST Bias in the Kiel Climate Model

Dissertation

zur Erlangung des Doktorgrades

der Mathematisch Naturwissenschaftlichen Fakultät

der Christian-Albrechts-Universität zu Kiel

vorgelegt von

Sebastian Wahl

Leibniz-Institut für Meereswissenschaften

Forschungsbereich 1

- Maritime Meteorologie -

Kiel, Oktober 2009

Contents

Teile dieser Arbeit wurden in Climate Dynamics zur Veröffentlichung akzeptiert:
Wahl, S., M. Latif, W. Park and N. Keenlyside: On the Tropical Atlantic SST Warm Bias in the Kiel Climate Model, Climate Dynamics, accepted, DOI: 10.1007/s00382-009-0690-9

Abstract

Until today, the Tropical Atlantic Ocean is a region which is difficult to represent in numerical models. Most of the current coupled general circulation models (CGCM) show a strong warm bias in the eastern Tropical Atlantic and are unable to reproduce the observed variability especially directly along the equator.

In this work various sensitivity experiments with the Kiel Climate Model (KCM) are described. A largely reduced warm bias and an improved seasonal cycle in the eastern Tropical Atlantic are simulated in one particular version of KCM. By comparing the stable and well-tested standard version with the sensitivity experiments and the modified version, mechanisms contributing to the reduction of the eastern Atlantic warm bias are identified and compared to what has been proposed in literature. The errors in the spring and early summer zonal winds associated with erroneous zonal precipitation seems to be the key mechanism, and large-scale coupled ocean-atmosphere feedbacks play an important role in reducing the warm bias. Improved winds in boreal spring cause the summer cooling in the eastern Tropical Atlantic via shoaling of the thermocline and increased upwelling, and hence reduced sea surface temperature (SST). Reduced SSTs in the summer suppress convection and favor the development of low-level cloud cover in the eastern Tropical Atlantic region. Subsurface ocean structure is shown to be improved, and potentially influences the development of the bias. The strong warm bias along the southeastern coastline is related to underestimation of low-level cloud cover and the associated overestimation of surface shortwave radiation in the same region. Therefore, in addition to the primarily wind forced response at the equator both changes in surface shortwave radiation and outgoing longwave radiation contribute significantly to reduction of the warm bias from summer to fall.

The better representation of the mean annual cycle in the Tropical Atlantic also improves the variability in the Tropical Atlantic. The different steps of the Bjerknes feedback mechanism are more realistically simulated in those version of KCM that have an better mean state. The improved representation of equatorial Atlantic variability is believed to be responsible for better potential predictability. No predictability that is significantly above persistence is found when hindcasting equatorial Atlantic SST between 1971 and 2004 using different configurations of KCM.

Zusammenfassung

Bis heute stellt der Tropische Atlantische Ozean eine Region dar, die sich nur schwer in globalen numerischen Modellen darstellen lässt. Die meisten der aktuellen gekoppelten Zirkulationsmodelle zeigen positive Meeresoberflächentemperaturabweichungen (SST[1] Abweichungen) im östlichen Tropischen Atlantik und haben Schwierigkeiten die beobachtete Variabilität, besonders unmittelbar am Äquator, wiederzugeben.

In dieser Arbeit werden unterschiedliche Sensitivitätsexperimente mit dem Kieler Klimamodell (Kiel Climate Model - KCM) beschrieben, unter anderem eine modifizierte Version des KCM, in der die positiven SST Abweichungen deutlich reduziert sind. Durch den Vergleich der stabilen und gutuntersuchten Standardversion mit den Sensitivitätsexperimenten und der modifizierten Version werden Mechanismen die zur Verringerung des SST Fehlers beitragen, identifiziert und mit Ergebnissen aus der Literatur verglichen. Daraus folgt, dass Fehler im zonalen Wind im Frühling und zu Beginn des Sommers in Zusammenhang mit Fehlern in der zonalen Verteilung des Niederschlags ein Schlüsselmechanismus darstellen. Grossskalige gekoppelte Ozean-Atmosphären Rückkopplungen spielen ebenfalls eine wichtige Rolle. Realistischere Winde im Nordfrühling verursachen die Abkühlung der SST im östlichen Tropischen Atlantik durch ein Abflachen der Thermokline und einen verstärkten Auftrieb, und tragen so zur Reduzierung des SST Fehlers bei. Kältere SST im Sommer unterdrücken die Konvektion und begünstigen die Entwicklung tiefer Wolken im östlichen Tropischen Atlantik. Die ozeanische Schichtung, die ebenfalls verbessert wurde, beeinflusst möglicherweise die Entwicklung des SST Fehlers. Der ausgepräge SST Fehler entlang der Südostküste des Tropischen Atlantik steht in Zusammenhang mit der Unterschätzung der tiefen Bewölkung und der damit zusammenhängenden Überschätzung der kurzwelligen Einstrahlung in der gleichen Region. Die Verringerung dieser Fehler trägt daher - neben den Fehlern in der äquatorialen Zirkulation - signifikant zur Reduzierung des SST Fehler im Nordsommer und -herbst bei. Die bessere Modellierung des mittleren Jahresgangs im Tropischen Atlantik verbessert ebenfalls die Darstellung der Variabilität. Die unterschiedlichen Schritte des Bjerknes-Rückkopplungsmechanismus werden realitätsnaher in den im mittleren Zustand verbesserten Ver-

[1] Sea surface temperature - Meeresoberflächentemperatur

sionen des KCM dargestellt. Die realistischerer Modellierung der Variabilität wird auch für die verbesserte potentieller Vorhersagbarkeit verantwortlich gemacht. Allerdings findet sich keine Vorhersagbarkeit die einer Persistenzvorhersage überlegen ist, wenn KCM zur Vorhersage der SST im östlichen tropischen Atlantik herangezogen wird.

1 Introduction

Representing the earth's climate in numerical atmosphere-ocean models remains a challenging task as many processes can currently not be represented correctly. These include, for example, processes such as the Madden-Julian Oscillation (Madden and Julian, 1971, 1994), or even large scale processes such as modeling the climate of the southern ocean (Randall et al., 2007).

The Tropical Atlantic region is another region where global numerical models have significant difficulties in modeling the correct climate and reasonable variability. In comparison to the Tropical Pacific Ocean, the climate state and the associated feedbacks in the Tropical Atlantic Ocean are much more difficult to represent in coupled climate models since the size of the Atlantic basin is roughly one third of the Pacific basin. All basinwide processes occur on a much smaller scale. In terms of a low resolution ocean or atmosphere model this means that only a small amount of gridpoints in the basin have to represent all mechanisms. Therefore, local errors have a much stronger impact. On top of that a very asymmetric coastline complicates the modeling efforts in the Tropical Atlantic. Altogether this causes coastal and land processes to have a strong influence on the basinwide circulation. Both the South American and African continent host two major centers of convection. The intense convection especially over the Sahel area directly influences the strength of the cross-equatorial trade winds in the eastern equatorial Atlantic, a fact already recognized more than 320 years ago (Halley, 1686). Stronger trades cause intensified upwelling and hence colder SST along the equator. In addition to the air-sea

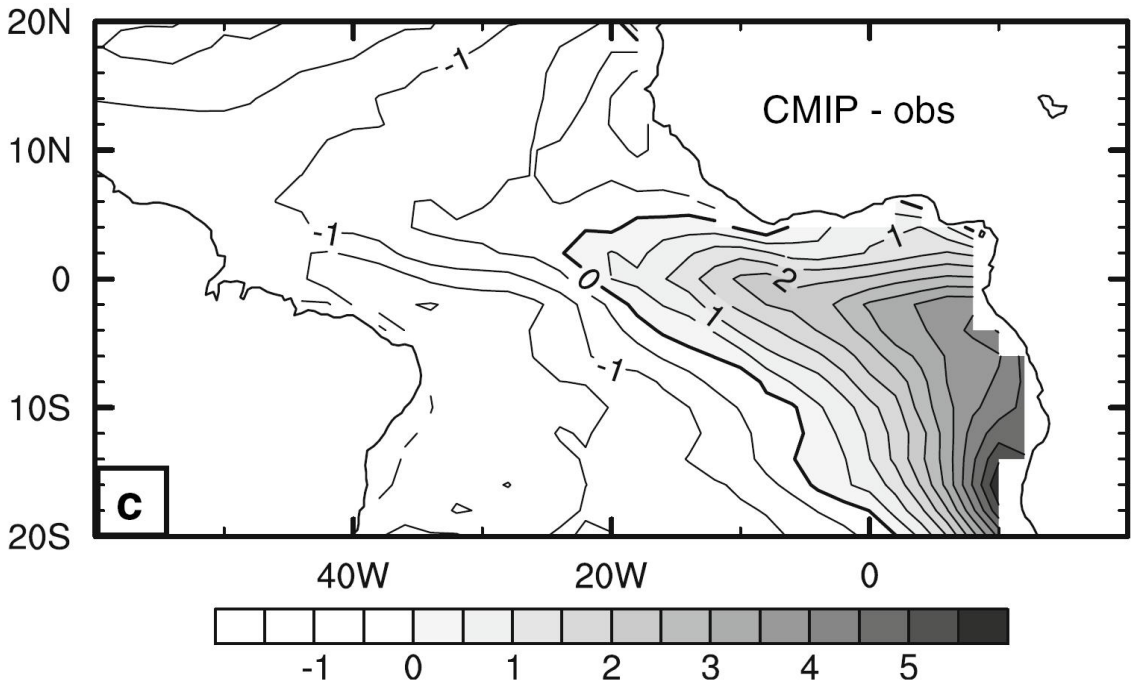

Figure 1.1: *Mean SST bias in eight coupled models that are part of last IPCC report (Randall et al., 2007). Figure adopted from Richter and Xie (2008).*

interaction over the open ocean, thus the correct representation of processes over land is essential. Despite the fact that horizontal, vertical and temporal resolution of global coupled general circulation models (CGCMs) has continuously increased during the last decades, and an increasing number of processes is accounted for in the models, the correct representation of Tropical and Subtropical Atlantic climate remains a challenging task. From the comparison of modelled sea surface temperatures (SSTs) to observed SSTs it is known that basically all current CGCMs exhibit a warm bias in the eastern and southeastern Tropical Atlantic that peaks during boreal summer (Figure 1.1). A similar warm bias is simulated in the Tropical Pacific both north and south of the equator, and in the eastern South Tropical Indian Ocean. However, the bias is particularly important in the Tropical Atlantic given its small basin size and the reversal of the SST gradient along the equator. The warm bias causes major problems in simulating present and future climate in the Tropical Atlantic, specifically precipitation. For example, eastern Tropical Atlantic SST

is important for the correct representation and forecast of the African Monsoon on seasonal and decadal timescales today as well as under future climate scenarios (e.g. Hulme et al., 2001).
In this work the following key questions will be discussed using different configurations of the coupled Kiel Climate Model (KCM, Park et al. (2009) and chapter 3.2):

- Which mechanisms contribute to the seasonal development of the warm bias in SST in the eastern Tropical and Subtropical Atlantic,
- how does the eastern Tropical Atlantic warm bias influence equatorial Atlantic variability and
- how do errors in the mean state and variability influence predictability of equatorial Atlantic SST?

In chapter 2 processes and feedback mechanisms contributing to the mean annual cycle and interannual variability are introduced, and current problems in modeling Tropical Atlantic climate in coupled models as well as limits in predicting equatorial Atlantic SST are discussed. Chapter 3 introduces the Kiel Climate Model (KCM) and the different configurations of the model used in this work. The mean state and the seasonal cycle as well as the processes that are important for the development of the strong warm bias in the equatorial Atlantic are discussed in chapter 4. Variability is investigated in chapter 5. Predictability in the equatorial Atlantic is subject of chapter 6. The last chapter provides the conclusions.

2 The Tropical Atlantic Ocean

2.1 Seasonal cycle

In the equatorial Atlantic the seasonal cycle in SST is governed by the seasonal movement of the Intertropical Convergence Zone (ITCZ). Due to the earth's inclination the ITCZ attains it's southermost position in boreal winter (December to February, DJF). Despite the fact that solar radiation at the top of the atmosphere is more or less symmetric about the equator in the annual mean, the ITCZ is located roughly along the equator over the Tropical Atlantic from December to February. During this time winds are weak along the equator and a relatively high and uniform distribution of SST is found between 10°S and 5°N (Figure 2.1a), which is related to various processes (Chang et al., 2007). Over the South American continent precipitation peaks at roughly 5°S to 10°S. As the ITCZ moves further north in spring and summer the southeasterly trades across the equator intensify rapidly. Due to the missing Coriolis force along the equator a zonal temperature gradient is established by the zonal component of the cross-equatorial trades. It drives the equatorial undercurrent and contributes to eastern Atlantic upwelling in summer and the formation of a cold tongue (Figure 2.1b). Increased entrainment and turbulent mixing of cold subsurface water into the mixed layer is an important contributor to the rapid development of the eastern equatorial cold tongue as Foltz et al. (2003) concluded from four years of Prediction and Research Moored Array in the Tropical Atlantic (PIRATA, Servain et al., 1998) data. The sudden cooling towards boreal summer is

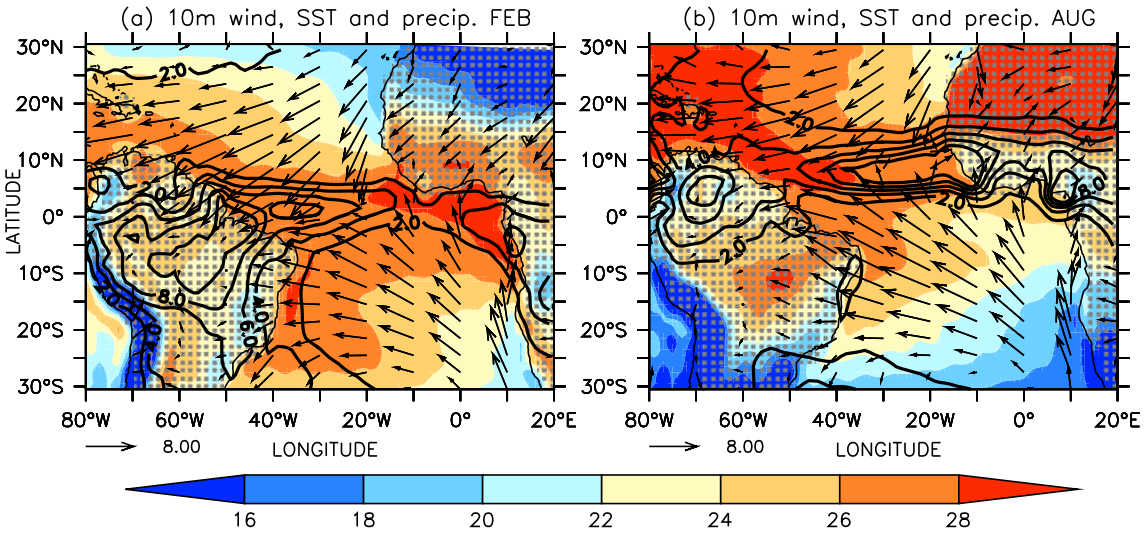

Figure 2.1: *Climatological SST (shading), 10m wind and precipitation (contours, contour interval is 2 mm/day) in the Tropical Atlantic in February (a) and August (b) from observed SST, winds and precipitation (data is described in chapter 3.3).*

enhanced by upwelling slightly south and downwelling slightly north of the equator driven by the cross-equatorial southern winds (Philander and Pacanowski, 1981). The rapid heating in the Sahel region after the spring equinox establishes a strong northward temperature gradient. As a consequence, a northward pressure gradient is established in the boundary layer, which accelerates the southerly winds over the Gulf of Guinea. The strengthened southerlies increase the eastern equatorial upwelling leading to a reduction in local SST. The equatorial cooling further strengthens the the southerly winds and pushes the convective activity northward into the Sahel region (Okumura and Xie, 2004, Hagos and Cook, 2009). Hence, a positive local interaction between the cold tongue, the cross-equatorial trade winds and convection in the Sahel region exists which is often referred to as the African monsoon (e.g. Okumura and Xie, 2004). The rapid cooling of eastern equatorial Atlantic SST also increases the zonal pressure gradient and thus strengthens the equatorial easterlies.

Oceanic Kelvin wavepropagation transport the cooling signal from the cold tongue area southward along the African coast (Chang et al., 2007, Florenchie et al., 2003, Polo et al.,

2008). In the southeastern Tropical Atlantic the SST cooling is possibly amplified by local cloud-radiation-SST feedbacks (Nigam, 1997, Klein and Hartmann, 1993, Philander et al., 1996, Huang et al., 2007). Reduced SST increases the lower tropospheric stability and favors the development of an inversion layer at the surface. At the upper boundary of the stable surface layer, marine stratocumulus form that reduce the incoming shortwave radiation at the surface and further contribute cooling of SST. This mechanism is most effective in late boreal summer to fall due to the peak in lower tropospheric stability as a consequence of the maximum strength of the subtropical high in that region at that time of year (Klein and Hartmann, 1993).

Compared to the Tropical Pacific, the seasonal cycle in Tropical Atlantic SST is of similar strength and seasonality (e.g. Ding et al., 2009). However, the seasonal cycle of ocean dynamics and their interaction with SST are very different (e.g. Philander and Pacanowski, 1986, Xie and Carton, 2004, Ding et al., 2009). Furthermore, in the Atlantic, the seasonal cycle is the dominant signal compared to interannual variability (see next section), while in the Pacific both the seasonal cycle and the interannual variability are of similar strength (Xie and Carton, 2004).

2.2 Variability and predictability

2.2.1 Major modes of variability

As early as the seventies, diagnostic investigations have shown the influence of large-scale patterns onto Sahelian rainfall (e.g. Lamb, 1978) and NE Brazil droughts (e.g. Hastenrath and Heller, 1977, Moura and Shukla, 1981, Enfield, 1996). Statistical analysis using empirical orthogonal functions (EOFs, e.g. early studies by Weare, 1977, Hastenrath, 1978) revealed two modes that are believed to be dominating equatorial

Atlantic variability.

The meridional mode (Weare, 1977, Moura and Shukla, 1981, Servain, 1991) describes the interhemispheric SST gradient maximizing in boreal winter and spring (Ruiz-Barradas et al., 2000) and exhibits interannual to decadal timescales (e.g. Moura and Shukla, 1981, Mehta and Delworth, 1995, Tourre et al., 1999, Latif and Grötzner, 2000). It is also the time of year where equatorial atmospheric circulation is most sensitive to changes in the meridional temperature gradient since mean SSTs are rather uniformely distributed (see previous section). A strong meridional mode corresponds to warmer-than-normal SST in the northern Tropical Atlantic and colder-than-normal SST in the southeastern Tropical Atlantic. It strengthens the southeastern trade winds, displaces the ITCZ northward, weakens the northeastern trades and is associated with deficient northeastern Brazil rainfall (Carton et al., 1996, Giannini et al., 2004) or strengthening of the African Monsoon (e.g. Nobre and Shukla, 1996, Servain et al., 1999). Chang et al. (1997) argue using forced ocean model experiments with different complexity and different strength of dynamic and thermodynamic coupling that the meridional mode variations on decadal timescales are primarily due to positive thermodynamic ocean-atmosphere interactions similar to the wind-evaporation-SST (WES) feedback. The WES feedback was originally described by Xie and Philander (1994) to explain the northward displacement of the climatological ITCZ position. Houghton and Tourre (1992), Mehta (1998), Dommenget and Latif (2000) and Dommenget and Latif (2002) show evidence that the meridional mode is a purely statistical mode and that the northern and southern hemisphere act independently. Carton et al. (1996) show that off-equatorial SST anomalies are dominantly influenced by local wind variability governing the surface latent heat flux in both hemispheres which does not imply interhemispheric coupling of the SST anomalies. While there is disagreement on the physical basis of the meridional mode a general agreement on the implications for e.g. Northeastern Brazil rainfall and ITCZ position exists.

Various studies have also shown the influence of El Niño and the Southern Oscillation (ENSO, e.g. Latif and Grötzner, 2000). It is generally seen as a warming of the northern

Tropical Atlantic a few month after the peak of ENSO (e.g. Huang et al., 1995), and thus influences the meridional mode (e.g. Penland and Matrosova, 1998).

The zonal mode is dominated by the seasonal cycle described in the previous section. On top of that variations in the eastern Tropical Atlantic occur, which are referred to as zonal mode or Atlantic Niño. This mode peaks during boreal summer and frequently exceeds 1°C, maximizing in the region of the summer cold tongue roughly between 6°S and 2°N and 20°W and 5°E. Due to the warmer temperatures the trade winds slow down and a corresponding southward shift of tropical convection occurs (e.g. Carton et al., 1996) bringing higher rainfall total to the Gulf of Guinea region and lower rainfall over the Sahel (Goddard and Mason, 2002). Using observational as well as ocean model results from the 1980s, Carton and Huang (1994) show that a warm event in summer is related to changes in equatorial winds in fall and winter or spring preceding the warm event. Weaker trade winds cause a deeper thermocline in the east and thus weaken surface cooling in summer. The impact of Atlantic Niños onto atmospheric circulation is captured by some atmospheric GCMs but only when forced by Atlantic Niño SST anomalies (e.g. Chang et al., 2000). The periodicity of Atlantic Niño warm events is roughly 30 month, and the reason for the periodicity is currently poorly understood (Xie and Carton, 2004). The zonal mode has some similarity with Pacific ENSO, a fact that has already been recognized since the 1980s (e.g. Merle et al., 1980, Hirst and Hastenrath, 1983). Cool anomalies of the zonal mode are less limited to boreal summer and have received less attention (Xie and Carton, 2004). A recent study by Hu and Huang (2007a) suggests a physical connection between southeastern Atlantic interannual to decadal anomalies along the coast and those found along the equator mainly through coupled low-cloud-SST variability (Huang and Hu, 2007). However, the validity of their results might be limited (last section in Hu and Huang, 2007a). Due to strong biases in the Tropical Atlantic in coupled GCMs which are discussed in the next section, Atlantic Niños are not found in coupled GCMs (e.g. Deser et al., 2006).

Both the zonal and meridional mode are related to changes in trade winds in the Tropical Atlantic. This means that both modes are related (Carton et al., 1996). The different

timescale in both modes is attributed to the fact that the zonal mode seems to be dynamically forced (e.g. Keenlyside and Latif, 2007) while the meridional mode is governed by thermodynamic processes at the sea surface (Chang et al., 1997). Servain et al. (1999) give strong evidence that the equatorial mode, the meridional mode and the latitudinal position of the ITCZ are linked at short and long timescales indicating that the processes involved are much the same as those that control the seasonal cycle. The strength of this relationship is possibly dependent on the timeperiod analyzed (Murtugudde et al., 2001). Improving the mean state in a coupled model therefore possibly improves the representation of Tropical Atlantic variability on longer timescales as well. This is especially true for the variability related to the zonal mode as the mean seasonal cycle and the zonal mode variability seem to be driven by similar mechanisms.

The Bjerknes feedback mechanism (Bjerknes, 1969) is closely related to the zonal equatorial variability and acts on an interannual timescale. The Bjerknes feedback is a positive feedback and contains three steps. First, colder (warmer) than normal SST in the eastern Equatorial Atlantic strengthen (weaken) the easterly winds in the central and western equatorial Atlantic. Second, the stronger (weaker) easterlies along the equator raise (deepen) the thermocline in the east. Third, the reduced (increased) thermocline depth in the east further contribute to a cooling (warming) of the local SST. Many studies have investigated individual components of the Bjerknes feedback in the Tropical Atlantic (an extended summary is given in the introduction of Keenlyside and Latif (2007)). Zebiak (1993) uses sensitivity experiments from a simplified coupled ocean-atmosphere model to show that on the one hand the Bjerknes feedback mechanism may be active in the Tropical Atlantic but on the other hand that some of the variability found in the Tropical Atlantic is externally forced. Chang et al. (2000) also note a Bjerknes type feedback in the Tropical Atlantic. Keenlyside and Latif (2007) show using observational data that all three components of the Bjerknes feedback are active in the Tropical Atlantic, but only at certain times of the year.

2.2.2 Predictability in the Tropical Atlantic

In contrast to the Pacific, relatively few studies have been performed to investigate (potential) predictability in the Tropical Atlantic, which might be partially due to the fact that the socio-economic impact of Atlantic variability is a lot smaller compared to Pacific (ENSO) variability. Another reason might be the fact, that variability is weaker in the Tropical Atlantic (Keenlyside and Latif, 2007) and that current coupled climate models exhibit large biases (Davey et al., 2002).

Chang et al. (1998) show using a relatively simple dynamical ocean-atmosphere model (Chang et al., 1997) and a linear inverse model (Penland and Matrosova, 1998) that a predictable pattern exist in the northern Tropical Atlantic (NTA). The predictability in the NTA has been related to ENSO by Penland and Matrosova (1998). Using an atmospheric general circulation model (AGCM) coupled to a simple mixed layer (ML) ocean model, Chang et al. (2003) indicate that (in addition to the NTA predictability due to ENSO influence onto the region) a significant part of NTA predictability is due to active air-sea feedback between surface heat flux and SST. Barreiro et al. (2005) further decompose the ENSO and non-ENSO part of seasonal predictability in the NTA and find that predictability depends on the fact whether the ENSO and the meridional mode influence on the NTA act together in a "constructive" or "destructive" way (as defined in Barreiro et al., 2005). They also address equatorial predictability explicitly - in contrast to the previous studies that mainly discuss predictability in the NTA region - and show that including ocean dynamics (which have been included in the Barreiro et al. (2005) AGCM-ML model in a simple statistical manner) significantly rises predictability along the equator on seasonal timescales. The fact that no predictability is found south of 10°S is attributed to the poor representation of the stratus cloud deck in the southern subtropics and the associated SST-cloud radiative feedback in the model (Tanimoto and Xie, 2002). Sutton et al. (2000) show with an uncoupled model run that the equatorial trades show a high level of potential predictability in MAM and JJA due to the fact that internal variance is small compared

to the total variance. The importance of both correct ENSO forcing and correct initial conditions in the Tropical Atlantic for forecasting the meridional mode index and South American precipitation is highlighted by Huang et al. (2009) using a AGCM coupled to a ML model.

The first more detailed study on equatorial Atlantic SST predictability is given by Stockdale et al. (2006) analyzing SST prediction by the ECMWF[1] and other DEMETER[2] (Palmer et al., 2004) models. Even when they try to account for the systematic wind bias along the equator (see next section) no skill above persistence is found for the southern Tropical Atlantic, and only weak skill is found along the equator and in the NTA. This is attributed to the fact that all models cannot reproduce the seasonal cycle of SST correctly (i.e. develop a warm bias in boreal summer) in conjunction with a misrepresentation of convection and winds in the equatorial Atlantic. Another large fraction of the forecast error is attributed to the uncertainties in the subsurface ocean data used to initialize the models as well as errors in coastal upwelling and the representation of coastal waves (Florenchie et al., 2003). A similar study based on the NCEP[3] coupled forecast system (Hu and Huang, 2007b) extracts the "most predictable pattern" by computing EOF patterns which maximize the signal-to-noise ratio to the predicted time series. These patterns indicate that the higher skill in the western part of the Tropical Atlantic is related to ENSO, while the low skill especially in the southeastern Atlantic is related to errors in the low-cloud-SST feedback (Hu et al., 2008) as well as the systematic SST bias in the same region. A recent study by Jansen et al. (2009) uses a conceptual model based on the delayed oscillator model by Burgers et al. (2005) to study predictability in the Tropical Atlantic. The simple model shows skill above persistence when hindcasting SST in the Atlantic 3 (ATL3, 20°W-0°E, 3°S-3°N). However, skill in the Jansen et al. (2009) study is still low.

[1] European Center for Medium Range Weather Forecast

[2] Development of a European Multi-Model Ensemble Prediction System for Seasonal to Interannual Prediction

[3] National Centers for Environmental Prediction

2.3 Problems in Coupled Modeling of Tropical Atlantic Climate

As mentioned earlier, the most pronounced error in basically all of the state-of-the-art coupled general circulation models (CGCMs) is the strong warm bias in sea surface temperature (SST) in the eastern Tropical Atlantic and peaks during boreal summer. The presence of the bias is therefore directly related to the inability of the CGCMs to simulate the correct annual cycle in the tropical Atlantic. Due to the presence of the strong SST bias in the eastern Tropical Atlantic the mean SST gradient along the equator is reversed (Davey et al., 2002, Figure 2 in Richter and Xie, 2008).

The SST bias in the equatorial Atlantic is present in all current CGCMs (Davey et al., 2002). Although effort has been taken to understand and minimize the large errors in the equatorial Atlantic, the mean biases summarized by Davey et al., 2002) are still present today. DeWitt (2005) argue that a westerly wind bias along the equator is the "most likely" cause for the development of the SST bias. It also leads to a vertical velocity distribution at the base of the mixed layer causing erroneous cooling of the SST both in the east and in the west. An important limitation of DeWitt (2005)'s experiments are the flux corrections used to prevent model drift. Okumura and Xie (2004) show that a westerly bias even prevails in an uncoupled AGCM. Chang et al. (2007) note that the westerly wind bias in the Tropical Atlantic is accompanied by deficient (excessive) rainfall over the Amazon region (Africa) indicating a weakened Walker-Circulation in the Atlantic. The most up-to-date study on the causes of Tropical Atlantic biases in CGCM has recently been published by Richter and Xie (2008). They show by comparing AMIP-type (Atmospheric Model Intercomparison Project, Gates, 1992) with CMIP (Coupled Model Intercomparison Project, based on IPCC-AR4 model output) experiments that a westerly surface wind stress bias in the central and western Tropical Atlantic already exists in the AGCMs, but only in boreal spring. This is due to anomalously high (low) sea-level pressure in the western (eastern) equatorial Atlantic, which Richter and Xie (2008) attribute to deficient (excessive) pre-

cipitation over tropical South America (Africa). These biases are amplified in the coupled model simulations. The westerly wind stress bias in spring causes the thermocline to be too deep in the eastern equatorial Atlantic preventing the development of a summer cold tongue. Chang et al. (2008) find similar results with CCSM3 (Community Climate System Model, version 3, Collins et al., 2006). They argue that the westerly bias in zonal wind stress in the Tropical Atlantic in boreal spring originates from a large precipitation bias in the eastern Amazon region. The precipitation bias is attributed to the inability of the AGCMs to correctly simulate the amount of convective precipitation over land. SST biases in the Tropical Atlantic region also cause errors in atmospheric circulation since strong ocean-atmosphere coupling is present in the Tropics. Stockdale et al. (2006) find that the interhemispheric SST gradient is important for spring precipitation in northeastern Brazil, while equatorial SST and the east-west SST gradient at the equator influences West African rainfall. Thus the circulation biases in the AGCMs, when run with prescribed observed SSTs, may be further amplified through ocean-atmosphere feedbacks in coupled mode (Richter and Xie, 2008).

Another source of error is the representation of low clouds in the southeastern part of the Tropical Atlantic and Pacific, in which also coupled feedbacks play an important role. While in the Pacific this problem has received attention more than 10 years ago (e.g. Ma et al., 1996, Nigam, 1997, Gordon et al., 2000, Yu and Mechoso, 1999), only recently work has been done on southeastern Tropical Atlantic low cloud representation in CGCMs. Huang et al. (2007) used a set of ensemble hindcasts from CFS (NCEP coupled forecast system, Saha et al., 2006) to analyze the warm bias in the southeastern Tropical Atlantic, which rapidly grows in boreal summer and peaks in November to December. They attribute the bias to excessive shortwave radiation reaching the surface which in turn causes the model to simulate too little low cloud cover in the region due to changes in lower tropospheric stability. Hu et al. (2008) find as well that the radiative flux directly affects the simulated SST. They show that the model produces too little low and too much high clouds amplified by a biased atmospheric stratification which might be responsible for a warm bias of up to 3K near the southeastern boundary. It has to be pointed out that

the NCEP-CFS has a relatively high resolution in the lower troposphere (20 sigma levels below 650hPa) so there is little hope that any of the current coarse resolution climate models can realistically simulate Atlantic low clouds and associated feedbacks.

In summary two main sources for the SST bias in the Tropical Atlantic due to atmospheric forcing seem to dominate the discussion. First, the westerly wind stress bias in AGCMs especially in spring that prevents summer cooling in the eastern Tropical Atlantic. Second, a local low cloud bias that causes excessive shortwave radiation and hence SST warming in the southeastern Tropical Atlantic.

While all of the above mentioned studies attribute the Tropical Atlantic SST bias to biases in atmospheric physics, there are also few studies attributing the source of error to the inability of the ocean model to simulate the observed strength of coastal upwelling (Large and Danabasoglu, 2006). It should be mentioned in this context that many ocean components of CGCMs have relatively poor horizontal and/or vertical resolution. Therefore, enhanced ocean model resolution may help to improve the simulation of coastal upwelling and thus SST. One study attributes the bias to poorly resolved mesoscale variability (Seo et al., 2006). Increased entrainment efficiency at the bottom of the mixed layer largely improved thermocline structure and SST bias in coupled model simulations analyzed by Hazeleger and Haarsma (2005). More recently Lee and Wang (2008) speculate using results from a simplified coupled model that a too strong meridional dipole mode could possibly contribute to the development of the warm bias. Breugem et al. (2008) attribute up to 2K of the eastern Tropical Atlantic SST warm bias to the formation of spurious barrier layers in the eastern and southeastern Tropical Atlantic. Barrier layers are found in tropical regions where a strong vertical salinity stratification occurs within the isothermal layer, which means that the isothermal layer depth and mixed layer depth differ. The difference between the isothermal and the mixed layer depth defines the thickness of the barrier layer. It acts as a barrier to the vertical penetration of heat into the ocean because, without a temperature gradient at the bottom of the mixed layer, entrainment of water from below does not remove any heat from the mixed layer. The occurrence of low sea surface salinities due to a southward displacement of the ITCZ in

boreal spring and summer produce unrealistic barrier layers. According to Breugem et al. (2008) the erroneous barrier layers enhance the SST bias, which in return contributes to the southward displacement of the ITCZ in the eastern Tropical Atlantic. This positive feedback mechanism has been termed the "BL-SST-ITCZ" mechanism by Breugem et al. (2008).

The large bias in SST and the atmospheric circulation in CGCMs have prevented modeling efforts of interannual variability in the equatorial Atlantic by means of CGCMs because errors in the simulation of seasonal climate are likely to cause similar errors in the representation of year-to-year variability (Chang et al., 2007). Despite the significant biases in their models, Stockdale et al. (2006) and Hu and Huang (2007b) investigate predictability in the equatorial Atlantic region (see previous section). On top of the mean biases in the CGCMs that spoil predictability, the low quality of ocean analysis data in the Tropical Atlantic compared to the Pacific poses another problem (Stockdale et al., 2006).

3 Model and Datasets

3.1 The Kiel Climate Model

The basis for this study is the coupled Kiel Climate Model (KCM, Park et al., 2009). The individual model components and their interaction, which will be described in the following and are depicted in Figure 3.1. As the atmospheric component ECHAM5 is used and is described in Roeckner et al. (2003). The mean climatology of the model is summarized in Roeckner et al. (2004). In the current low resolution configuration of KCM the atmospheric component uses T31 horizontal resolution (approximately 3.75° by 3.75°) with 19 vertical levels up to 10 hPa and a temporal resolution of 40min. Convective processes are accounted for by a mass flux scheme by Tiedtke (1989) with modifications for deep convection as suggested by Nordeng (1994). The stratiform cloud scheme follows Lohmann and Roeckner (1996). Subgrid variability of clouds is taken into account with a scheme by Tompkins (2002) approximating the subgrid distribution of cloud condensate by a prognostic β-distribution. Even though this scheme provides information about the subgrid variability of clouds in each grid cell, this information is currently not used for the radiative transfer calculations, but effort is taken to use this additional information (Pincus et al., 2003, Räisänen et al., 2007). The shortwave radiation transfer calculation follows Fouquart and Bonnel (1980) while for the longwave part a rapid radiative transfer model (RRTM) scheme by Mlawer et al. (1997) is used. Surface turbulent fluxes are described in the next section. For all further details about the model the reader is referred

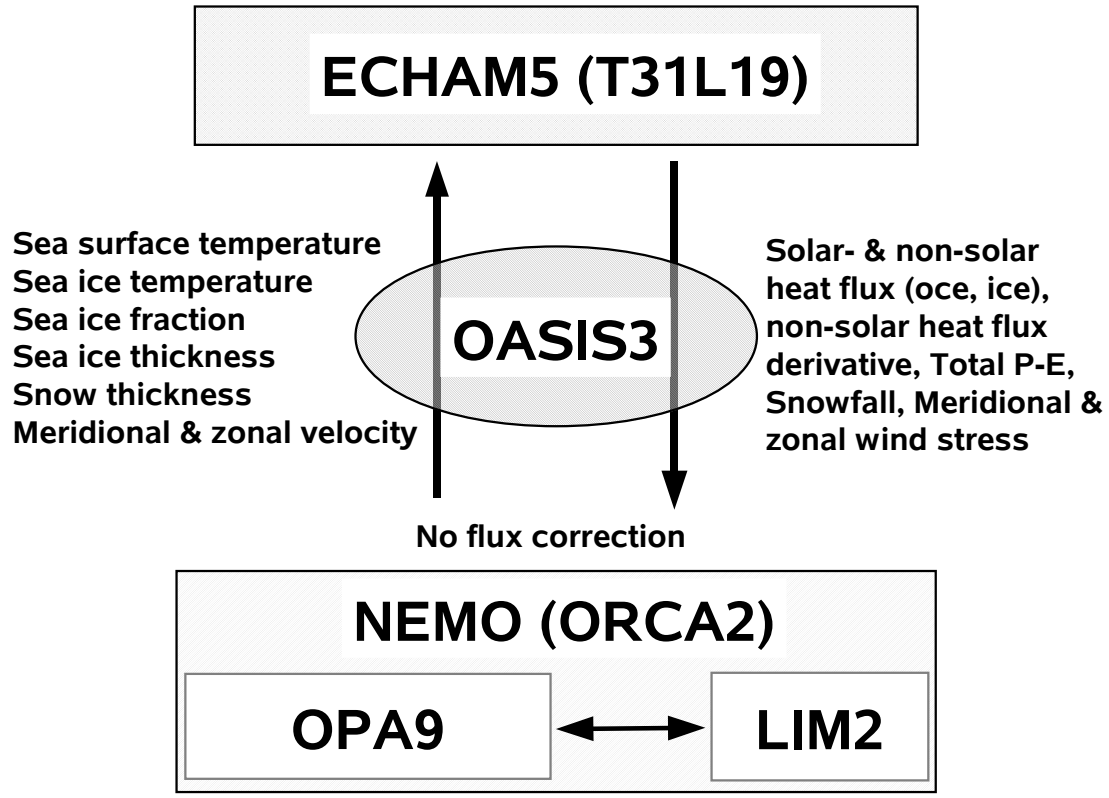

Figure 3.1: *Components of the Kiel Climate Model KCM. Atmosphere-Ocean (Ocean-Atmosphere) exchange parameters are listed on the left (right). Adopted from Park et al. (2009)*

to Roeckner et al. (2003).

The ocean model component is the Nucleus for European Modeling of the Ocean (NEMO; Madec, 2008). It uses the primitive equations for tracers and velocities which are solved on an ARAKAWA-C type grid (Arakawa and Lamb, 1977). In this setup the tracer point T resides in the middle of the grid box, and the U- and V- grid points are located on the sides of each grid box. The horizontal resolution is 2° with a equatorial latitudinal refinement of 0.5°. To avoid the singularity problem at the north pole a tripolar grid is used with one pole over Greenland and a second pole over Asia. In the vertical the model uses z-based coordinates with 31 levels. The ocean model includes an interactive sea-

ice model (Louvain-la-Neuve sea ice mode, LIM, Fichefet and Morales Maqueda, 1997, Goose et al., 1999). More details on the ocean model configuration can be found in Madec et al. (1998), Madec (2008), Scheinert (2008) and Park et al. (2009).
Coupling of the atmosphere and ocean component of the model is achieved via the Ocean Atmosphere Sea Ice Soil version 3 (OASIS3, Valcke et al., 2006) once per day. The parameters exchanged through OASIS3 are indicated on Figure 3.1. The detailed coupling strategy applied in KCM is described in Park et al. (2009).
In its current setup the model has been used to study long-term internal variability (Park and Latif, 2008), forced variability (Latif et al., 2009), and the sensitivity to global increase in CO_2 concentration (Park et al., 2009).

3.2 Model configurations

The reference run (REF) is essentially the same as the one described in Park et al. (2009) except for a few minor model modifications which are not relevant for the problems discussed in this work. For this study a set of sensitivity experiments have been performed that will be described in the following and are summarized in Table 3.1.
In the radiation (RAD) experiment the SW radiation penetrating into the ocean is reduced by 30% and 15% at certain gridpoints along the coast (Figure 3.2). This experiment is used to assess the effect of excessive surface radiation at the surface on the SST bias in the southeastern Tropical Atlantic. The values are chosen at those gridpoints where the mean SST bias is largest and roughly correspond to a reduction in surface shortwave radiation of 40 - 80 W/m^2. These values are in the range of excessive shortwave radiation in the southeastern Atlantic as suggested by Hu et al. (2008). This approach is somewhat inconsistent with previous results, which show that the biases in low cloud and surface radiation extend further off the coast (Hu et al., 2008 and Figure 4.2 in chapter 4). However, it allows us to quantify the direct impact of excessive shortwave radiation in the region where the warm bias is strongest.

Exp. ID	Years	Modifications with respect to REF experiment:
REF	120	REF experiment, see Park et al. (2009).
REFUC	20	uncoupled version of REF.
MOD	120	modified parameters as described in section 3.
MODUC	20	uncoupled version of MOD.
FLX	120	flux-corrected (global, 40°S - 40°N) version of KCM.
RAD	50	modified SW radiation in the southeastern Atlantic as depicted in Figure 3.2.
WIND4	50	climatological wind stress between 4°S and 4°N in the Atlantic.
WIND10	50	climatological wind stress between 10°S and 10°N in the Atlantic.

Table 3.1: *Configurations of the Kiel Climate Model KCM used in to discuss the mean state in the equatorial Atlantic.*

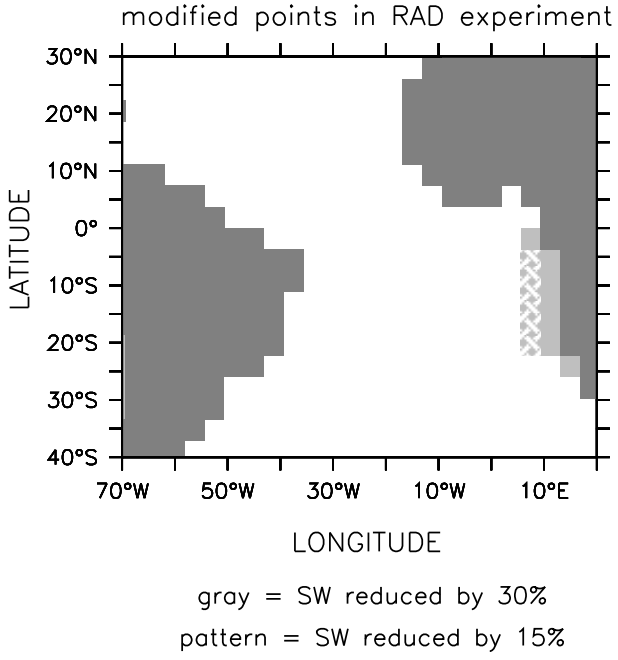

Figure 3.2: *Modifications in the RAD run as denoted on the figure, for details see text.*

Richter and Xie (2008) and Chang et al. (2008) claim the westerly wind in the western Tropical Atlantic to have a strong influence on the development of the SST bias. To evaluate the importance of this mechanism a run with climatological wind stress between 4°S and 4°N in the Atlantic has been performed, which will be referred to as WIND4. North (south) of 4°N (4°S) a linear transition between the climatological wind stress and the model generated wind stress is applied to avoid spurious effects due to a rapid change in wind stress along 4°S and 4°N. The wind stress climatology has been calculated from monthly NCEP-NCAR Reanalysis data from 1950 to 2004, and is linearly interpolated online onto the corresponding time step during the model run. The same experiment has been repeated with climatological wind stress merged into the model between 10°S and 10°N, and will be referred to as WIND10.

Flux-corrections are often used to overcome the problems associated with model biases but do not necessarily fix subsurface errors in the ocean circulation. To calculate the flux-corrections a 50 year run with restoring towards climatological SSTs at all ice free grid points has been performed. The last ten years of this run have been used to calculate a flux-correction climatology, which has been applied on a daily basis in the FLX run between approximately 40°S and 40°N. North (south) of 40°N (S) flux corrections are linearly reduced towards zero.

The modified version of KCM (MOD experiment) contains modifications in the physical parameterizations of the atmospheric model, which mainly affect the turbulent surface transfer of heat and moisture at the ocean surface. Generally, the surface flux of a variable is controlled by turbulent fluxes, which must be parameterized in GCMs using bulk-parameterizations because of the small scale nature of turbulent processes. The turbulent fluxes of heat and moisture at the surface mainly depend on the roughness of the surface, horizontal wind speed and atmospheric stratification above the sea surface. The turbulent flux of a variable χ is obtained from the bulk transfer relation (Roeckner et al., 2003):

$$(\overline{\omega'\chi'})_S = -C_\chi |V_L|(\chi_L - \chi_S), \tag{3.1}$$

where C_χ is the transfer coefficient. The subscripts L and S refer to values at the lowest model level and the surface layer, respectively, and V_L is the horizontal wind vector at level L. The transfer coefficient for moisture and heat can be expressed as

$$C_{qh} = C_N f_{qh}, \tag{3.2}$$

where C_N is the neutral transfer coefficient and f the stability function representing the ratio of C_{qh} (q and h denote moisture and heat, respectively) to the respective value under neutral conditions (Roeckner et al., 2003). The stability function f are defined separately for land, ice and water surfaces and stable and unstable conditions, respectively. Following Miller et al. (1992) in unstable conditions over sea, an empirical interpolation between the free convection limit and the neutral approximation is used to ensure that free convection conditions prevail:

$$f = \left(1 + {C_R}^{1.25}\right)^{1/1.25} \tag{3.3}$$

$$C_R = \beta \frac{\left(\triangle\Theta_v\right)^{1/3}}{C_N |V_L|}. \tag{3.4}$$

In the MOD version mainly β in equation 3.4 is increased. The change in β increases the transfer coefficient of heat and moisture being most effective at low windspeeds and large instabilities (i.e. large $\triangle\Theta_v$). Over land the transfer parameter f depends on surface roughness and vegetation index and has not been changed.

A set of three uncoupled experiments has been additionally performed. They consist of two AMIP-type experiments both with MOD and REF configuration, which will be referred to as MOD uncoupled (MODUC) and REF uncoupled (REFUC), respectively. The uncoupled ocean run (OCE) covers the period 1958 to 2002 and is forced with the CORE dataset by Large and Yeager (2004), which provides the atmospheric state at 10m. All required atmosphere-ocean fluxes are then computed via bulk formulae (Kara et al., 2000).

If not stated otherwise, 20 years from the end of a run are used for calculating the mean fields and climatologies. For the runs which are only 50 years or shorter the last 10 years are used.

3.3 Observational datasets

Observational SST are taken from the NCEP/NCAR reanalysis (Kalnay et al., 1996) covering the period from 1950 to 2004. Latent heat flux at the ocean surface has been taken to the Hamburg Ocean–Atmosphere Parameters and Fluxes from Satellite Data (HOAPS, Andersson et al., 2007), which covers 1978 to 2005. Observed high and low cloud cover is taken from International Satellite Cloud Climatology Project (ISCCP, Rossow and Schiffer, 1991) from year 1984 to 2000. To calculate the amount of high and low cloud cover from model data, assumptions about the vertical overlap of clouds have to be made. Total cloud cover in KCM is calculated using the maximum random overlap assumption, which means that adjacent cloud layers are maximally overlapped while non-adjacent are randomly overlapped. Total low cloud has been calculated in two ways and compared to the ISCCP derived low cloud cover. In the first case, low clouds are defined as all clouds occurring below 680 hPa and are assumed to be maximally overlapped (MAX). In the second case clouds are assumed not to be overlapped at all, i.e. the sum of the cloud cover in all model layers below 680 hPa is taken, which can be seen as the most extreme case of the random overlap assumption (RAN). Comparing the MAX and RAN calculation to ISCCP low cloud cover shows that bias patterns are in principle the same but low cloud cover is generally 10-15% lower in the MAX method. In the figures discussed in this work the MAX method has been used.

Observed precipitation is taken from the dataset by Xie and Arkin (1997), which extends from 1979 to 2006. Zonal and meridional wind components as well as total windspeed are compared to 6 years (2000-2005) of high resolution quickscat observations (Graf et al., 1998). To evaluate subsurface temperature and salinity the Simple Ocean Data Assimilation (SODA version 1.4.2, Carton and Giese, 2008) reanalysis dataset from 1980 to 1999 is used.

4 Mean state and seasonal cycle in the Tropical Atlantic Ocean

4.1 Mean state in the REF experiment compared to observations

While Park et al. (2009) provide an extensive discussion of KCM biases with respect to observations for the Pacific, such an analysis has not been performed for the Atlantic. In the following, a short comparison of the mean climate in the Tropical Atlantic in the REF experiment with various observed parameters will therefore be provided.

Figure 4.1 shows the mean SST bias in the tropical and Subtropical Atlantic in the REF experiment towards observed SST. Along the southeastern coast of Africa the bias exceeds 8°C at some gridpoints. Along the equator a mean bias of 2-4°C is found east of 10°W with higher values towards the coast. Due to this bias the gradient along the equator is reversed in KCM (see section 4.2.3). The cold bias north of 20°N is related to the strong cold bias in the northern Atlantic (see discussion in Park et al., 2009). The seasonal development of the SST bias is depicted in Figure 4.2a. In May the bias is smallest and limited to coastal areas. Towards August the bias grows rapidly and spreads westward along the equator. The largest areal extent is found in November. Throughout the winter months the bias decreases and shifts south of the equator in the central equatorial Atlantic.

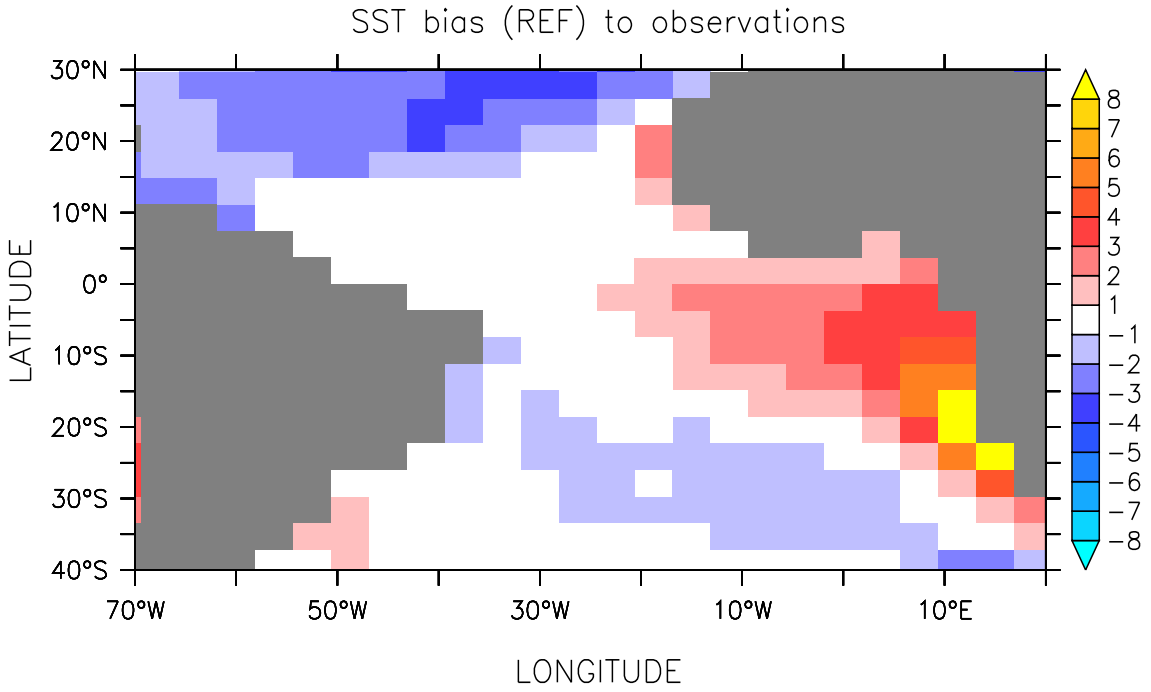

Figure 4.1: *Mean SST bias with respect to observations in the REF experiment.*

While SST varies between almost 29°C in the eastern equatorial Atlantic in spring and 24°C in late summer, almost no seasonal variation in the eastern Tropical Atlantic SST if found in KCM, and SST stays at around 29°C.

Three major regions with precipitation biases can be identified. One area is located between 15°S and 5°S and 40°W to 20°W, where the REF configuration of KCM overestimates precipitation from January to March (shown for February in Figure 4.2d). Towards boreal summer and fall this pattern shifts towards the central Tropical Atlantic. The second important bias pattern is the underestimation of precipitation in Northeastern Brazil from January to July (shown for February and May in Figure 4.2d) with peak values from February to April. Another region where KCM overestimates precipitation is located in the southeastern Atlantic north of 20°S shifting into the Gulf of Guinea in boreal summer. In late fall to early winter precipitation is too high over central South America (only November value shown in Figure 4.2d).

The bias in the 10m wind field (Figure 4.2b) shows that the trade winds are too strong

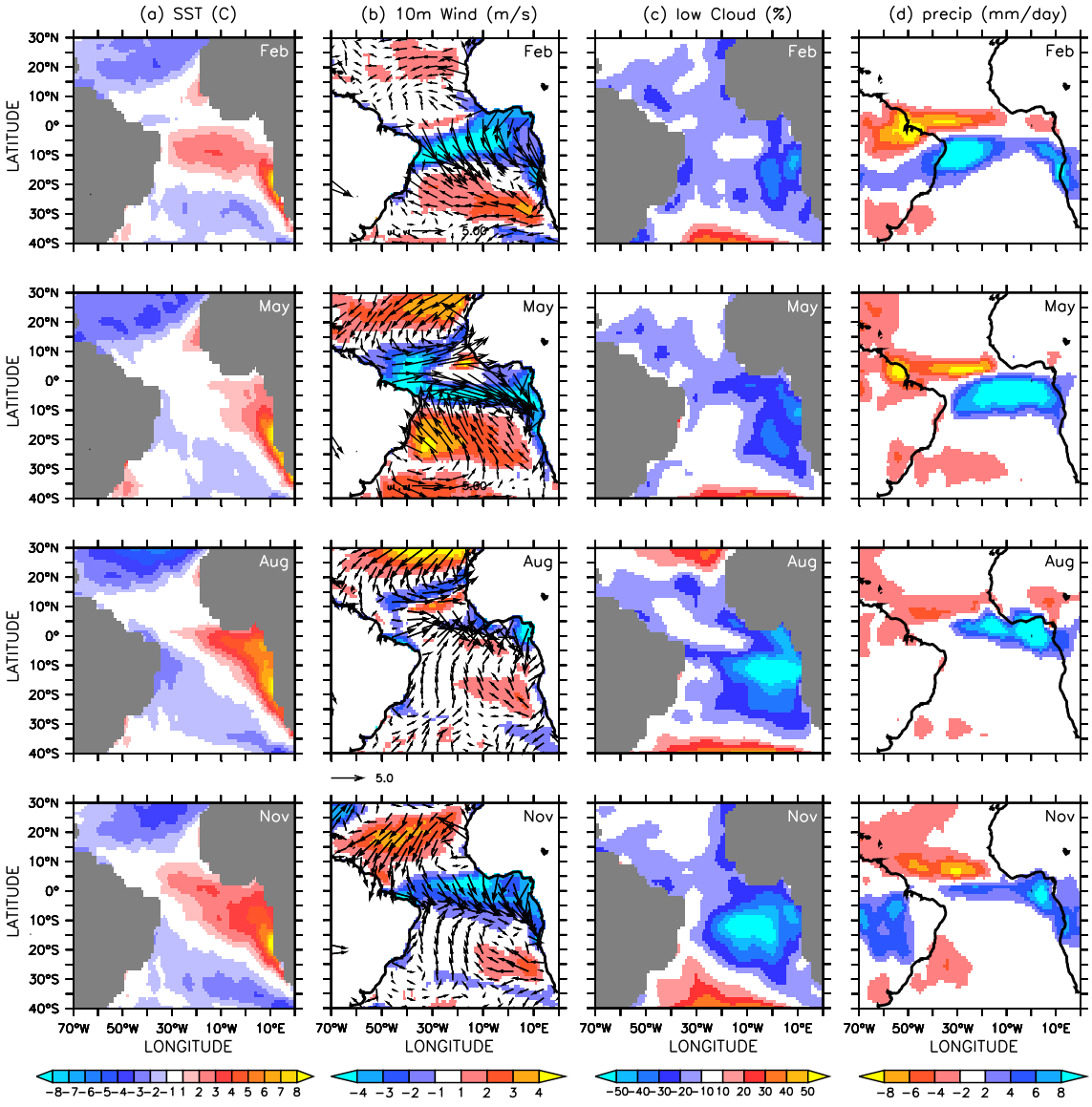

Figure 4.2: *Seasonal cycle of bias in SST (a), 10m winds (b), low cloud cover (c) and precipitation (d) in the REF experiment relative to observed values. The respective observational datasets are introduced in section 3.3. The shading in (b) shows the differences in absolute windspeeds calculated as* $(\sqrt{(u10)^2+(v10)^2})_{REF} - (\sqrt{(u10)^2+(v10)^2})_{OBS}$. *The length of a standard array is indicated below the figure in the third row.*

south and north of the ITCZ with the largest bias occurring in MAM (SON) in the southern (northern) hemisphere at approximately 10-20°S (20-30°N). In both hemispheres the

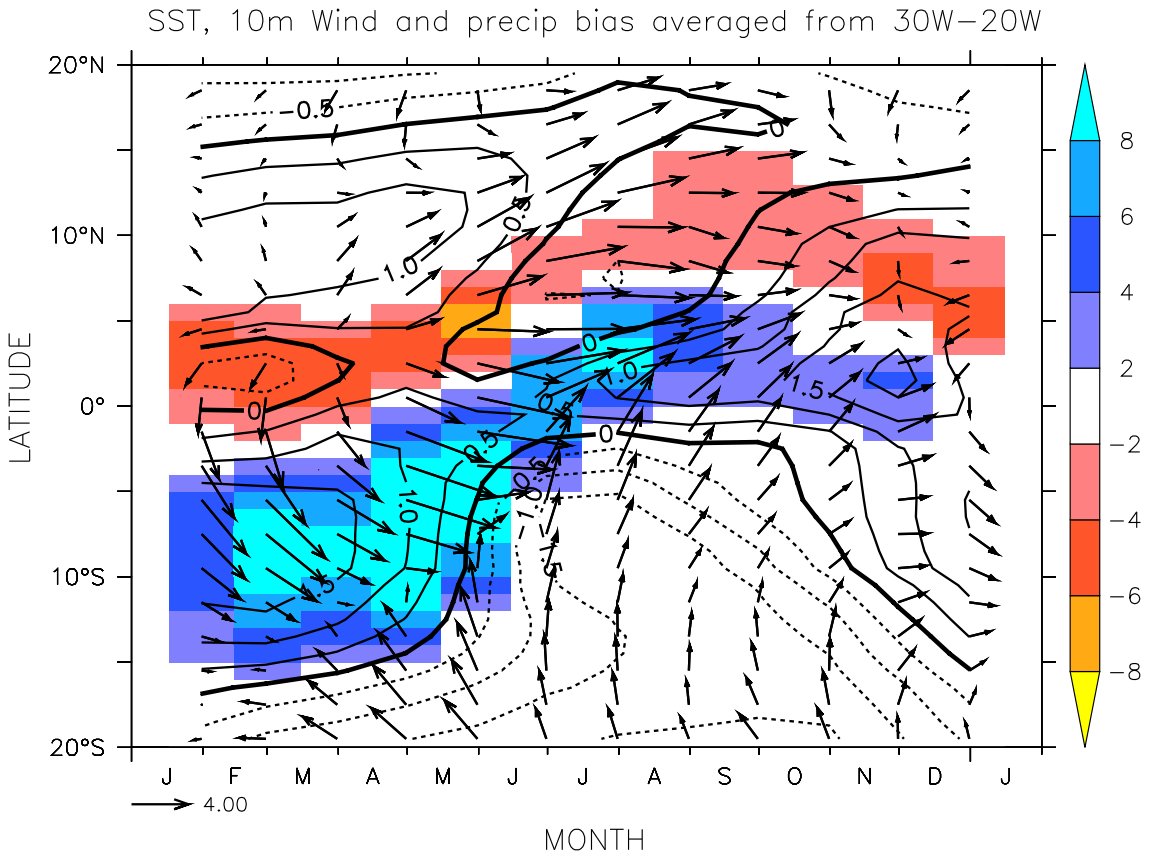

Figure 4.3: *Seasonal cycle of bias in SST bias (contours), 10m winds (arrows) and precipitation (shading, mm/day) averaged from 30°W to 20°W.*

subtropical wind bias follows the seasonal cycle of the ITCZ. Between roughly 10°S and 10°N an west to northwesterly wind bias of 3 to 4 m/s is found. The westerly to northwesterly wind bias peaks in May when the bias exceeds 4 m/s.

SST, wind and precipitation biases in the central to western equatorial Atlantic (averaged from 30°W to 20°W) as a function of calendar month are shown in Figure 4.3. The strong positive precipitation bias follows the strongest warm bias in SST. In every month of the year, a negative precipitation bias is located towards the north of the positive precipitation bias. This corresponds to a southward shift of the ITCZ all year round, since precipitation between 30°W to 20°W is tied to the position of the ITCZ. The strongest deviation from the observed mean ITCZ position is found from January to June where the mean ITCZ

position in KCM is approximately at 5-10°S. In observations the center of the mean ITCZ is located just north of the equator. Consistent with the southward shift of the ITCZ position, a northwesterly to southwesterly wind bias is found to the south of the observed ITCZ position in the model.

As discussed in section 2.3 low cloud cover represents an important parameter in Tropical Atlantic climate. Figure 4.2c shows that low cloud cover is underestimated east of 20°W and south of the equator. The bias is weakest from January to March (February value shown in Figure 4.2) with a peak bias of 30% along the southeastern coast between 20°S and 10°S. From May to July the bias grows rapidly along the coast and exceeds 50% in August. In late summer to fall the center of the bias is located further offshore between 10°W and 0°E. During boreal winter the bias reduces and underestimation of low cloud cover is mostly below 30% in February and May.

The biases in the atmospheric state in the Tropical Atlantic in the REF experiment project onto the ocean subsurface state. Figure 4.4 shows the seasonal cycle of the temperature and salinity biases in the ATL3 and ETA region. Especially in the ETA region a strong subsurface bias in temperature is present peaking from May to September. In addition surface and subsurface salinities are too low during all seasons. These biases have similar magnitude compared to those found in other state-of-the-art GCMs (Breugem et al., 2008).

Although the mechanisms leading to SST and atmospheric biases in KCM are discussed extensively in the following chapters, some conclusions can be drawn already. The ITCZ is located too far south in boreal winter especially in the western Tropical Atlantic along the South American coast as seen in precipitation. In the Gulf of Guinea precipitation is too high due to strong convective activity as a result of high SST. It is consistent with a northerly wind bias in that region and too little precipitation over the Sahel area. This shows that the African Monsoon doesn't develop properly and that the ITCZ remains in its equatorial position in boreal summer. Winds along the equator are too weak and show a west to northwesterly bias in KCM. Low cloud cover in the central and eastern Atlantic south of the equator is underestimated. In the ocean, biases in temperature and salinity

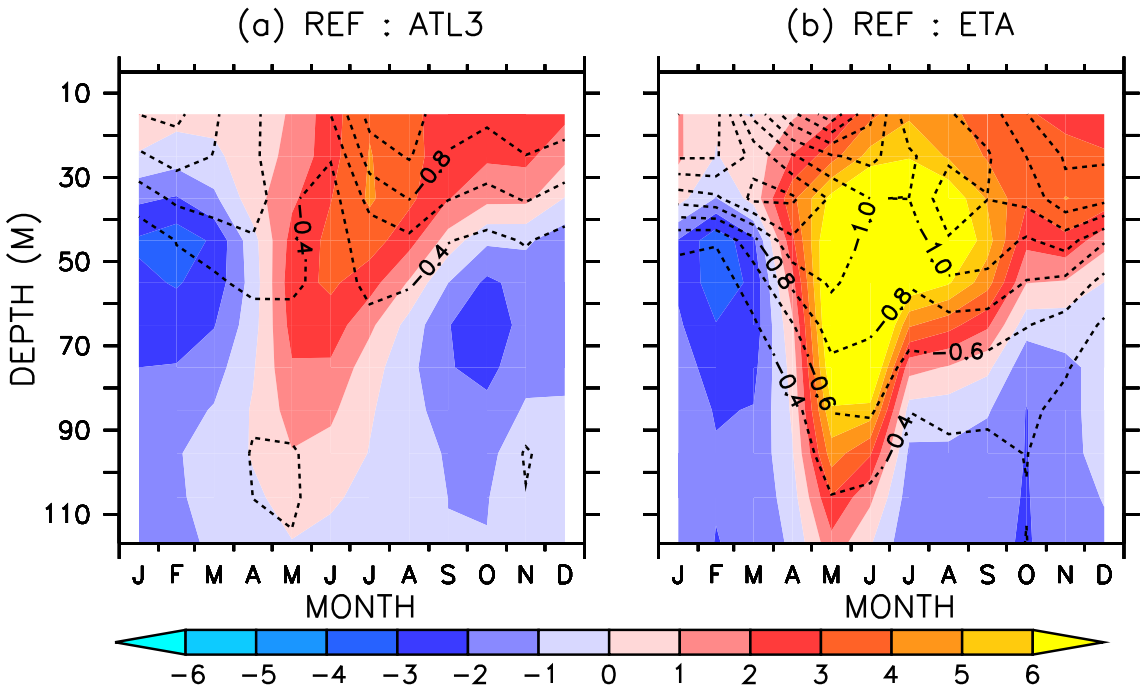

Figure 4.4: *Seasonal cycle of temperature bias (shading) and salinity (contours) in the REF experiment with respect to a 20 year climatology calculated from SODA data in the ATL3 box (a) and ETA box (b).*

develop, which favor the development of erroneous barrier layers that may contribute to the development of the SST bias during boreal summer (Breugem et al., 2008).

4.2 Sensitivity of biases in Tropical Atlantic climate to wind and surface radiation

In this section the two major causes for the development of the eastern Atlantic warm bias are discussed, namely the excessive surface shortwave radiation in the southeastern Atlantic due to deficient low cloud cover (Huang et al., 2007), and the errors in equatorial winds along the equator (Richter and Xie, 2008) that prevent the development of the

summer cold tongue in the eastern equatorial Atlantic. Both mechanisms are studied in KCM by means of sensitivity experiments.
In sections 4.2.1, 4.2.2 and 4.3 the focus is on the impact on the atmospheric circulation in the Tropical Atlantic. Section 4.4 provides a more detailed discussion of the subsurface temperature and salinity structure and its influence on the SST bias in all experiments.

4.2.1 WIND4 and WIND10 experiment

Figure 4.5 shows the SST differences of the WIND4, WIND10 and RAD experiment with respect to the REF experiment. In the WIND4 experiment the SST is reduced up to 3°C just south of the equator in the eastern Tropical Atlantic. Along the southeastern coast the reduction of the warm bias is weak and stays below 1.5°C. In the WIND10 experiment the difference in mean SST with respect to the reference experiment (Figure 4.5b) is stronger than in the WIND4 experiment. Along the southeastern Atlantic coast a reduction of SST by more than 3°C is found. The difference between the WIND10 and WIND4 experiment might be related to stronger southerly wind stress along the coast between 4°S and 10°S. It removes the north to northwesterly wind stress bias close to the coast which is present in the REF experiment (Figure 4.2b). Stronger southerly wind stress along the African coast possibly increases coastal upwelling, and colder water reaches the surface. Off-equatorial wave dynamics (Ding et al., 2009, Schouten et al., 2005) might also play a role but have not been studied in detail (see also section 4.4).
The seasonal development of the SST bias in the WIND10 experiment is shown in Figure 4.6a. In spring (Figure 4.6a), a warm bias in SST tends to develop east of 20°W. The realistic wind stress merged into the model enhances the equatorial upwelling and suppresses the development of the bias in boreal summer (Figure 4.6a). Further to the south (and weaker also to the north), a coastal warm bias is still present, but is reduced compared to the large warm bias in the REF experiment. The colder SST along the equator seems to spread south- and northward along the coast reducing the off-equatorial coastal SST bias,

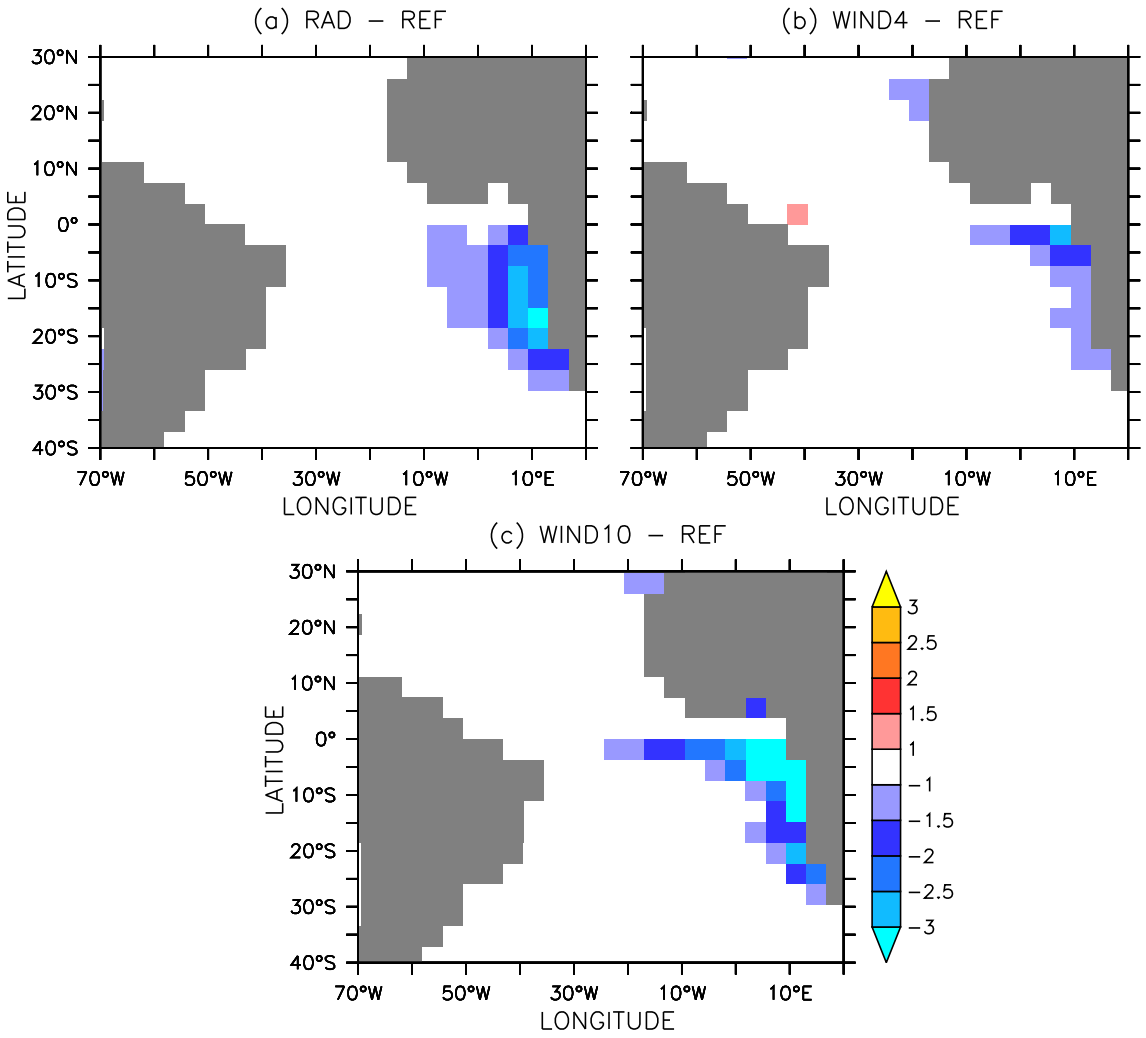

Figure 4.5: *SST difference of the RAD (a), WIND4 (b) and WIND10 (c) experiment with respect to the REF run.*

and resembles the coastal Kelvin wave propagation discussed by Florenchie et al. (2003) and Polo et al. (2008). Florenchie et al. (2003) show that the source of the Benguela Niño (positive SST anomaly in spring centered at roughly 15°S along the African coast) can be tracked back to the west to central Tropical Atlantic perturbations in the thermocline. The signal travels north- and southward as a downwelling Kelvin wave and takes about two month to propagate from the central Tropical Atlantic to 15°S (Polo et al., 2008).

The reduced SST in the eastern Tropical Atlantic destroy the excessive convection in the

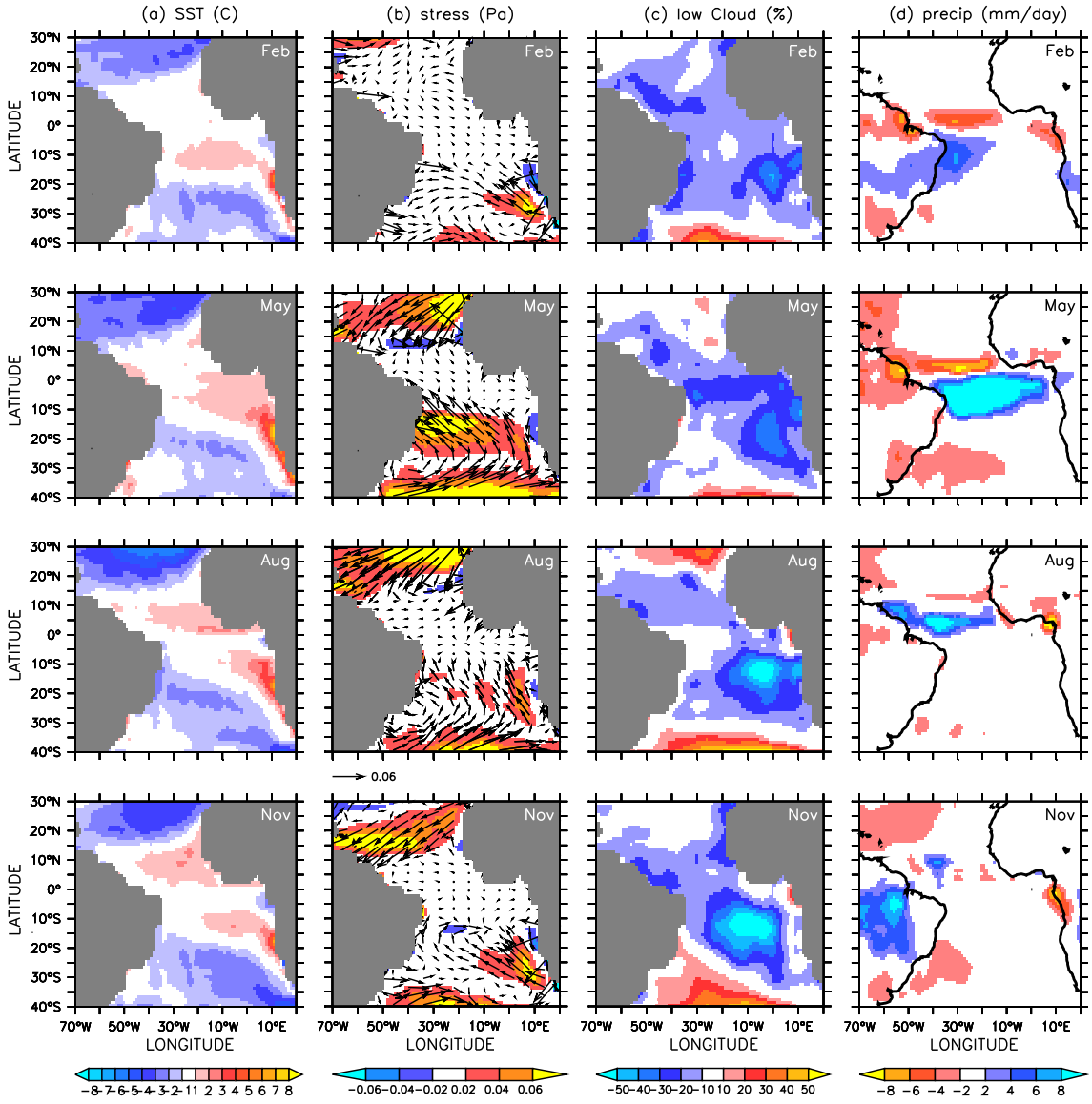

Figure 4.6: *Seasonal cycle of bias in SST (a), surface wind stress (b), low cloud cover (c) and precipitation (d) in the WIND10 experiment towards observational datasets. The respective observational dataset have been introduced in section 3.3. The shading in (b) shows the bias in total windspeed. The shading in (b) shows the differences in absolute absolute wind stress calculated as* $(\sqrt{u^2+v^2})_{WIND10} - (\sqrt{u^2+v^2})_{OBS}$. *The length of a standard array in (b) is indicated below the figure in the third row. As wind stress between 10°S and 10°N is replaced in WIND10, wind stress insted of 10m wind is shown in this figure.*

Gulf of Guinea turning the overestimation of precipitation in REF into a small dry bias from August to February (Figure 4.6d). In the central and western Tropical Atlantic a significant reduction of the precipitation biases in the REF experiment are also found in the same months. Despite the improvements in SST, both the WIND4 and the WIND10 experiment show a substantial wet bias in precipitation between 10°S and 5°N (Figure 4.6d) in conjunction with a dry bias towards the north and northwest in May. It shows that the ITCZ is still shifted southward.

The reduction of the SST bias has a significant impact on the evolution of the low cloud bias along the African coast (Figure 4.6c). In boreal fall the low cloud bias disappears east of 5°E. The strengthening of the low cloud deck along the coast contributes to the reduction of the low cloud bias via the cloud-radiation-SST feedback (Huang et al., 2007). In late summer to fall the shortwave radiation reaching the surface is reduced by up to 40W/m^2(not shown), consistent with an increase in low cloud cover by more than 25% with respect to the REF experiment (compare Figures 4.2c and 4.6c). Although slightly reduced, the strong bias in low cloud cover remains further off the coast in August and November. Nevertheless, the SST warm bias is reduced by 1-2°C in this area in August and November. To further quantify the contribution of southeastern Atlantic low cloud and surface radiation onto the SST bias in the southeastern Atlantic and at the equator, the RAD experiment (as described in section 3.2) has been set up and will be discussed in the following section. The impact on the subsurface temperature and salinity stratification will be discussed in section 4.4.

4.2.2 RAD experiment

In the annual mean SST bias pattern (Figure 4.5) the reduction of shortwave radiation reaching the surface in the RAD experiment has a large impact with local cooling more than 2.5K (Figure 4.5b). To assess the temporal development of the bias in these experiments, Figure 4.5 has been compared to similar figures for year 5-10 and 80-100 of the

same runs (not shown). Comparing those figures shows that the realistic wind stress in the WIND4 and WIND10 experiments have an immediate effect on the bias pattern i.e. Figure 4.5b does not change much over time. For the RAD experiment the cooling grows continuously over time and stabilizes with a pattern close to the one shown in Figure 4.5a. The artificial reduction of the shortwave radiation penetrating into the ocean continuously removes energy (in the form of shortwave radiative energy) without any compensation from the coupled system.

The seasonal development of the differences between the RAD and REF experiment in SST, wind, low cloud cover and precipitation are shown in Figure 4.7. Despite the fact that the artificial reduction in surface SW radiation is constant throughout the year, a pronounced seasonality of the SST, 10m wind, low cloud and precipitation differences with respect to the REF experiment occurs (Figure 4.7a). The reduction (increase) in eastern Atlantic SST (low cloud cover) in RAD with respect to REF is largest in August and November. During the same months the biases in eastern Atlantic SST and southeastern Atlantic low cloud cover are largest in the REF experiment with respect to observations (Figure 4.2a,c). It indicates that eastern Tropical Atlantic climate is most sensitive to changes in surface radiation along the southeastern coast during boreal summer and fall. In the REF experiment the northward shift of convective activity into the Sahel zone in boreal summer is inhibited as favorable conditions for convection remain over the Gulf of Guinea due to the SST bias. In the RAD experiment SST is reduced in the southeastern Tropical Atlantic thus forcing the convection to move northwards in spring and follow the change in solar inclination. In Figure 4.7d this is seen as reduced precipitation just south of the equator in the eastern Tropical Atlantic and an increase in precipitation towards the north. The increase in precipitation in the western and northwestern Tropical Atlantic indicates a strengthening of the zonal circulation. The relocation of the convective activity increases the southeasterlies along the equator (Figure 4.7b), resulting in a cooling of SST in the cold tongue region by about 1-2°C in August. Compared to February and May, the reduction of the SST warm bias in the RAD experiment is larger along the southeastern coast in August and May. The largest increase in low cloud cover with respect to the REF

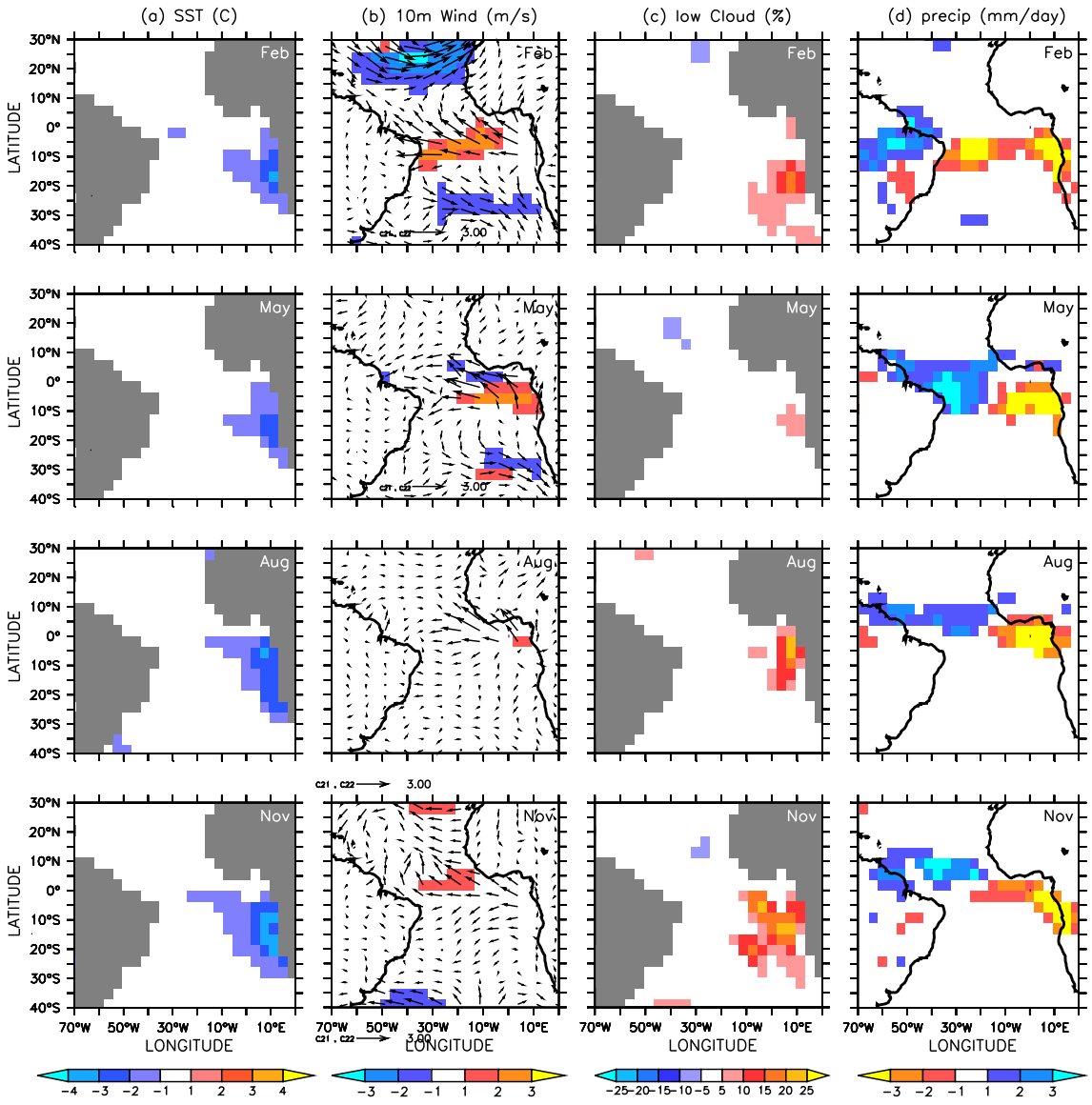

Figure 4.7: *February (top), May (second row), August (third row) and November (bottom) of SST (a), 10m Wind (b), low cloud cover (c) and precipitation (d) differences between RAD and REF in the Tropical Atlantic. Units are indicated in the headings. The shading in (b) shows the differences in absolute windspeeds calculated as* $(\sqrt{(u10)^2+(v10)^2})_{RAD} - (\sqrt{(u10)^2+(v10)^2})_{REF}$. *A standard array as indicated below the third Figure in column (b) corresponds to 3 m/s.*

experiment is found in November. Consistent with Huang et al. (2007), this indicates that low cloud cover has an significant impact on the southeastern Atlantic SST bias and its seasonal cycle, and that low cloud cover and SST are tightly coupled. Huang et al. (2007) show that the large bias in low cloud cover in their coupled model analysis has a significant impact on the southeastern Atlantic SST bias from boreal summer to fall, and is related to the low-cloud-radiation-SST feedback mechanism. As already stated in chapter 2.1, this mechanism is most effective in late boreal summer to fall due to the peak in lower tropospheric stability as a consequence of the maximum strength of the subtropical high in that region at that time of year (Klein and Hartmann, 1993).

In boreal winter the modifications imposed in the RAD experiment only have a small impact on SST at the equator in the eastern Tropical Atlantic. This can be explained as follows: In boreal spring the decrease in SST in the southeastern Tropical Atlantic "kicks off" the natural northward shift in convective activity that is inhibited in REF due to the presence of the strong SST bias. In boreal fall and winter no such northward shift in convective activity is supported by the solar inclination. However, the positive precipitation bias and the northwesterly wind bias just south of the equator, which both are present in the REF experiment (Figure 4.12b,d), are reduced in the RAD experiment. The weakening of the trade winds north of 15°N in February due to changes in southeastern Atlantic radiation remains unclear.

In summary, the RAD experiment shows that the southeastern Atlantic coastal warm bias has the potential to contribute to the biases in the atmospheric circulation in the Tropical Atlantic, which are believed to be responsible for the SST bias along the equator. To quantify the overall impact of the southeastern surface radiation bias, another sensitivity experiment, which has the surface radiation bias corrected further off the coast as well, would be helpful.

The modifications applied to the atmosphere also cause significant changes in the mean ocean state, which will be discussed together with the results from the MOD experiment in section 4.4.

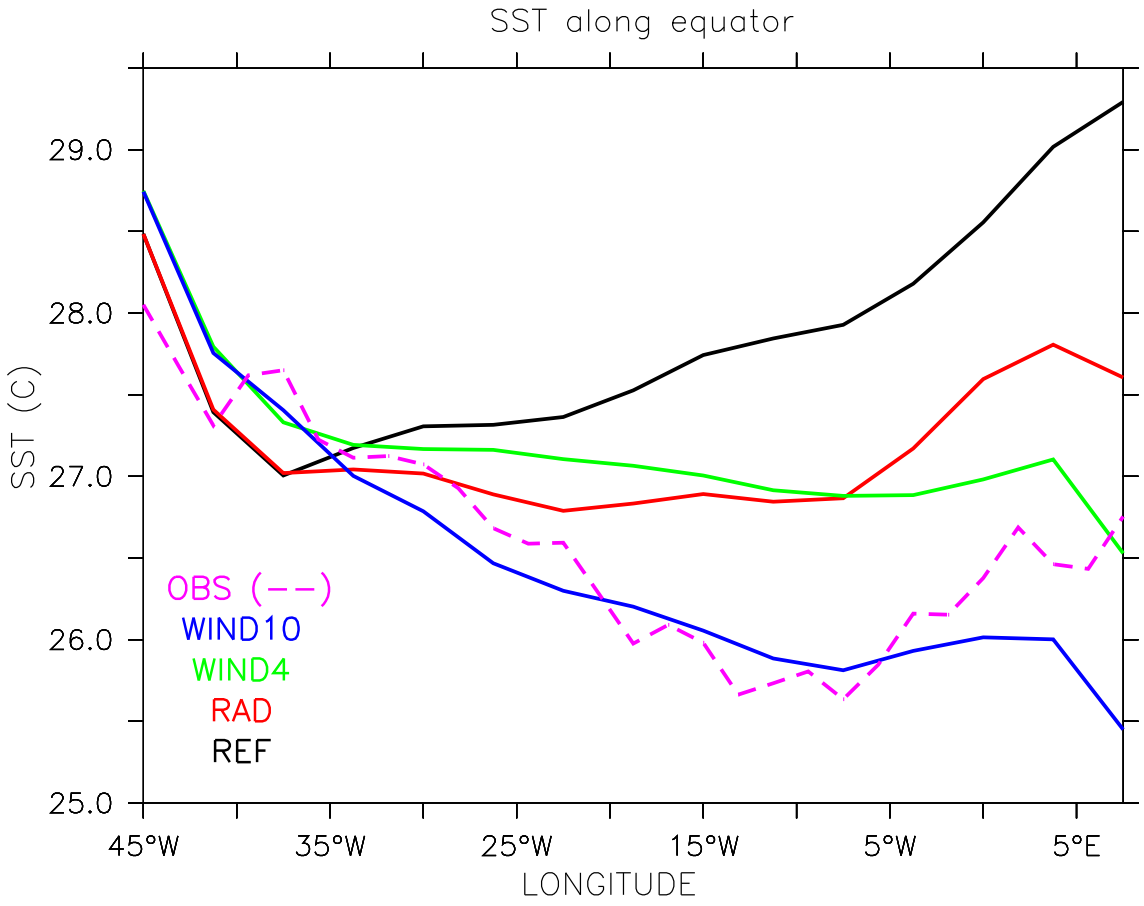

Figure 4.8: *SST along the equator in different sensitivity experiments as indicated on the figure as well as observed SST.*

4.2.3 Equatorial SST gradient in the sensitivity experiments

Errors in the mean SST gradient along the equator in the Atlantic are related to the SST warm bias in the eastern equatorial Atlantic (Davey et al., 2002). The SST along the equator for the three sensitivity experiments is shown in Figure 4.8. Consistent with the large bias in the eastern Tropical Atlantic a very large error in the SST gradient along the equator is found in the REF experiment. The WIND4 and RAD experiment show a significant improvement in the bias. The WIND10 experiment shows a equatorial SST gradient that compares nicely with the observed zonal SST gradient. The differences

in the zonal gradient in the experiments discussed here confirm the findings from the previous sections. First, realistic equatorial *and* off-equatorial winds are necessary to get a correct east-west SST gradient along the equator and are primarily responsible for a realistic SST gradient. Second, the error in surface shortwave radiation along the southeastern coast has a significant impact on the zonal SST gradient along the equator.

4.3 Atmospheric and surface response in the MOD experiment

In the experiments discussed above artificial modifications have been applied to KCM to further understand the causes of the bias and compare to what has been discussed in literature. In the MOD experiment modifications are in the physical parameters concerning air-sea exchange as described in section 3.

The most striking difference between REF and MOD is the strong reduction of the warm bias that exceeds 3°C in the eastern part of the basin (Figure 4.9a). Figure 4.9b shows clearly that the reduction in the SST bias in MOD is most pronounced in those areas where the largest bias in REF is found. Consistent with the reduction of the bias in the eastern Tropical Atlantic the SST gradient along the equator is significantly improved (Figure 4.9c). The cold biases south of 20°S and north of 15°N, which are already present in the REF experiment, are not reduced.

As stated earlier, the eastern Atlantic warm bias in the REF experiment shows a pronounced seasonality (Figure 4.10). Along the equator the warm bias starts to develop around May, peaks in July-August-September and weakens towards December. In the MOD experiment the warm bias is considerably reduced. A weak warm bias, however, is still present in summer (Figure 4.10). At the same time a slight cold bias develops in the western part, which is due to the general cooling of approximately 1°C over the whole

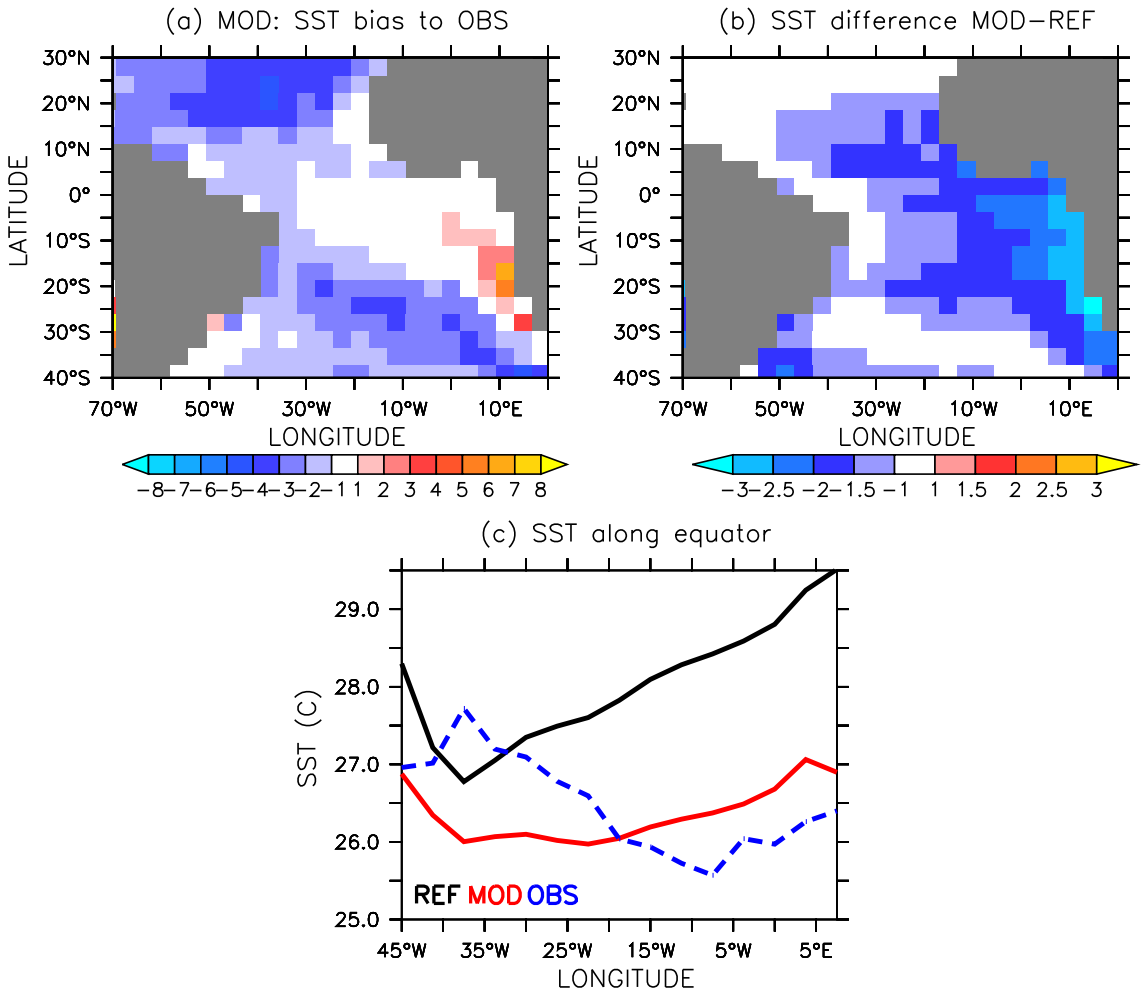

Figure 4.9: *(a) SST bias to observed SST in the MOD experiment; (b) SST difference of MOD to REF experiment; (c) SST along the equator in MOD, REF and observations.*

Tropical Atlantic (Figure 4.9).

Consistent with previous work (e.g. DeWitt, 2005, Richter and Xie, 2008) the changes in SST in boreal summer in MOD in the eastern Tropical Atlantic (i.e. the reduction of the bias) are related to changes in western Tropical Atlantic wind stress (Figure 4.11). In May, the westerly bias is reduced by up to 0.04 N/m^2. It corresponds to a change from a westerly component in REF to a weak easterly component in the zonal wind stress in the central Tropical Atlantic. The corresponding geographical distribution of the differ-

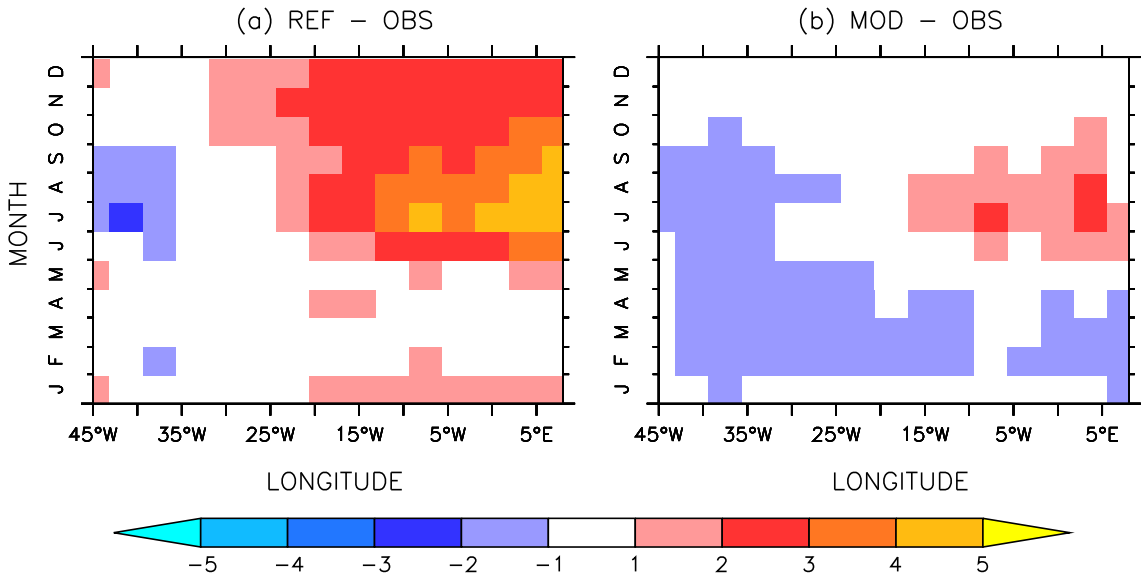

Figure 4.10: *Difference in Seasonal cycle of SST relative to observations along the equator (averaged from 2°S - 2°N) in MOD (a) and REF (b). Units are °C.*

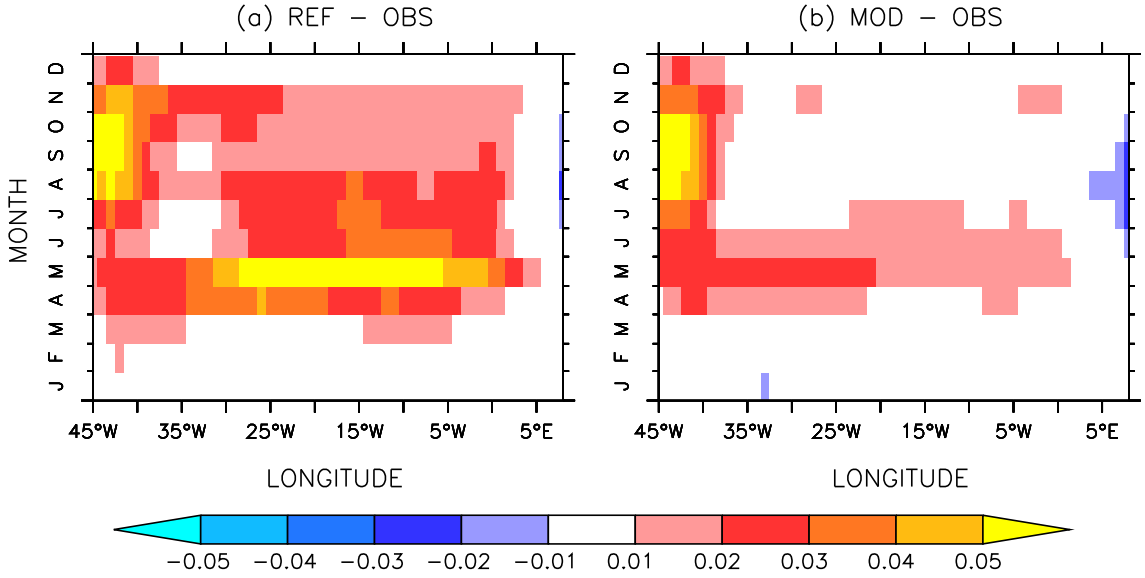

Figure 4.11: *Same as Figure 4.10 but for zonal wind stress. Units are* N/m^2.

ences between MOD and REF in the 10m wind field are shown in Figure 4.12b. It shows that the reduction in the wind bias in MOD can clearly be related to a strengthening of the southeastern trades. The strengthening of the spring easterlies is connected with increased precipitation west of 20°W peaking off the eastern coast of Brazil (Figure 4.12b). This is not in agreement with observations, which indicate deficient precipitation over northeastern Brazil as well as excessive precipitation along the equator west of 20°W in late boreal winter and spring in the MOD experiment (not shown). This indicates that the ITCZ is located too south in boreal winter and spring in the western Tropical Atlantic. Since a warm bias is not present in the MOD experiment in boreal winter and spring (and relatively small in the REF experiment, see Figure 4.2a), the southward shift might be related to the cold bias in towards the north, which favors a southward displacement of the ITCZ (Chang et al., 2007). At the same time, precipitation is reduced in the Gulf of Guinea in the MOD experiment (Figure 4.12), thus significantly reducing the large precipitation bias that is present in the REF experiment (Figure 4.2). Even though the location of the precipitation increase in the western Tropical Atlantic is not correct with respect to observations, it sets up a pressure gradient, which enhances easterly flow along the equator. These changes are consistent with an intensified Atlantic Walker circulation. Downward motion is enhanced in the east and upward motion enhanced in the western part of the Tropical Atlantic that is due to enhanced (reduced) convection in the western (eastern) Tropical Atlantic. This is confirmed by seasonally resolved differences in vertical velocity along the equator (Figure 4.13) as well as upper tropospheric zonal wind speed (not shown). Comparing absolute values of SST between MOD and REF shows that SST in the REF experiment in the eastern Tropical Atlantic is roughly 28°C or above all year round while in MOD no SSTs above 28°C can be found (not shown). According to e.g. Fu et al. (1994) a SST of 28°C is believed to be a critical value for deep convection to develop and possibly explains the reduction in convective activity over the eastern Tropical Atlantic in the MOD experiment (Figure 4.13 and Figure 4.12d). This is supported by reduced amount of high clouds (as analyzed on the 300 hPa level), which spread in the upper troposphere due to convective towers (not shown). A reduction in cloud cover in the

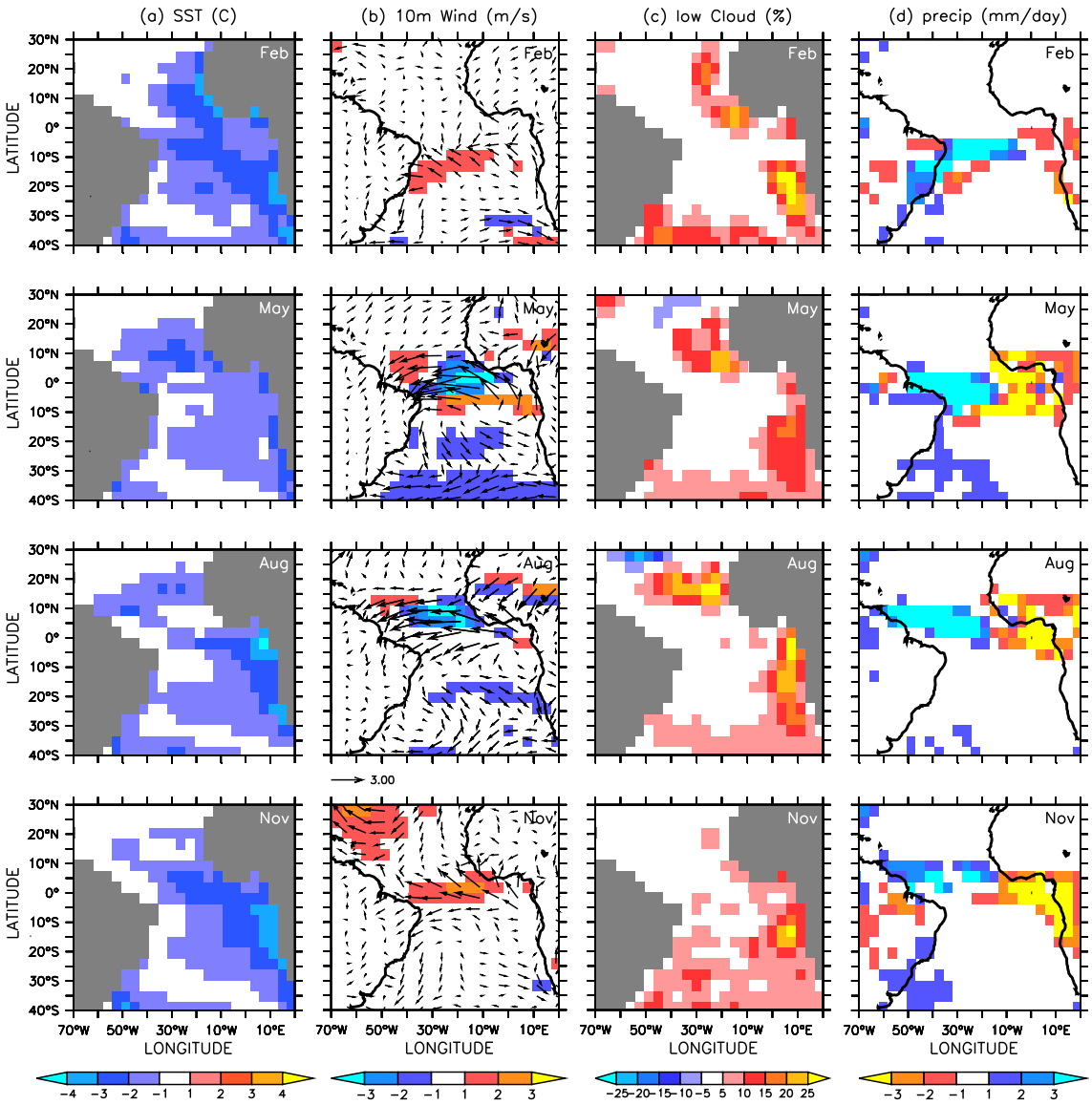

Figure 4.12: *February (top), May (second row), August (third row) and November (bottom) of SST (a), 10m Wind (b), low cloud cover (c) and precipitation (d) differences between MOD and REF in the Tropical Atlantic. Units are indicated in the headings. The shading in (b) shows the differences in absolute windspeeds calculated as* $\sqrt{(u10)^2+(v10)^2}_{MOD} - \sqrt{(u10)^2+(v10)^2}_{REF}$. *A standard array as indicated below the third Figure in column (b) corresponds to 3 m/s.*

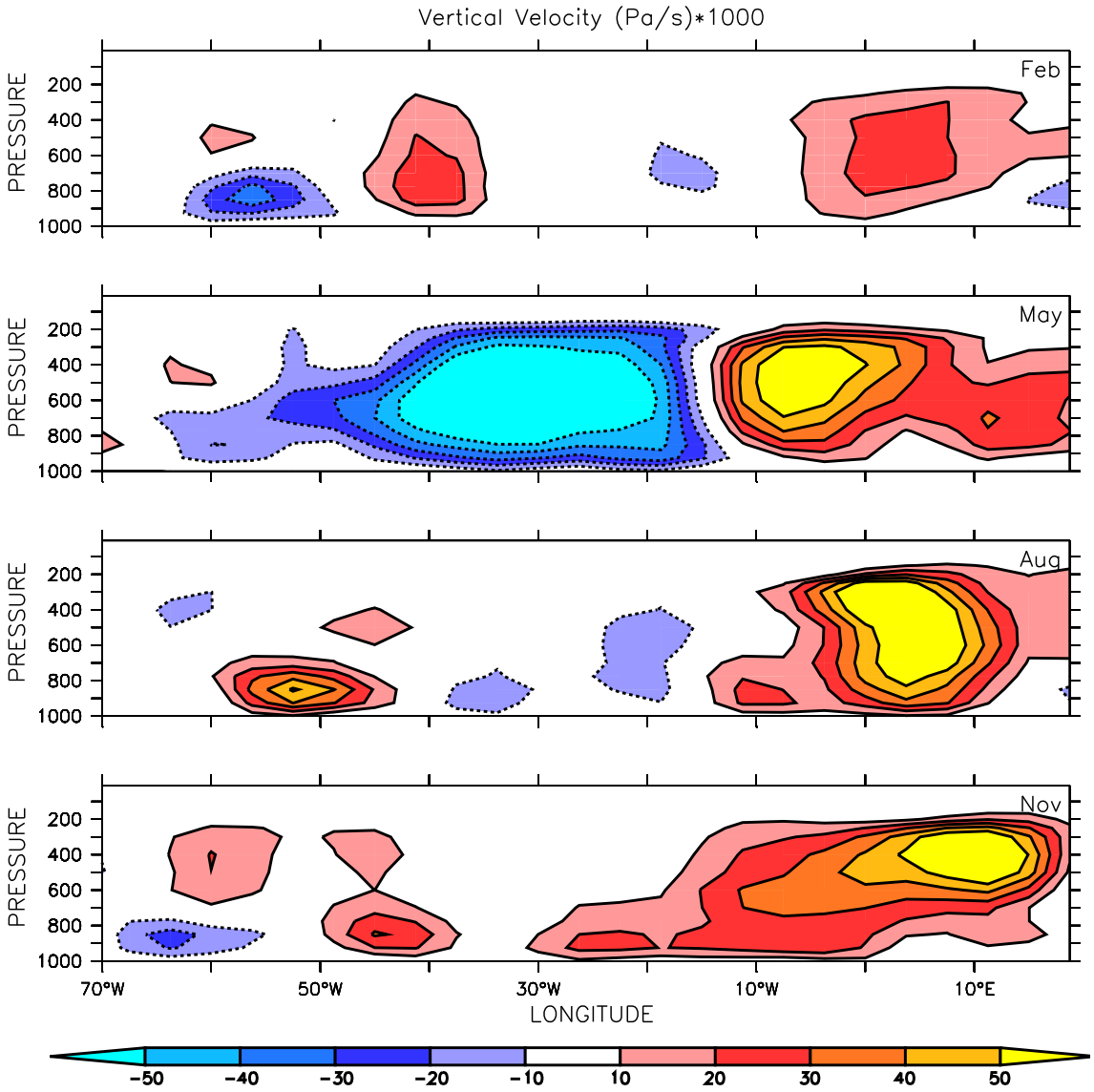

Figure 4.13: *Difference between MOD and REF in vertical velocity along the equator in February (top), May (second from top), August (third from top) and November (bottom). Positive (negative) values indicate stronger downward (upward) motion. Units are* $Pa/s \times 10^3$.

model levels in the upper troposphere as well as drying of the upper atmospheric layers increases the amount of outgoing longwave radiation (OLR, Figure 4.14) in all seasons in the eastern Tropical Atlantic via the water vapor feedback. An increased amount of OLR

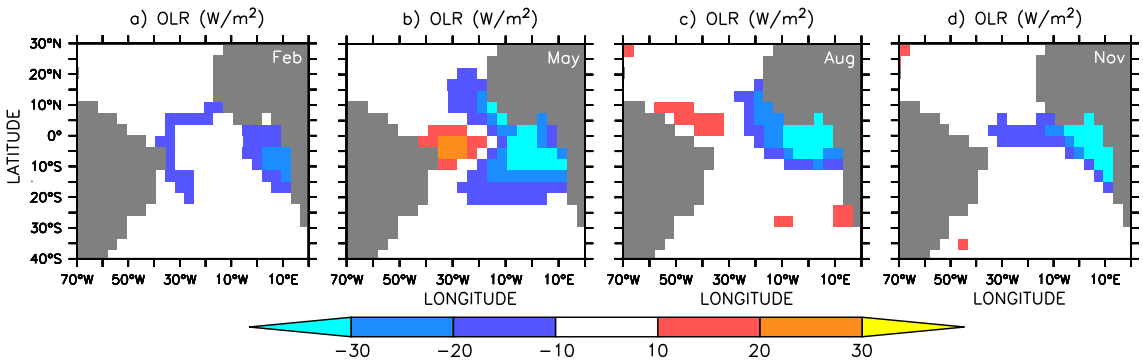

Figure 4.14: *Difference between MOD and REF in OLR at the top of the atmosphere in February (a), May (b), August (c) and November (d). Negative values indicate an increased amount of OLR.*

contributes to cooling of the atmospheric column that may indirectly contribute to SST cooling. In those areas in the Gulf of Guinea where low cloud cover does not increase (Figure 4.12c) the increased amount of OLR is balanced by more SW radiation reaching the surface. The reduced amount of OLR in the western Tropical Atlantic in May is due to increased convection (Figure 4.13), which increases upper tropospheric humidity as well as the amount of high cloud cover (not shown).

Figure 4.12c shows that an increase of low cloud cover is most pronounced further to the south between 10°S and 20°S. As stated earlier, SST and the evolution of low cloud cover are tightly coupled and exhibit a positive feedback. Low cloud cover is hence not the driver of the reduction of the SST bias but acts as an amplifier once the SST is cold enough to support the development of low clouds. This is supported by comparing low cloud cover of the uncoupled version of the reference run (REFUC) to the coupled REF experiment (not shown). The former shows significantly higher low cloud cover in the eastern and southeastern Tropical Atlantic. Even compared to the (fully coupled) MOD experiment low cloud cover is higher in the REFUC experiment. The latter is due to the fact that a small warm bias still exists in the MOD experiment.

So what drives the reduction of the eastern Atlantic SST bias in the MOD experiment? To

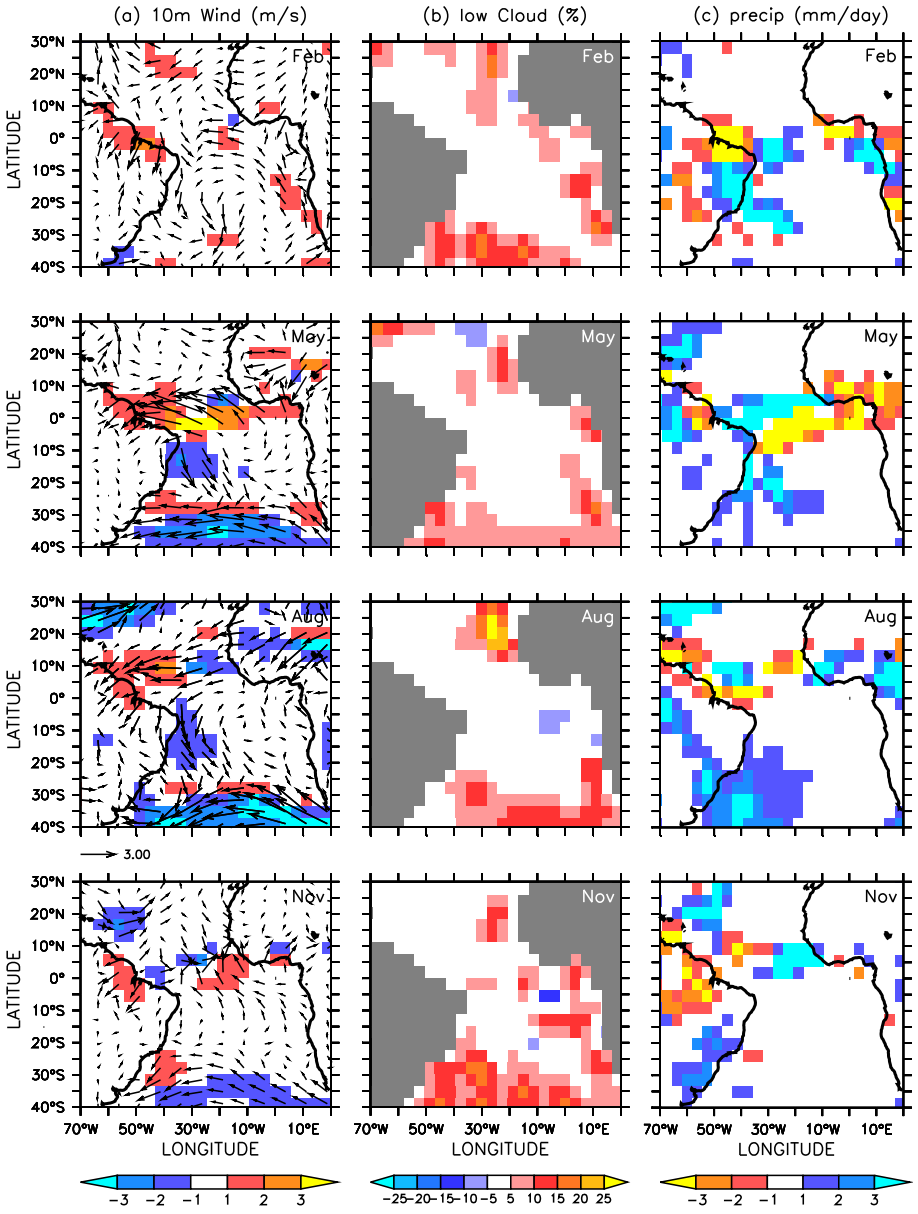

Figure 4.15: *February (top), May (second row), August (third row) and November (bottom) of 10m winds (a), low cloud cover (b) and precipitation (c) differences between MODUC and REFUC in the Tropical Atlantic.*

further understand this, wind stress, precipitation distribution and cloud cover in different levels in the REFUC as well as the MODUC experiment are analyzed (Figure 4.15). In May a strengthening of the cross-equatorial easterlies is found in the MODUC experi-

ment (Figure 4.15b). Differences in precipitation patterns between MODUC and REFUC (Figure 4.15d) indicate that this can be related to a northwestward shift of the ITCZ in the Tropical Atlantic in May. An increase in low cloud cover in MODUC relative to REFUC in the eastern and southeastern Tropical Atlantic by 10-20% is found especially from boreal fall to winter (Figure 4.15c) thus reducing the negative bias in low cloud cover (not shown). It indicates that the relation between SST and low cloud cover in the southeastern Tropical Atlantic is improved in the MODUC run with respect to the REFUC run as SSTs are the same in both uncoupled experiments. Altogether, differences in low cloud cover, zonal winds and precipitation in the Tropical Atlantic in the uncoupled runs (MODUC relative to REFUC) resemble those found for the MOD experiment with respect to the REF experiment. However, only the MOD configuration maintains the mean state which is beneficial to the reduction of the eastern Atlantic warm bias in coupled mode. Both the MODUC and REFUC run still contain errors with respect to observations in e.g. the zonal winds along the equator, but they are smaller compared to what is seen in the coupled REF experiment. This is consistent with Richter and Xie (2008) who show that uncoupled models already contain biases in the Tropical Atlantic which amplify when models are used in coupled mode.

From the comparison of the uncoupled (MODUC, REFUC) to the coupled (MOD, REF) experiments the following conclusions can be drawn: In the MODUC version of KCM the parameters which have been identified to be important for the reduction of the warm bias (spring easterlies along the equator, eastern and southeastern Atlantic low cloud cover, distribution of convection and associated precipitation patterns, etc.) show an stronger "signature" compared to the REFUC experiment, i.e. slightly stronger spring easterlies and increased low cloud cover in the eastern and southeastern Tropical Atlantic.

Nevertheless the key difference has to be in the modified treatment of surface exchange in the MOD as described in section 3. The stronger evaporation in the subtropical trade wind regions (Figure 4.16) caused by modifications in the MOD experiment can be seen as a starting point for the mechanism leading to a the reduction of the eastern Atlantic warm bias. Enhanced evaporation in the subtropics can be found in both the MOD and MODUC

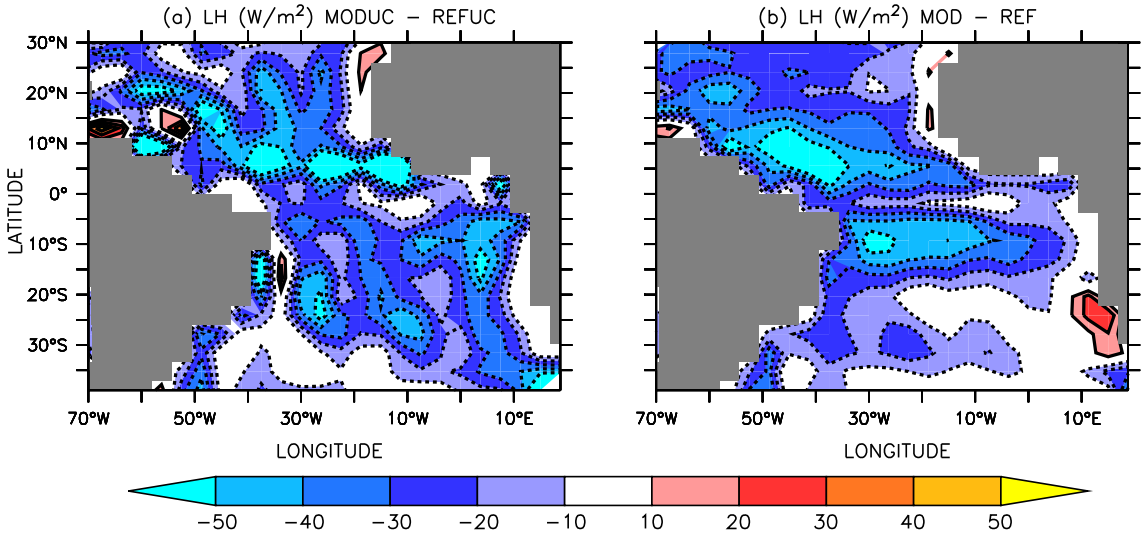

Figure 4.16: *Mean latent heat flux differences between MODUC and REFUC (a) and MOD and REF experiment (b). Negative values denote higher latent heat flux from the ocean into the atmosphere in the MOD and MODUC experiment, respectively.*

experiment compared to REF and REFUC, respectively (Figure 4.16). In the MODUC experiment, the increase of latent heat flux is more evenly distributed in the Tropical and Subtropical Atlantic with respect to the REFUC experiment (Figure 4.16a). The surface latent heat flux in the MOD experiment compared to the REF is primarily found in the western part of the Subtropics of both hemispheres. The additional availability of moisture enhances convection in the western Tropical Atlantic driving stronger easterlies along the equator in spring. This causes the thermocline to be closer to the surface (see Figure 4.18 and discussion in section 4.4.2) in the eastern Tropical Atlantic and brings colder water to the surface. The surface cooling in the eastern Tropical Atlantic reduces convection accordingly (Figure 4.12d). Together with stronger convection in the western Tropical Atlantic region this corresponds to an intensified Walker circulation along the equator in the Atlantic (Figure 4.13). Colder surface water together with suppressed convection through changes in the Walker circulation provides favorable conditions for the formation of low clouds (Figure 4.12c). Increased amount of low cloud reduces surface shortwave radiation, which further contributes to cooling of SST. This mechanism is most effective

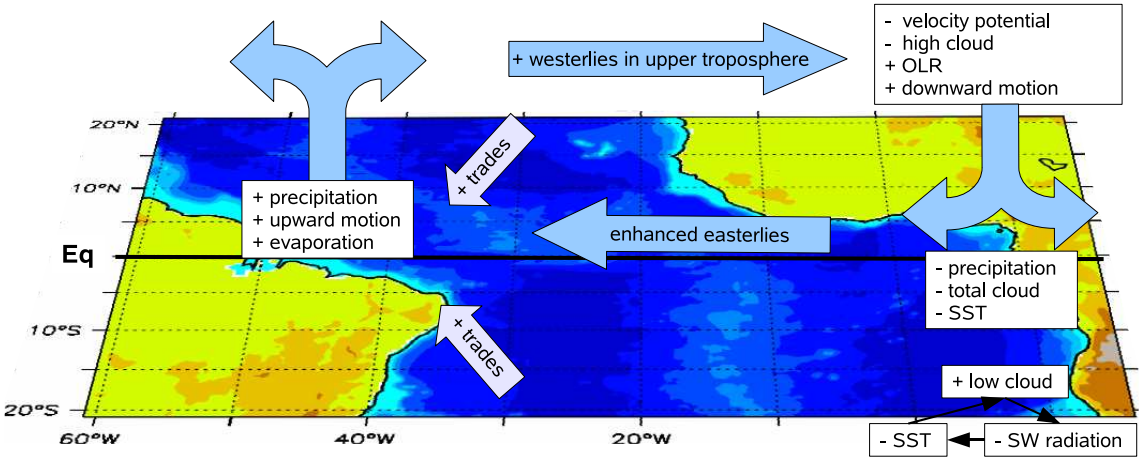

Figure 4.17: *Summary of the differences in the atmospheric circulation between the MOD and REF configuration. "+" ("-") indicates an increase (decrease) in the parameter following the "+" ("-"). Some of the parameters shown here are neither introduced nor discussed in the text (e.g. velocity potential). Nevertheless they are included in this summary.*

in the southeastern Atlantic in late summer to fall. Although reduced, a significant warm bias remains directly along the southeastern coast between approximately 25°S and 10°S in all experiments. Weaker-than-observed southerly winds along the coast (present in all experiments but only shown for the REF experiment in Figure 4.2b) that can cause too weak coastal upwelling are one possible reason. Consistently, this bias is also present in the WIND4 and WIND10 experiments since correction of the wind field is only applied between 4°S (10°S) and 4°N (10°S) in these experiments (Figure 4.6b).

To conclude this section, Figure 4.17 provides a schematic summary of the differences between the MOD and REF experiment.

4.4 Ocean response

The modifications applied in the atmospheric component (MOD experiment) or at the interface between atmosphere and ocean (WIND4, WIND10, RAD, FLX experiments) have an non-negligible impact on the ocean subsurface structure, which will be discussed in the following sections. As a reference temperature and salinity from the SODA dataset (Carton and Giese, 2008) and a forced ocean run (OCE experiment) will be used.

4.4.1 Methodology

Breugem et al. (2008) point out the importance of barrier layers as a mechanism that can have an amplifying effect on the SST bias in the eastern Tropical Atlantic. They define the top of the thermocline, or equivalently the isothermal layer depth (ILD), as the depth where the potential temperature has dropped by 0.2°C with respect to the value at 10m depth. The mixed layer depth (MLD) is defined as the depth where the potential density has increased with respect to the values at 10m by an amount that corresponds to a drop in potential temperature by 0.2°C. In mathematical form, the above definitions can be expressed as:

$$\begin{aligned} ILD &= z(\Theta_{10m} - 0.2) \\ MLD &= z(\sigma(S_{10m}, \Theta_{10m} - 0.2)) \end{aligned} \tag{4.1}$$

where Θ is the potential temperature, S is the salinity and σ the potential density computed from the 1980 UNESCO International Equation of state (IES80; Gill, 1982). If MLD and ILD differ a barrier layers is present (Breugem et al., 2008).

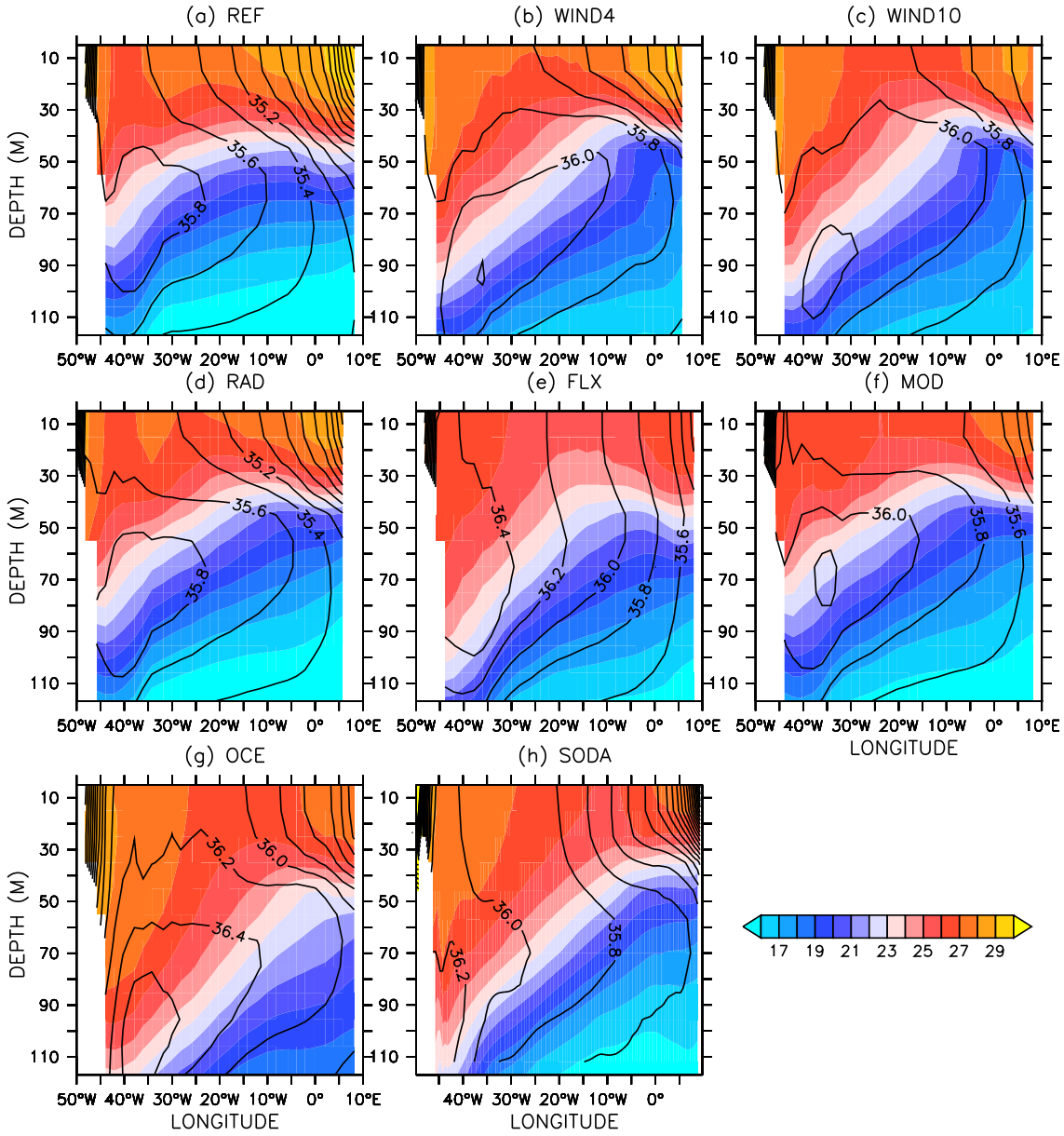

Figure 4.18: *Zonal section of SST (shading, C) and salinity (contours, psu) along the equator from REF (a), WIND4 (b), WIND10 (c), RAD (d), FLX (e), MOD (f) and OCE (g) experiment as well as the SODA dataset (h).*

4.4.2 Mean State and Seasonal Cycle

Figure 4.18 shows the 20 year mean temperature and salinity sections along the equator from the REF, WIND4, WIND10, RAD, FLX, MOD and OCE experiments as well as from SODA. The OCE experiment shows the most realistic tilt of the thermocline followed by the WIND4, WIND10, FLX and RAD experiments. For the OCE and WIND4/10 experiments this is due to realistic wind stress forcing. In the FLX experiment the westerly wind stress bias at the equator is reduced (not shown) due to the fact that an amplification of the bias due to coupling (Richter and Xie, 2008) is inhibited via the restoring towards the observed SST climatology. This results in an improved representation of the tilt of the thermocline. However, the thermocline is less sharp than in the WIND10 experiment. The RAD and MOD experiments still show a small bias in SST. Zonal winds along the equator that are improved with respect to the REF experiment, but remain too weak compared to observations. The REF experiment has the strongest bias in zonal wind stress along the equator (Figure 4.2), and almost no tilt of the thermocline is simulated (Figure 4.18a). Thus consistent with the theory of equatorial ocean dynamics, the representation of the tilt of the thermocline can hence be to first order related to the strength of the equatorial easterlies in the different experiments.
Surface salinities drop continuously towards the east and are below observed values in all levels in the upper 100m in the REF run. At the surface this is consistent with too high precipitation compared to observations over the eastern Tropical Atlantic in the REF configuration all year round. In all other configurations salinity increases with depth in the upper ocean, however, in the FLX run the increase is very weak. With respect to salinity the mixed layer is very shallow in the WIND4 experiment.

Figure 4.19 shows the seasonal development of the temperature and salinity bias with respect to the SODA dataset in various experiments. The very strong subsurface warm bias in boreal summer in the REF experiment is reduced in all other configurations of KCM. However, a subsurface cold bias in boreal winter remains in the MOD and RAD

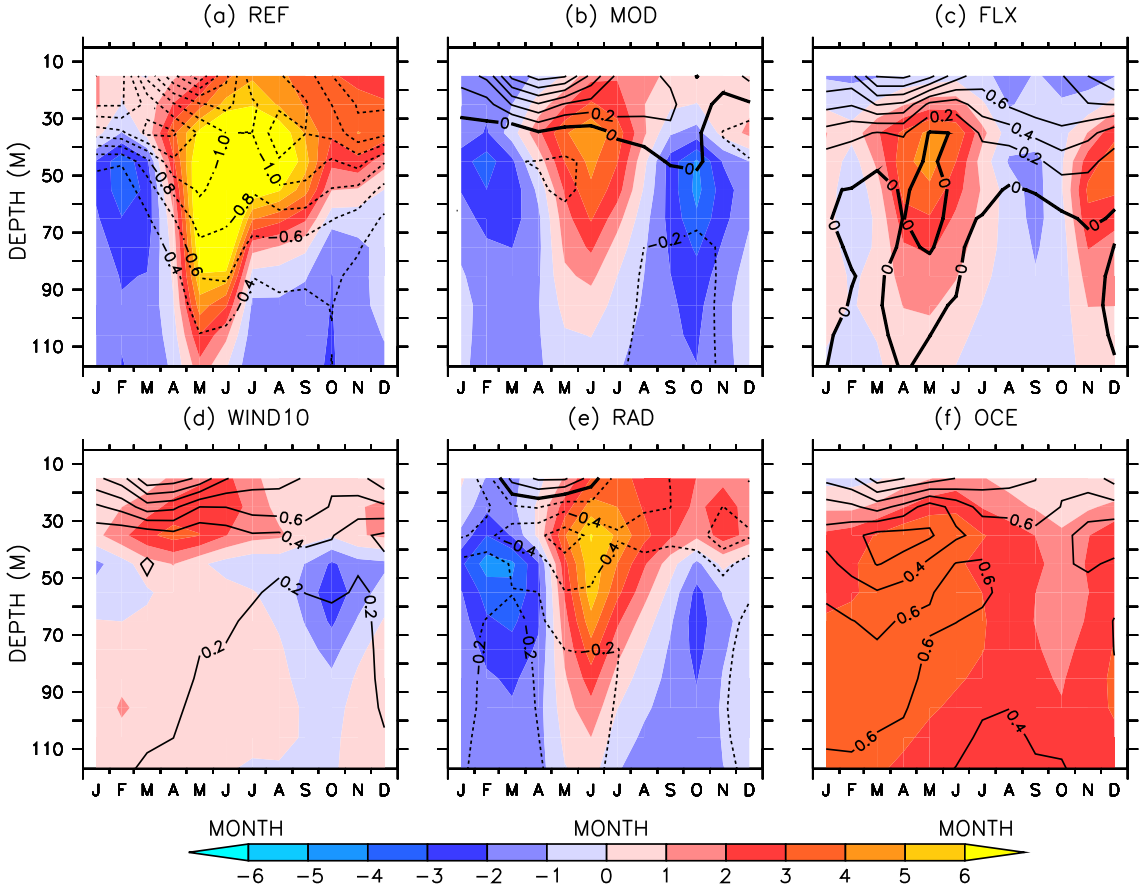

Figure 4.19: *Mean seasonal cycle of SST bias (shading, °C) and salinity bias (contours, psu) with respect to SODA in the ETA region (0°E-8°E, 2°S-2°N) in REF (a), MOD (b), FLX (c), WIND10 (d), RAD (e) and OCE (f).*

setup. Consistent with the reduction in eastern Tropical Atlantic precipitation, the pronounced negative salinity bias disappears in the WIND10, MOD and FLX experiments. The higher salinity with respect to SODA in the upper ocean layers in the WIND10, MOD and FLX experiments seems to be inherent to the ocean model as this bias is also present in the forced ocean run. The largest biases both in temperature and salinity remain in the RAD experiment. Comparing the subsurface temperature structure in the WIND10 (Figure 4.19d) to the other configurations shows that realistic wind forcing (together with the associated feedbacks such as reduction of eastern Tropical Atlantic precipitation bias due to reduction of the SST bias) seems to be a key parameter in determining a realistic

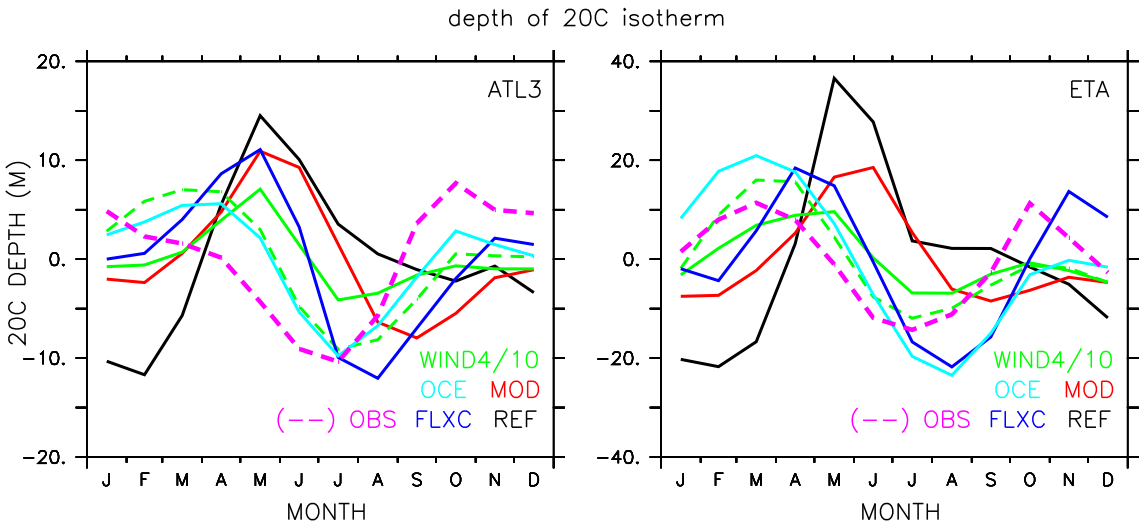

Figure 4.20: *Depth of 20°C isotherm (mean removed) for ATL3 (left) and ETA (right) for various experiments as indicated on Figure. The solid (dashed) green line denotes the WIND4 (WIND10) experiment. The pink dashed lines shows the values from SODA. Positive (negative) values indicate a deep (shallow) 20° isotherm. Please note the different scale on the y-axis.*

subsurface ocean stratification in a coupled model.

Figure 4.20 shows the mean seasonal cycle (mean removed) of the depth of the 20°C isotherm for REF, MOD, WIND4, WIND10, FLX and OCE as well as observed values in the Atlantic 3 region (ATL3, 20°W-0°, 3°S-3°N) and a box in the eastern equatorial Atlantic (ETA, 0°E-8°E, 2°S-2°N). The 20°C isotherm depth (hereafter 20C depth) in the ETA box is shown as it is the region where the largest improvement in the SST bias is simulated in the MOD experiment. As expected the best representation of the seasonal cycle in the ATL3 region is found in the OCE experiment. The strength of the seasonal cycle is well captured, especially the minimum in 20°C depth in summer. In spring the 20°C isotherm is too deep both in the ATL3 and ETA region, consistent with the general subsurface warm bias in the OCE runs compared to SODA (Figure 4.19f). In the ETA region, the uncoupled OCE run overestimates the strength of the seasonal cycle. Assuming

that the OCE experiment is the best in reproducing the mean seasonal cycle of the 20C depth, the following comparison focuses on the differences with respect to the OCE run. In the WIND4 experiment the seasonal cycle is very weak. The WIND10 experiment has a seasonal cycle in 20C depth that is nearly identical to the one found in the OCE experiment in the ATL3 region (Figure 4.20a). In the ETA box the seasonal cycle in the WIND10 experiment is weaker but has the same seasonal structure as in the OCE experiment. In both the ATL3 and the ETA region the seasonal cycle in 20C depth is weaker in the WIND4 than in the WIND10 experiment. The differences between the WIND4 and WIND10 experiments indicate the importance of off-equatorial winds on the subsurface structure. These difference have not been studied in detail.

In the REF experiment, the minimum in 20C depth in summer is not simulated properly. Nevertheless, it is interesting that a seasonal cycle in 20C depth (Figure 4.20) in REF exists, in contrast to SST, which does not have a seasonal cycle at all (not shown). Therefore the seasonal cycle in 20C depth (which is primarily forced by WTA winds) does not project onto the variations in SST. In conjunction with weaker than observed cross-equatorial winds that cause reduced upwelling, this discrepancy might be related to the positive precipitation bias in the ETA that develops in spring and persists until late fall (Figure 4.2d). As a consequence, reduced surface and subsurface salinity introduces a strong vertical salinity gradient. The combination of a negative salinity bias with a strong positive subsurface temperature bias in boreal spring and summer, and consistent with the results by Breugem et al. (2008), this leads to the formation of an erroneous barrier layer in the ETA from April to August (Figure 4.21). The presence of a barrier layer in REF possibly causes further warming of the surface layers enhancing the peak in the ETA warm bias in boreal summer (Figure 4.2a).

The representation of the seasonal cycle of the 20C depth in the MOD experiment is improved, although the 20°C isotherm is about 10m closer to the surface in the annual mean (compare Figure 4.18f and 4.18h). Both the unrealistic minimum in 20C depth boreal winter and the maximum in 20C depth in spring in REF are significantly reduced (Figure 4.20). Consistent with observations, a minimum in 20C depth in the ATL3 region (and

less pronounced in the ETA region) is found in the MOD experiment in boreal fall. Although the seasonal cycle in 20C depth is caught, it is shifted by roughly two months. The improvements just described are primarily related to improved equatorial easterlies (Figure 4.11). Reduced errors in the vertical temperature and salinity stratification (Figure 4.19) possibly contribute to reduction in the SST bias. The significant reduction of the precipitation bias in the eastern equatorial Atlantic (Figure 4.12) in the MOD experiment reduces the surface and subsurface salinity bias and prevents the formation of an erroneous barrier layer in the ETA region (Figure 4.21).

Flux corrections at the surface significantly reduce the subsurface temperature bias compared to the REF experiment in all seasons (Figure 4.18e). Compared to the WIND10 experiment, which exhibits the smallest subsurface temperature bias in all seasons, biases in 20C depth are large in the FLX experiment. Again, this indicates that realistic wind-forcing at the surface is more important for the seasonal cycle of 20C depth than correct surface fluxes.

As depicted in Figure 4.21 and consistent with the large SST and salinity bias discussed above, only the REF experiments develops a barrier layer during boreal summer. In the RAD experiment which shows the largest SST bias in boreal summer (apart from the REF experiment) no barrier layer is found in the ETA (Figure 4.21b) owing to the reduced subsurface biases in temperature and salinity (Figure 4.19e). This indicates that the impact of barrier layers on the SST bias is limited. As precipitation, surface and subsurface salinity biases as well as the errors in the trade winds across the equator form a coupled feedback (Breugem et al., 2008), it is difficult to clarify the relative importance of the erroneous barrier layers in the eastern Tropical Atlantic with the methods applied in this work. More sensitivity experiments (e.g. using freshwater flux corrections at the surface) are needed to finally quantify the relative importance of the erroneous barrier layers.

In summary it is found in accordance with the results by Breugem et al. (2008) that surface errors, specifically errors in freshwater flux in response to errors in precipitation, introduce errors in the vertical density stratification. Although the SST bias in the eastern

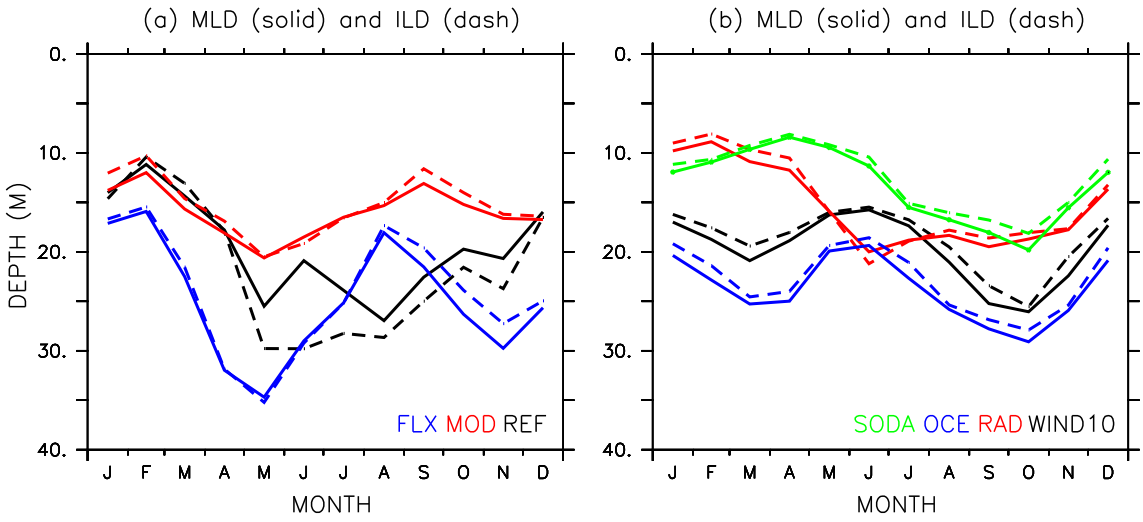

Figure 4.21: *mean seasonal cycle of MLD depth (solid lines) and ILD depth (dashed lines) averaged over the ETA box in the REF, MOD, and FLX (left) as well as WIND10, RAD, OCE experiment and from the SODA dataset (right).*

Tropical Atlantic has shown to be primarily wind forced, errors in the vertical temperature and salinity stratification possibly amplify the SST bias in the eastern Tropical Atlantic via the formation of unrealistic barrier layers. Correcting SST by implementing flux corrections does not provide a solution either as they cause a weaker-than-observed salinity stratification in the model, and significant subsurface temperature biases remain.

5 Variability in the Tropical Atlantic: Sensitivity to model biases

5.1 Experimental Setup

In this chapter the variability, which occurs on top of the seasonal cycle, shall be discussed. Table 5.1 lists the configurations of KCM which have been used to study equatorial Atlantic variability. The REF, MOD and FLX configuration have already been introduced in section 3.2. In the FLX experiment, the errors in the mean annual cycle of SST in the Tropics are removed by means of flux corrections (chapter 3.2). Although flux corrections are not much used anymore in current coupled climate models (Randall et al., 2007), they provide useful information how errors in the mean seasonal cycle of SST possibly affect the variability of SST on interannual to decadal timescales. As shown in the previous chapter, errors in the mean seasonal cycle of the equatorial wind field in the Atlantic are the major source of error of the SST bias there. Therefore, an additional experiment has been set up, which corrects the error in the mean seasonal cycle of the equatorial Atlantic wind field without inhibiting the evolution of interannual variability. This procedure is commonly termed anomaly coupling. The wind anomaly experiment (Wano experiment) uses anomaly coupling with respect to zonal (τ_x) and meridional (τ_y)

Exp. ID	Years	Modifications with respect to REF experiment:
REF	120	REF experiment, see Park et al. (2009).
MOD	120	modified parameters as described in section 3.
FLX	120	flux-corrected (global, 40°S - 40°N) version of KCM.
Wano	50	Anomaly coupling for u-/v-stress between 10°S and 10°N in the Atlantic.

Table 5.1: *Configurations of KCM used to study Atlantic variability.*

wind stress in the Tropical Atlantic between 10°S and 10°N:

$$\tau_x = \tau_x - (\overline{\tau}_{x,REF} - \overline{\tau}_{x,obs}) \equiv \overline{\tau}_{x,obs} + \tau'_{x,REF} \tag{5.1}$$

$$\tau_y = \tau_y - (\overline{\tau}_{y,REF} - \overline{\tau}_{y,obs}) \equiv \overline{\tau}_{y,obs} + \tau'_{y,REF}. \tag{5.2}$$

Values with an overbar denote climatological values from the REF ($\overline{\tau}_{x,REF}$, $\overline{\tau}_{y,REF}$) and NCEP ($\overline{\tau}_{x,obs}$,$\overline{\tau}_{y,obs}$), respectively. $\tau'_{x,REF}$ and $\tau'_{y,REF}$ are the zonal and meridional wind anomalies in the model, respectively. This method ensures that a correct climatology is present in the model without inhibiting variability. The correction terms $\overline{\tau}_x - \overline{\tau}_{x,obs}$ and $\overline{\tau}_y - \overline{\tau}_{y,obs}$ are calculated using the difference between a NCEP climatology from 1950-2004 for zonal and meridional wind stress and a 20 year climatology calculated from the REF experiment.

Figure 5.1 *(facing page)*: *SST anomalies along the equator (averaged from 3°S-3°N) for a 20y period for the REF (a), MOD (b), FLX run (c) and Wano (d) experiment as well as observations (e). Contour lines indicate zonal wind anomalies (contour interval 1 m/s except (e) where an additional contour line at -0.5 m/s and 0.5 m/s is drawn). For (a)-(d) the last 20 years of each experiment are taken; for (e) year 1980 to 1999 are shown.*

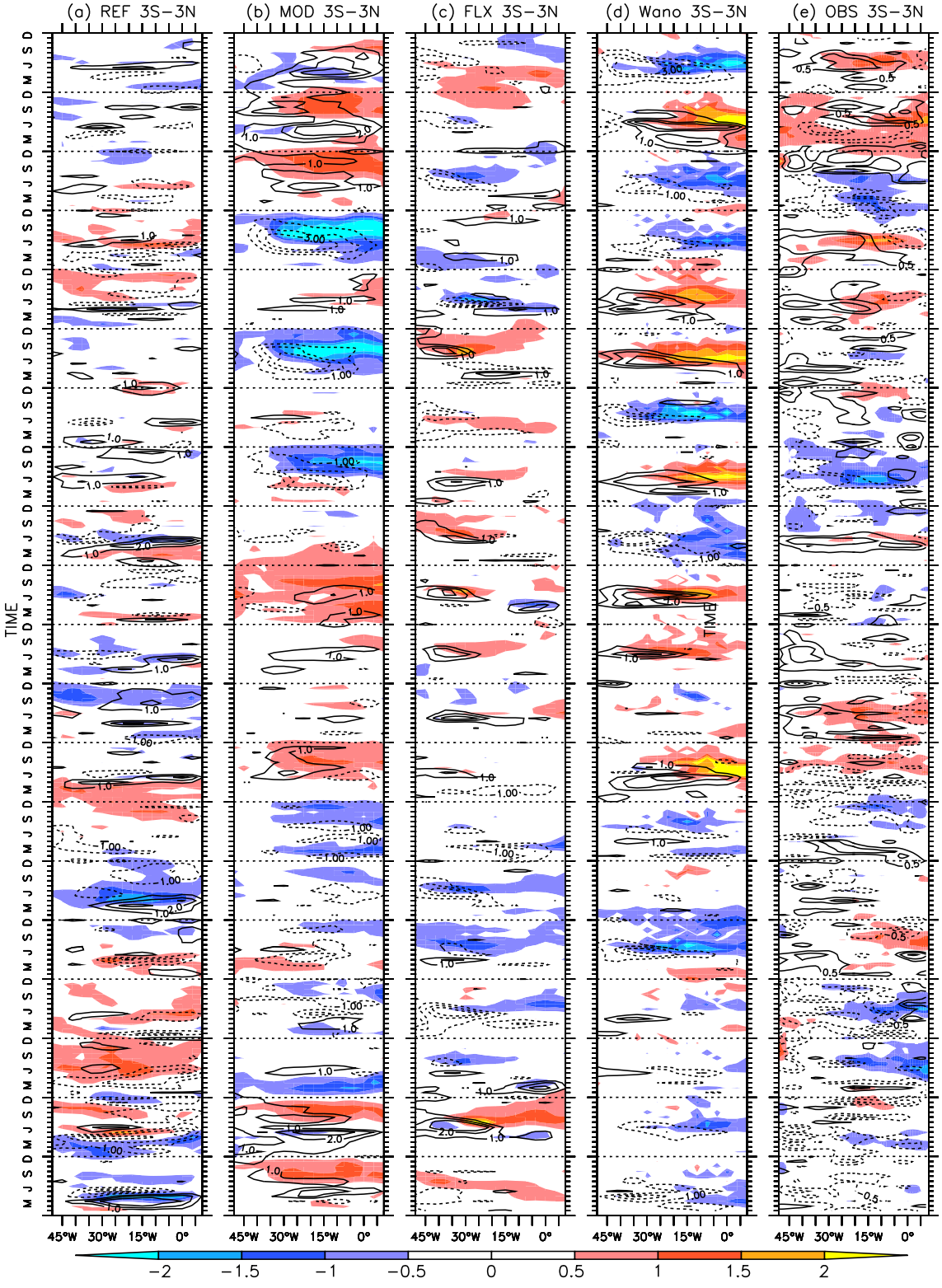
(a) REF 3S–3N
(b) MOD 3S–3N
(c) FLX 3S–3N
(d) Wano 3S–3N
(e) OBS 3S–3N
TIME
J F M A M J J A S O N D J F M A M J J A S O N D J F M A M J J A S O N D J F M A M J J A S O N D J F M A M J J A S O N D
45°W 30°W 15°W 0°
−2 −1.5 −1 −0.5 0 0.5 1 1.5 2

5.2 Results and Discussion

Numerous studies summarized in section 2.2 have shown significant SST variability on different timescales to be present in the Tropical Atlantic. In this section the discussion focuses on the Bjerknes feedback, which has shown to be present in the equatorial Atlantic (Keenlyside and Latif, 2007) in observations, and how its representation in the model depends on the mean state.

Figure 5.1 shows 20 year long examples of the zonal distribution of the SST anomalies along the equator of the REF, MOD, FLX and Wano experiment as well as a 20 year period from observations. Monthly resolved standard deviations of ATL3 SST anomalies are shown in Figure 5.2. In the REF experiment SST anomalies in the eastern part of the equatorial Atlantic are weak, and the largest SST anomalies are found in the central and western equatorial Atlantic. This is not in agreement with observations, which show the largest SST anomalies in the eastern equatorial Atlantic. In the ATL3 region an unrealistic peak in SST variability occurs in May, and the maximum in SST variability centered about boreal summer is too broad. The MOD version of KCM shows an, with respect to observations, improved zonal structure of the SST anomalies along the equator, but the peak in SST variability is shifted towards fall by two months (Figure 5.2). The zonal distribution of SST anomalies in the FLX experiment indicates that too much variability is present in the western equatorial Atlantic. However, SST variability is well represented in the ATL3 region (Figure 5.2). The zonal structure of SST variability along the equator is improved in the Wano experiment, but SST variability is too strong compared to observations and too much phase-locked to the annual cycle.

In observations, cold SST anomalies are preceded by negative (i.e. easterly) anomalies in zonal wind that occur in the central and western equatorial Atlantic. They cause stronger equatorial upwelling and colder water reaches the surface. This relation is captured in the MOD, FLX and Wano experiment but not in the REF experiment. This is most likely related to the large biases in the mean wind field as shown later.

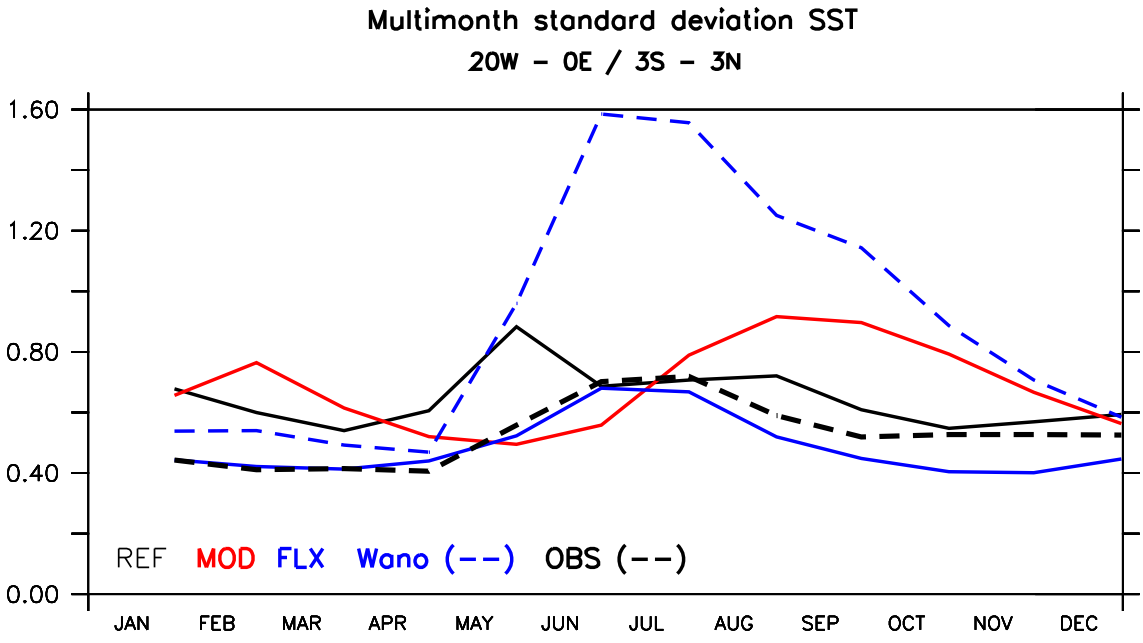

Figure 5.2: *Seasonally resolved standard deviation of ATL3 SST in the experiments indicated on the figure.*

In addition to local interaction among cross-equatorial winds and upwelling the interaction between wind, SST and subsurface structure known as the Bjerknes feedback mechanism significantly contributes to eastern Tropical Atlantic variability (Keenlyside and Latif, 2007). Before comparing the model results to observed values, the difference amongst observed values and a forced ocean run in the three components that form the Bjerknes feedback mechanism are evaluated (Figure 5.3). The regression of ATL3 SST anomalies onto equatorial Atlantic zonal wind stress anomalies indicates a stronger sensitivity of western equatorial Atlantic wind stress variability to SST anomalies in the ATL3 region when using only the last 25 years of the SODA dataset instead of the complete dataset (44 years). This might be related to the large uncertainty in long-term observational datasets in the Tropical Atlantic; a fact already noted by e.g. Stockdale et al. (2006). The significant improvement in data coverage in Tropical Atlantic observations at the end of the 1970s due to the begin of the satellite era might also play a role (e.g Bengtsson et al.,

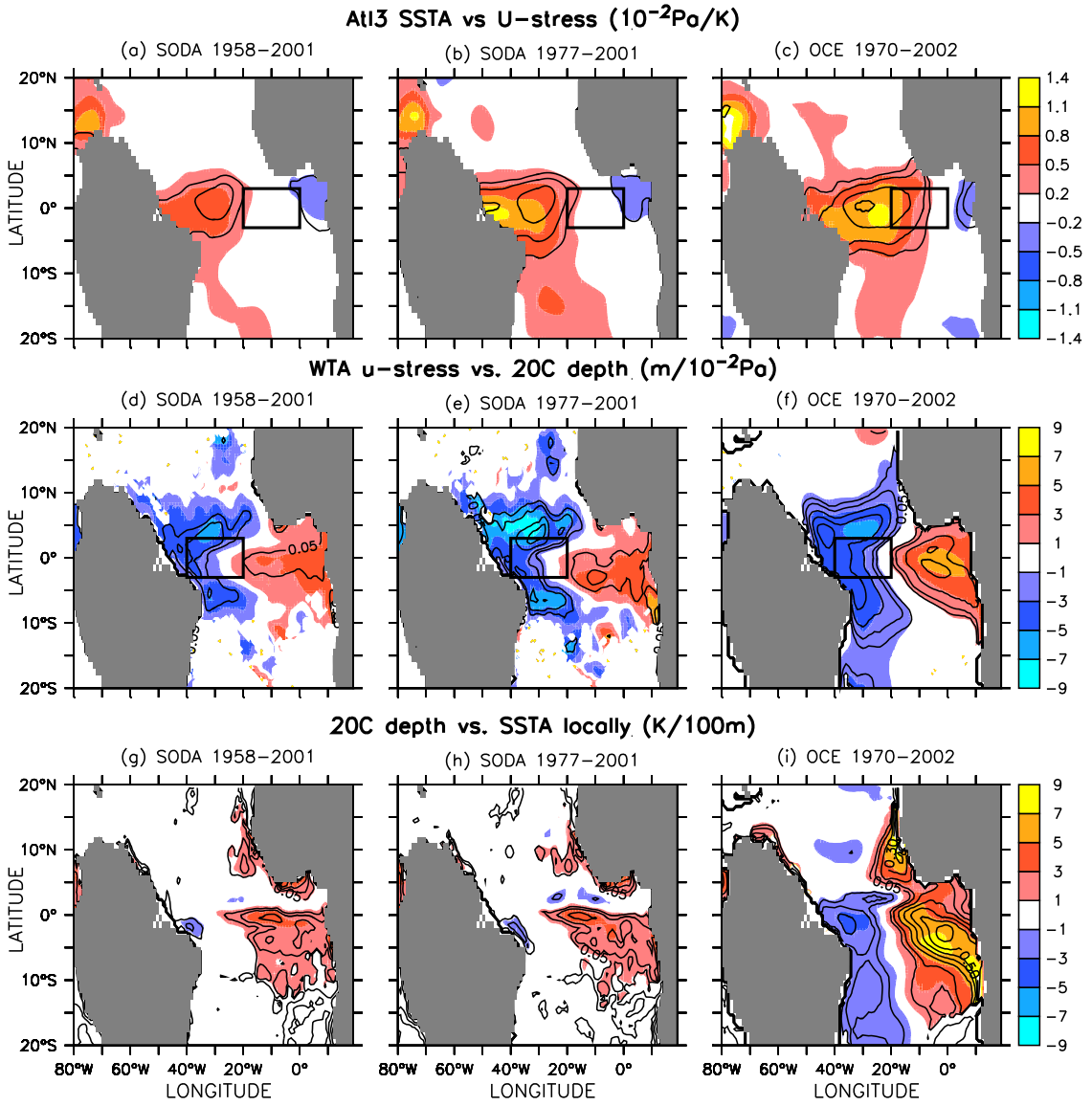

Figure 5.3: *The three components of the Bjerknes feedback in the Atlantic. Upper row: regression of ATL3 SST anomalies on zonal wind stress anomalies from SODA (a,b) and the forced ocean run (c). Center row: regression of WTA zonal wind stress anomalies onto 20C depth from SODA (d,e) and the forced ocean run (f). Bottom row: regression of 20C depth anomalies on to SST anomalies locally; figures (g) and (h) are from SODA and (i) from the forced ocean run. Explained variance is overlayed on all figures with contour levels at 0.05, 0.1, 0.2, ...*

2004). Decadal fluctuations in the meridional mode (e.g. Tourre et al., 1999) and hence the ITCZ position may also influence the strength of the feedbacks along the equator. This may also explain the differences in the strength of the Bjerknes feedback in the equatorial Atlantic between the different time periods considered here. The same regression calculated from the forced ocean run for the period 1970-2002 is shown in Figure 5.3c. A similar regression calculated from a uncoupled ocean run with the Max-Planck Institute for Meteorology ocean model (MPIOM, Marsland et al., 2003) forced with NCEP winds shows regression values that are slightly weaker (and less explained variance) than those found in the OCE experiment. This shows that the changes in western equatorial Atlantic wind stress associated with changes in ATL3 SST might be too strong in the OCE experiment (Jansen et al. (2009)).

The relation between western Atlantic wind stress variability and variability in eastern Atlantic 20C depth (Figure 5.3d-f) is weaker (in both observational periods considered) compared to that of the forced ocean model. In the latter up to 30% of the total variance in 20C depth can be explained by WTA zonal wind stress variability, and an increase in the WTA easterly wind stress by 0.01 N/m^2 corresponds to more than 5m rise in eastern Tropical Atlantic 20C depth. These values agree well with results from a similar analysis performed with data from the MPIOM by Jansen et al. (2009).

The last component of the Bjerknes feedback describes the relation between subsurface variability and SST variability. Comparing Figure 5.3g and 5.3h with 5.3i shows that the SST response to variations in 20C depth is roughly twice as strong in the forced ocean run compared to the SODA estimates. Explained variability exceeds 50% in the OCE run compared to 10-20% in the SODA results. This indicates that surface temperature in the ocean model is very sensitive to subsurface perturbations.

In summary the Bjerknes feedback mechanism is stronger in the forced ocean experiment and explains more variability than the SODA dataset suggests, but broadly agrees with other forced model results (Keenlyside and Latif, 2007, Jansen et al., 2009).

The three components of the Bjerknes feedback for the REF, MOD and FLX experi-

ment are shown in Figure 5.4. The response of zonal wind stress anomalies in the western Tropical Atlantic to ATL3 SST anomalies in the REF experiment is very weak with little explained variance. In the eastern Tropical Atlantic a negative relation between SST and zonal wind stress is found, meaning that weakened easterlies (or strengthened westerlies as the zonal wind component is positive when blowing towards the east) go along with reduced SST. An unrealistic thermodynamic feedback between local SST and zonal wind stress develops due to fact that the third step of the Bjerknes feedback (relation between subsurface temperature variations and SST, see below) is not present in the REF experiment. This is in disagreement to what is expected from previous work (Keenlyside and Latif, 2007) and observations (Figure 5.3). A very strong response to ATL3 SST anomalies in zonal wind stress in the western Tropical Atlantic is found in the FLX experiment, but explained variance is low. Only in the MOD experiment a response is found where both explained variance and strength of the feedback reasonably compare well with observed and forced model results.

The influence of western Tropical Atlantic zonal wind stress anomalies onto 20C depth anomalies is depicted in Figure 5.4d-f. Positive values indicate a shoaling of the thermocline due to increased easterlies in the WTA. Explained variance exceeds 20% of the total variance in the REF and FLX experiment in the ATL3 region and reaches up to 50% in the MOD experiment. The latter also shows the strongest response in 20C depth variations in the eastern equatorial Atlantic due to WTA wind variations. Negative correlations between WTA wind anomalies and 20C depth variations in the western equatorial Atlantic that compare reasonably to the range suggested by observations are found in in the FLX and MOD experiments.

The impact of 20C depth variations onto SST anomalies in the eastern Tropical Atlantic is best captured in the MOD and FLX experiment (Figure 5.4g-i). Compared to the values from the SODA data (Figure 5.3h) the feedback is too strong and explains too much variance. The strong relation between 20C depth and SST seems to be inherent to the ocean model as it is already found in the uncoupled ocean run (Figure 5.3i). The patterns found for the REF experiment are the least comparable with those suggested by the forced run

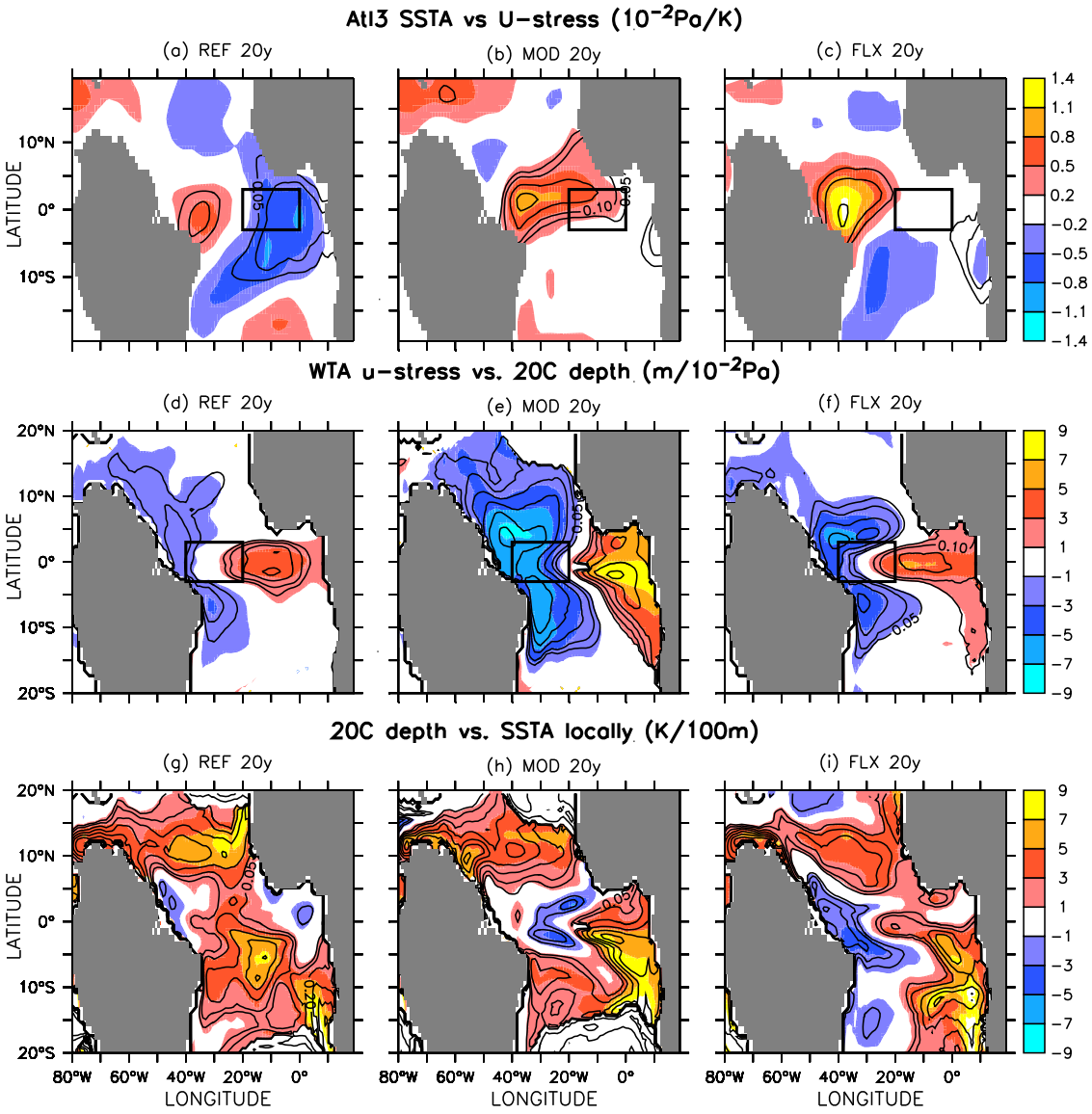

Figure 5.4: *The three components of the Bjerknes feedback in the Atlantic from different configurations of KCM. Upper row: regression of ATL3 SST anomalies on zonal wind stress anomalies from REF (a), MOD (b) and FLX (c). Center row: regression of WTA zonal wind stress anomalies onto 20C depth from REF (d), MOD (e) and FLX (f). Bottom row: regression of 20C depth anomalies on to SST anomalies locally from REF (a), MOD (b) and FLX (c). Explained variance is overlayed on all figures with contour levels at 0.05, 0.1, 0.2, ...*

and the observed patterns.

The discussion of the Bjerknes feedback in the Tropical Atlantic would be incomplete without shortly discussing the variability in the Wano experiment (anomaly coupling with respect to zonal and meridional wind stress in the Tropical Atlantic, see Table 3.1). As shown in Figure 5.2, ATL3 SST variability is at least twice as large as in the other experiments during boreal summer. A significant part of the large variability during boreal summer is related to an overly strong Bjerknes feedback mechanism (Figure 5.5a-c). Figure 5.5 shows that the regression patterns are similar to those found in the MOD and FLX. However, the strength of the Bjerknes feedback as well as explained variance is overestimated in every step of the Bjerknes feedback in the Wano experiment. Wind anomaly coupling hence causes too large sensitivity to SST and zonal wind perturbations in the model.

Summarizing the four model configurations it is found that the MOD and FLX experiment have the most realistic representation of the individual components of the Bjerknes feedback compared to the forced ocean model and the observed values. Improving the representation of the mean annual cycle in SST is hence essential for a realistic representation of important feedback mechanisms in the Tropical Atlantic such as the Bjerknes feedback. Nevertheless, both the MOD and FLX configuration seem to overestimate the strength of the Bjerknes feedback as seen in large explained variances in the individual components of the Bjerknes feedback mechanism. An important point here is that the overestimation of the strength of individual steps of the Bjerknes feedback is already found in the ocean-only run (Figure 5.3c,f,i). To further improve the representation of equatorial Atlantic variability, errors in the ocean model need to be considered further (e.g. Hazeleger and Haarsma, 2005).

In the REF experiment the strong bias inhibits correct variability in the eastern Tropical Atlantic. Although a positive relation between ATL3 SST anomalies and western equatorial Atlantic zonal wind stress anomalies is found in the REF experiment, an unrealistic negative relation between ATL3 SST anomalies and zonal wind stress in the eastern

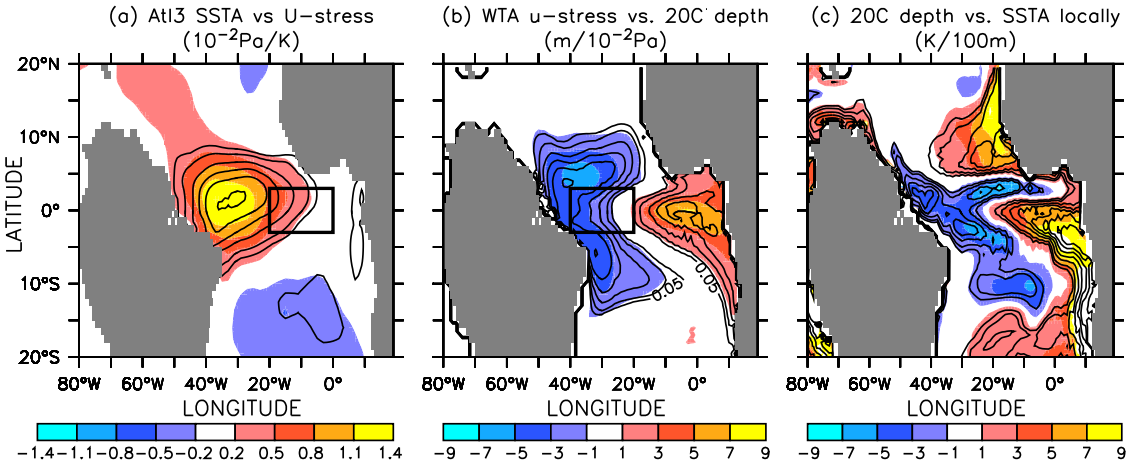

Figure 5.5: *The three components of the Bjerknes feedback in the Atlantic in the Wano experiment: regression of ATL3 SST anomalies on zonal wind stress anomalies (a), regression of WTA zonal wind stress anomalies onto 20C depth (b) and regression of 20C depth anomalies on to SST anomalies locally (c); Explained variance is overlayed on all figures with contour levels at 0.05, 0.1, 0.2, ...*

equatorial Atlantic occurs. The second component of the Bjerknes feedback mechanism is present in the REF experiment (Figure 5.4d), but is weaker than in the FLX and MOD configuration. The third component of the Bjerknes feedback mechanism, which describes the local relationship between thermocline depth and SST variations in the eastern equatorial Atlantic, shows the largest errors in the REF experiment (Figure 5.4g). Variability in thermocline depth therefore does not influence SST variability in the eastern equatorial Atlantic. This is due to the fact that winds in the eastern equatorial Atlantic contain a westerly component in all seasons in the REF experiment (Figure 4.2). The zonal wind bias inhibits upwelling, and hence the entrainment of colder subsurface water in the surface layers is suppressed. Consequently, variability in 20C depth and SST are not correlated. Additionally, erroneous barrier layers that occur during boreal summer in the eastern Tropical Atlantic in the REF experiment (section 4.4) suppress entrainment cooling of the ocean surface mixed layer (Breugem et al., 2008). The unrealistic barrier layers in the mean state of the REF experiment, which form due to the large biases in the

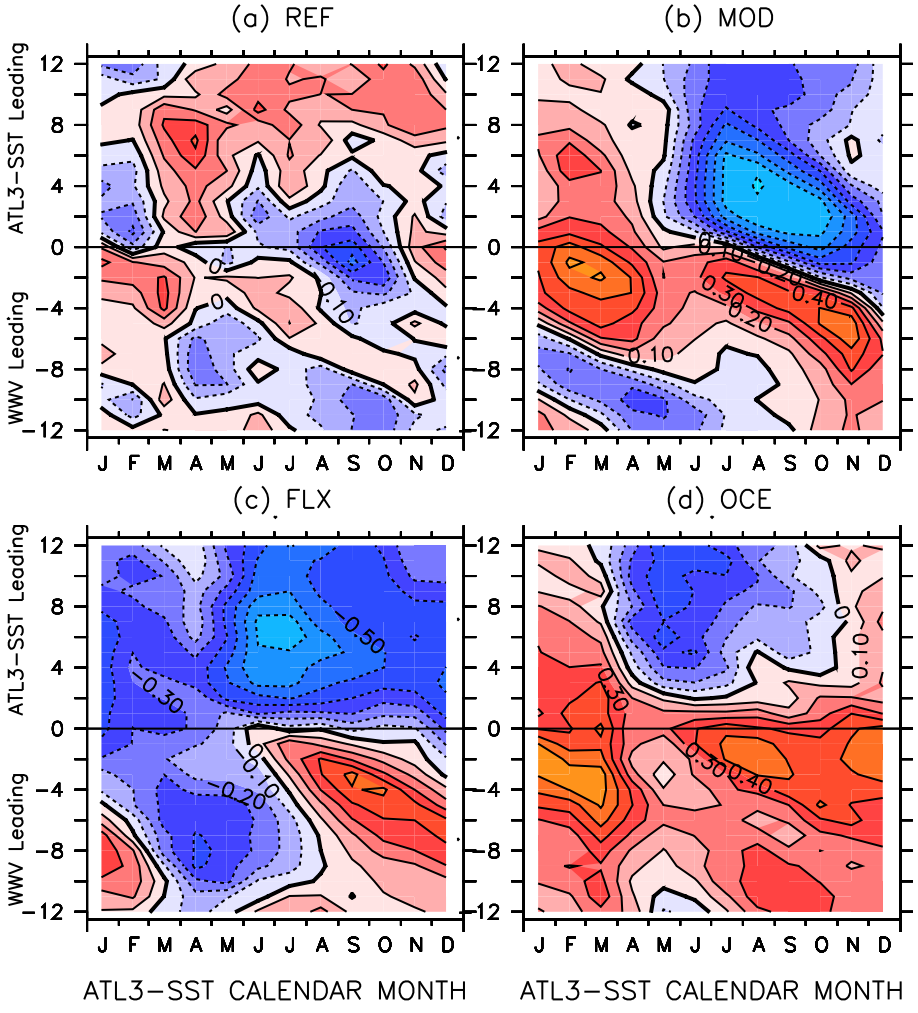

Figure 5.6: *Seasonally resolved cross-correlations between ATL3 SST and Atlantic WWV in the REF (a), MOD (b) FLX (c) and OCE (d) experiment.*

atmosphere, possibly contribute to the disruption of the Bjerknes feedback in the Tropical Atlantic and the weak variability in the eastern equatorial Atlantic in boreal summer.

Based on the results of a forced model and the SODA dataset, Jansen et al. (2009) show that a delayed feedback between the equatorial Atlantic warm water volume (WWV; following Meinen and McPhaden, 2000, Jansen et al., 2009 define the Atlantic equatorial warm water volume as the volume of water warmer than 20°C between 5°S and 5°N in that basin) and ATL3 SST is present. However, Jansen et al. (2009) find that the feedback

is weaker than in the Pacific.

The relationship between WWV and ATL3 for the REF, MOD, FLX and the OCE configuration is shown in Figure 5.6, which shows the seasonally resolved cross correlations between WWV and ATL3 SST anomalies. The overall pattern in the forced ocean run (Figure 5.6d) is in good agreement with the results by Jansen et al. (2009). WWV leads ATL3 SST anomalies by 2 to 6 months, and the strongest correlations occur at 2 to 4 month lead time in boreal winter and summer.

No correlation between WWV and ATL3 SST anomalies is found in the REF experiment. This is consistent with the results from the analysis of the Bjerknes feedback, which do not indicate an impact of thermocline variations onto eastern equatorial Atlantic SST. In the MOD experiment the 2 to 6 month lead of WWV anomalies with respect to ATL3 SST anomalies as well as the seasonally varying strength of the crosscorrelation is well represented. However, the negative correlation when ATL3 SST anomalies lead WWV anomalies are too strong. In the FLX configuration a positive correlation of WWV and ATL3 SST anomalies is only found from boreal summer to fall.

Meridional mode variability as well as equatorial variability on longer timescales in the various KCM setups are not discussed, although a preliminary analysis of EOF patterns of SST indicate that the improvement of the mean state in the MOD experiment results in an improved representation of both variability modes (not shown). Further work and possibly more sophisticated analysis methods such as a joint singular value decomposition to analyze Tropical Atlantic variability (Chang et al., 1997) are necessary to provide a better understanding of the variability modes in the different experiments in the Tropical Atlantic.

Overall, the improvement of the mean state in the Tropical Atlantic results in a better representation of the Bjerknes feedback in the equatorial Atlantic. However, if realistic (OCE and Wano experiment) or improved (MOD experiment) wind stress forces the ocean model, the Bjerknes feedback seems to be stronger compared to the SODA dataset. Especially the large variations of eastern Tropical Atlantic SST associated with thermo-

cline variations (third step of the Bjerknes feedback) in the same region may indicate that vertical mixing in the ocean model is too strong compared to observations.
Whether this improved representation of variability affects (potential) predictability shall be discussed in the following chapter.

6 Predictability in the Tropical Atlantic

6.1 Potential Predictability

As stated already in the introductory part of this work, the study of (potential) predictability of SST variability on seasonal timescales in a coupled general circulation model in the equatorial Atlantic has so far been refrained from due to the presence of the large SST bias.

In general, the potential predictability or "perfect model" approach has widely been used on monthly to seasonal timescales. Older methods include the estimation of the random variance calculated from daily data in relation to the seasonal variance (e.g. Madden, 1976, Zwiers, 1987) or the comparison of two GCM runs with climatological and interannual varying SSTs, respectively (e.g. Lau, 1985). A more detailed summary of those methods can be found in Rowell (1998). From the mid 1990s onward, ensemble of simulations, in which the individual ensemble members usually differ in the atmospheric initial conditions, are generally used to study potential predictability of different parameters (e.g. Kumar and Hoerling, 1995, Harzallah and Sadourny, 1995, Rowell et al., 1995, Boer, 2000). Although different in detail, the methods used to assess potential predictability generally relate the variability amongst the ensemble members to the internal

variability in the model itself. If the variability amongst the ensemble members is small compared to the natural variability, potential predictability is believed to be present. The simple method to evaluate potential predictability used in this work follows this idea and will be described in the following section.

6.1.1 Experimental setup and analysis method

The basis for the forecast runs are the REF, MOD and FLX control runs, whose setup, mean state and variability has been discussed in the previous sections. To analyze potential predictability in the equatorial Atlantic a set of ensemble experiments has been performed. From year 25 to 120 of REF and MOD control run four (initially perturbed) ensemble members were started every 5 years on January 1st, April 1st, Jun 1st and Oct 1st (i.e. four in Jan/Apr/Jun/Oct 1st, 0025, four in Jan/Apr/Jun/Oct 1st, 0030, etc until year 0120), which adds up to a total of 320 experiments for REF and MOD, respectively. Forecast length for each ensemble member is six month. A smaller set of experiments (same setup as above but only from year 0015 to 0050) has been performed with the flux-corrected version of KCM (FLX), which certainly limits the comparability with the runs using the REF and MOD configuration. The set of experiments based on the FLX version of KCM thus only consists of 208 experiments (13 years with 4 ensemble members per season). The four ensemble members only differ in their atmospheric initial states. Technically the perturbations are introduced by using atmospheric restart files from the two previous and two following month with respect to the actual start date. Additionally the unperturbed reference run is included in the analysis. Therefore five ensemble members in total are available. A limitation of this setup is the rather strong initial perturbations compared to what is used in other forecast studies (e.g. Saha et al., 2006) to initialize seasonal forecasts. As shown below, the use of an atmospheric state of the months preceding (following) the initialization month of the forecast introduces large spread in the first month following the initialization.

Following earlier studies on potential predictability (see above), the perfect model predictability in KCM has been assessed by calculating the mean ensemble spread of the ensemble members (including the reference run itself) x_j with respect to the ensemble mean y_i (time indices on all variables are omitted for clarity):

$$ES = \frac{1}{N}\sum_{i=1}^{N}\sqrt{\frac{1}{M-1}\sum_{j=1}^{M}(x_j - y_i)}. \tag{6.1}$$

N denotes the total number of forecasts started in January, April, July and October, respectively (REF, MOD: year 15, 20,...,120, i.e. N=20; FLX: year 15,20,...,50, i.e. N=13). M gives the number of ensemble members used per forecast (M=5). The ensemble mean consists of the four perturbed runs and the reference run itself. Additionally, the ensemble spread has been calculated by replacing the ensemble mean in equation 6.1 with the value from the reference run instead of the ensemble mean which yielded similar results as using the definition in equation 6.1. Since natural variability is not constant throughout the year, a scaled quantity is additionally used which relates the spread amongst the ensemble members to the seasonally varying variability:

$$\langle ES \rangle = \frac{ES}{\sigma} \tag{6.2}$$

where ES is the ensemble spread from equation 6.1 and σ the local standard deviation as a function of calendar month (Figure 5.2). This approach gives an indication of the "rate of separation" of the solutions and therefore the error growth rate of the system (Boer, 2000).

6.1.2 Results and Discussion

Figure 6.1 shows an example of the ensemble members for three particular years for the REF, MOD and FLX configuration, respectively. The mean ensemble spread of all forecasts calculated using equation 6.1 and 6.2 is shown in Figure 6.2. Except for the forecasts initialized in October, the smallest spread among the ensemble members is found in the

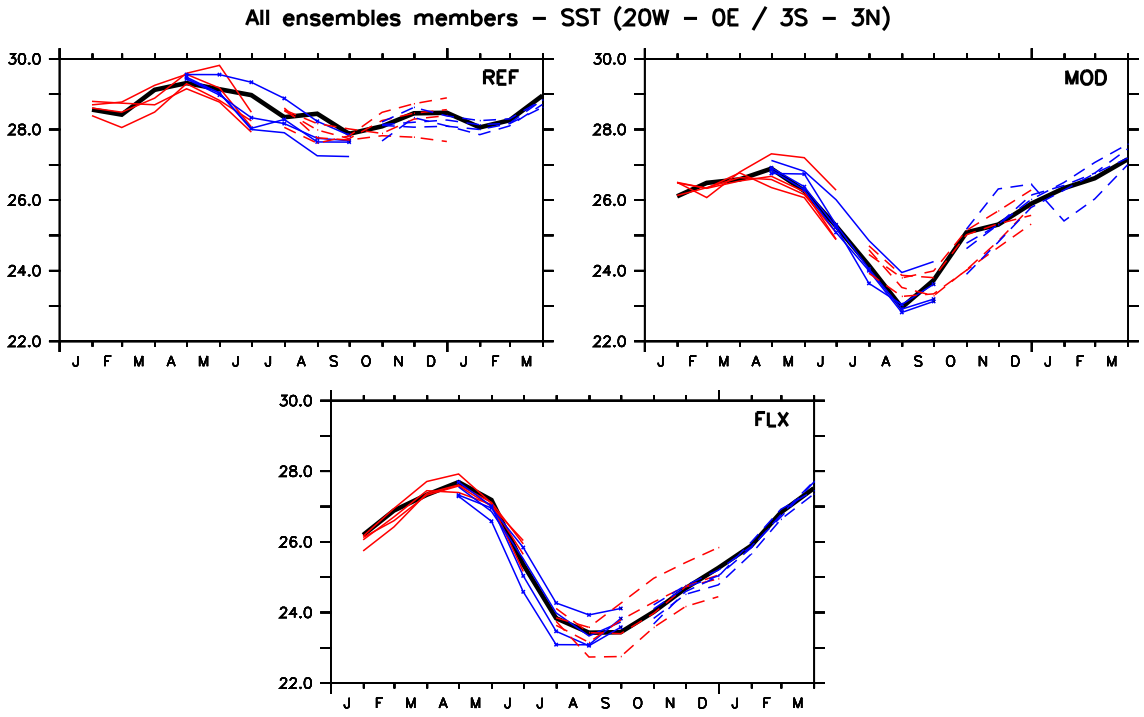

Figure 6.1: *Examples of the ensemble runs performed with REF (top left), MOD (top right) and FLX (bottom). The thick line represents the control run, the thin lines show the individual ensemble members started on January 1st (red, solid), April 1st (blue, solid), July 1st (red, dashed), October 1st (blue, dashed).*

MOD experiment. The FLX experiment shows an ensemble spread that is similar to the REF experiment for all forecast runs started in January, July and October. For the forecasts initialized in April, ensemble spread is below the spread found in the REF experiment but above that of the MOD experiment.

For the forecasts initialized in July, the ensemble spread spread in the MOD experiment is well below the spread in the FLX and REF configuration. This may be related to the lag-lead relationship between WWV and ATL3 SST that is best represented in the MOD configuration (Figure 5.6b) and may explain the improved potential predictability for the forecast initialized in July. On the other hand, WWV anomalies also lead ATL3 SST anomalies by 2 to 6 month from July to November in the FLX configuration, respectively

(Figure 5.6c). However, ensemble spread is larger in the FLX experiment than in the MOD experiment. It is therefore speculated that errors in surface fluxes, which are possibly larger in the FLX configuration, may be responsible for the rapid increase in ensemble spread in the FLX experiment in the forecasts initialized in July. This interpretation of the results is supported by the fact that the FLX and REF experiment use the same atmosphere configuration. Therefore, similar errors in atmospheric surface processes (and variability) might be present that possibly contribute to a rapid increase in spread among the ensemble members. Given the fact that correlations of WWV and ATL3 SST anomalies are weak (in the Pacific correlations reach 0.7, Meinen and McPhaden, 2000) further investigations are required to evaluate the importance of Atlantic WWV for the predictability of ATL3 SST in boreal summer.

Reduction of ensemble spread in the MOD (and to a smaller extent also in th FLX) is found in the forecasts initialized in April. Both WWV anomalies (Figure 5.6) and local 20C depth anomalies (not shown) show a minimum in correlation with ATL3 SST anomalies at all lead times of WWV in April and May. Hence, improved representation of atmospheric surface processes (e.g. surface fluxes) that influence ATL3 SST variability in April and May, which have not been identified yet, must be present. At lead times longer than 2 month, the positive correlation with WWV may act to reduce the spread in the MOD experiment. Consistent with the results for forecasts initialized in July, the positive relation between WWV and ATL3 SST anomalies (which is found for the FLX experiment at similar lead times) does not contribute to the reduction in ensemble spread in ATL3 SST among the ensemble members in boreal summer in the FLX configuration.

Overall the reasons for the reduction of ensemble spread primarily in the MOD configuration are still not well understood. However, the reduction in ensemble spread in the MOD experiment with respect to the REF experiment might be related to the improved representation of equatorial Atlantic variability. Although the representation of equatorial variability is improved in the FLX experiment (chapter 5), the ensemble spread is similar or even larger compared to the REF experiment. Further detailed analysis of all processes

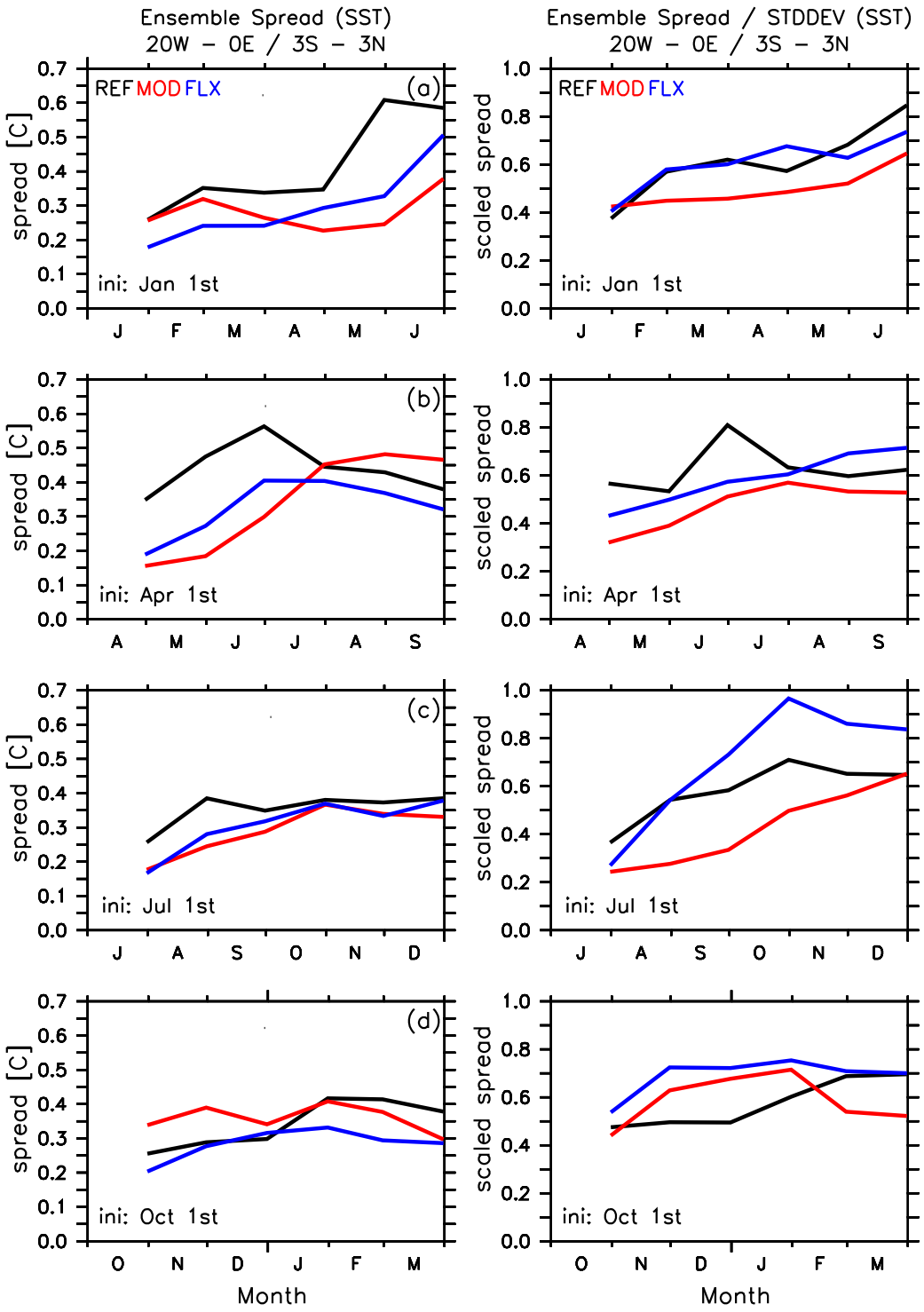

Figure 6.2: *Mean ensemble spread for the forecasts started in January (a), April (b), July (c) and October (d) in the ATL3 region. Figures in the left column show the scaled ensemble spread. Please note that the first value shown in each Figure is the spread one month after the initial date.*

contributing to eastern Atlantic SST variability is therefore necessary.

6.2 20th century hindcasts

In the previous section some evidence is given that modifications in the atmospheric configuration (MOD experiment) and (to a smaller extent) flux corrections (FLX experiment) may improve the predictive skill in boreal summer in the equatorial Atlantic. Therefore, different configurations of KCM are used for hindcasting observed SST in the Tropical Atlantic from 1971 to 2004.

6.2.1 Experimental setup

The configurations of KCM used for the hindcast study are summarized in Table 6.1. The idea behind this setup is to test the sensitivity of the forecast skill towards mean errors in surface heat fluxes, surface stress or a combination of both. Additionally the MOD configuration has been applied in two configurations of KCM (table 6.1).
The FLX version uses the same flux corrections as introduced in section 3.2. In the MFLX version both the FLX and MOD configuration are combined (Flux corrections are recomputed to "fit" the errors in mean surface fluxes in the MOD configuration). In the FLX+Wano setup the same flux corrections as in FLX are applied. On top of that the wind stress is corrected as in Wano (5.1) except that $\overline{\tau}_{x,REF}$ and $\overline{\tau}_{y,REF}$ are replaced by $\overline{\tau}_{x,FLX}$ and $\overline{\tau}_{x,FLX}$, respectively. Different corrections are used since biases towards observed wind stress differ in the REF and FLX experiment. In this setup biases in mean SST can occur in the Tropical Atlantic as wind stress corrections are applied on top of the SST flux corrections. To test the sensitivity of the hindcast to this shortcoming, the Wano+FLX configuration has been set up. In this case flux corrections are additionally applied in the Wano configuration. The flux correction climatology is derived from a control run where

Exp. ID	Years	Modifications with respect to REF experiment:
FLX	120	flux-corrected (global, 40°S - 40°N) version of KCM.
MFLX	120	combination of FLX and MOD.
Wano	50	Anomaly coupling for u-/v-stress between 10°S and 10°N in the Atlantic.
FLX+Wano	50	FLX run with additional anomaly coupling as in Wano.
Wano+FLX	50	Anomaly coupling as in Wano and flux-corrections to remove the mean SST bias in Wano.
WFM	50	Same as Wano+FLX but MOD atmosphere configuration.

Table 6.1: *Configurations of the Kiel Climate Model KCM used for hindcasts in the equatorial Atlantic. "Years" in the second column mean the length of a control run using the model configuration detailed in the third column.*

wind stress corrections and SST restoring is applied simultaneously. Flux corrections are then calculated as described for the FLX run. Although FLX+Wano and Wano+FLX principally contain corrections of the mean seasonal error of the same parameters (surface fluxes and wind), differences in equatorial variability (Bjerknes feedback strength, WWV and SST variability) between the two configurations are present (not shown). Therefore both experiments are included. The WFM is based on the Wano+FLX configuration but additionally contains modifications to the atmospheric component of KCM as described in chapter 3.

The REF version without flux-corrections has not been used for the hindcasts. If flux-corrections are not applied, the model just drifts from it's initial state towards it's biased state. This is especially true for spring and summer where the inability of the model to produce eastern Atlantic drop of SST becomes noticeable. Although the mean state as well as variability are improved in the MOD configuration with respect to the REF configuration (chapter 4.3) an initial drift is still present thus making realistic hindcasts impossible.

The experimental setup of the hindcasts is as follows. For each of the configurations of KCM listed in table 6.1, one hindcast (i.e. only one ensemble member) is started at the first of every month from January 1971 to December 2004 making a total of 408 runs per configuration. Length of each hindcasts is six month. The initial conditions for the hindcasts were obtained using the "coupled assimilation" scheme of of Keenlyside et al. (2008). In this simple scheme a coupled model run with realistic 20th century greenhouse gas forcing and strong restoring to observed SSTs is used to generate the initial conditions. The SST restoring is applied between approximately 40°S and 40°N decreasing linearly towards 0 between 40°N (S) and 60°N (S). This "initialization run" has been started on January 1st, 1920 from a 1000 year control run that assumes “present day” values of greenhouse gases (CO_2 = 348 ppm), and is comparable to the 20th century run discussed in Park et al. (2009). From 1920 to 1950 the model runs without restoring using 20C greenhouse gas forcing. From January 1950 onwards SST restoring towards observed SST is applied additionally. For the hindcasts using the MOD configuration (MFLX and WFM, see table 6.1) separate initialization runs using SST restoring as well as the MOD atmosphere configuration (and wind anomaly coupling for the WFM run) are used to provide the initial conditions.

6.2.2 Results and Discussion

To evaluate the forecast skill in the different configurations of KCM (Table 6.1) seasonally resolved correlations of ATL3 SST with observed values for the FLX, MFLX, Wano, FLX+Wano, Wano+FLX and WFM configuration are shown in Figure 6.3. The correlations are calculated by grouping all hindcasts starting in January, February, ..., December from 1971 to 2004, making a total of 34 six month hindcasts for each month of the year. The timeseries from each forecast step is then correlated with the timeseries of observed SST in the given month. Hence, as an example, the value in the lower left corner of each subfigure in Figure 6.3 is the correlation of the forecasted monthly mean

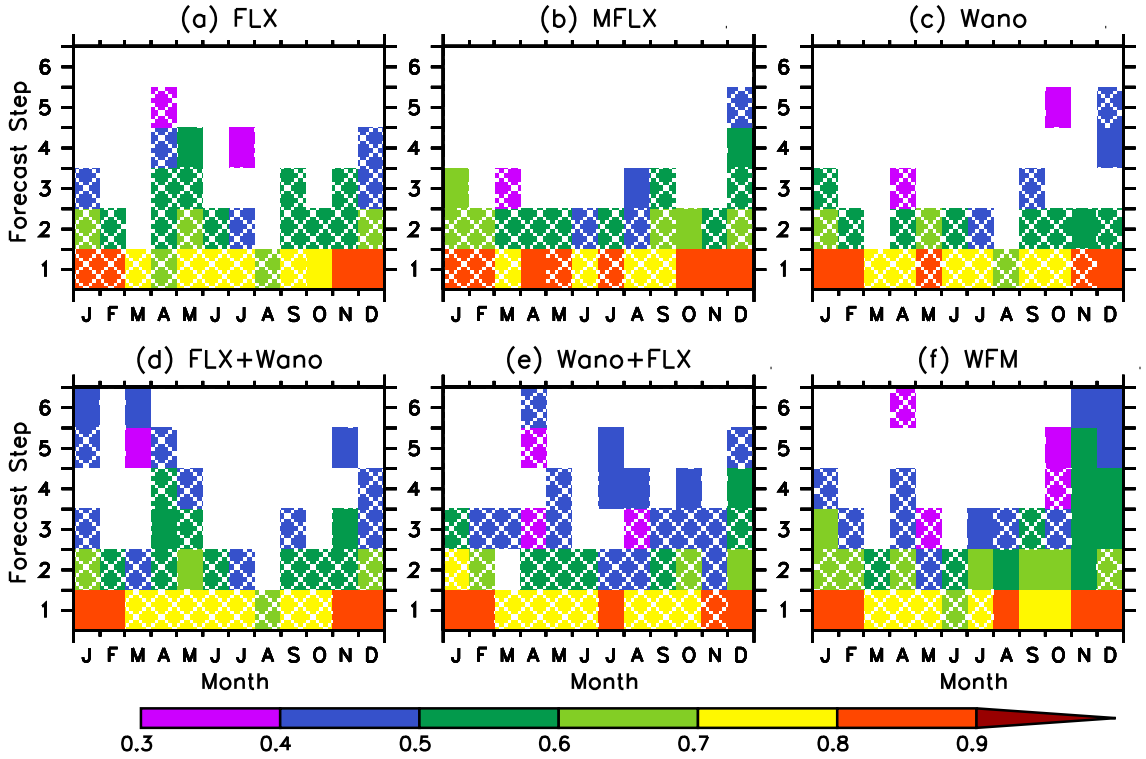

Figure 6.3: *Correlation of hindcasted ATL3 SST with observations of all hindcasts using the FLX (a), MFLX (b), Wano (c), FLX+Wano (d), Wano+FLX (e) and WFM (f) configuration as a function of calendar month. The x-axis indicates the initialization month, and the y-axis the hindcast step. Values which are not significant at the 95% level are shown in white. Hashed values indicate skill below persistence.*

ATL3 SST for January with the observed mean value in January for all hindcasts started January 1st between 1971 to 2004. White boxes mark values which are not significant at the 95% level. Significance has been calculated using a standard T-test (Press et al., 1992, chapter 14). Values where forecast skill is below observed persistence (Figure 6.4) are hashed.

When evaluating forecasts of a meteorological parameter, a persistence forecast is often used as a standard of comparison in measuring the degree of skill of forecasts. Persistence forecasts correlate the current value of a parameter with a value in the future. A perfect persistence forecast hence means that future weather conditions will be the same as the

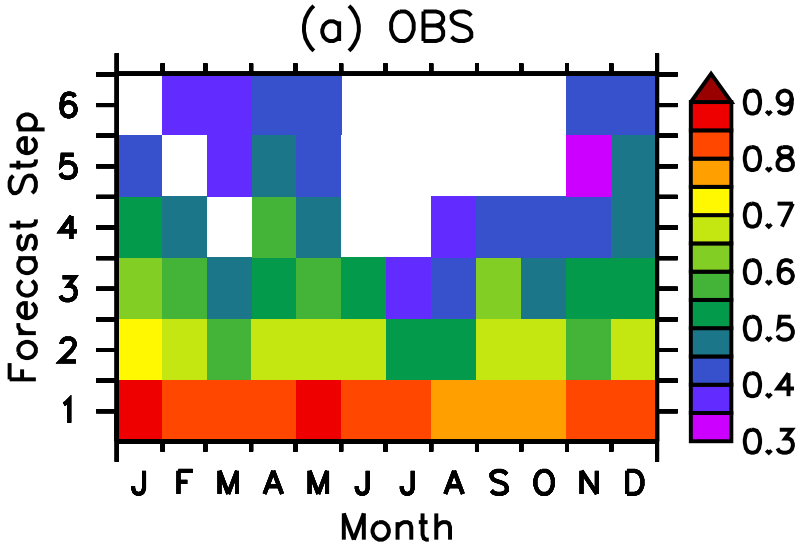

Figure 6.4: *Persistence calculated from observations (1971-2004) as a function of calendar month. The x-axis indicates the initialization month, and the y-axis the hindcast step. Values which are not significant at the 95% level are shown in white.*

present conditions.

Comparing observed persistence (Figure 6.4) to the forecast skill in the ATL3 region (Figure 6.3) shows that forecast skill is mostly below persistence in every month, irrespective of the model configuration used. It shows that removing the mean bias in surface fluxes (FLX) or wind stress (Wano) or even a combination of both (FLX+Wano, Wano+FLX) is not enough to get forecast skill above persistence. The KCM configurations that use the modified atmosphere (MFLX, WFM) show the largest skill in the hindcasts starting in November and December, and skill above persistence is found in the WFM configuration. The reason for the larger skill in those specific configurations compared to the other KCM setups remains unclear and is not discussed further.

The skill of all hindcasts using an ensemble mean of all KCM configurations listed in table 6.1 is shown in Figure 6.5 for all forecasts initialized May 1st and December 1st. Ensemble skill is calculated by computing an average over all ensemble members before correlation with observed values is performed. For the ensemble hindcasts started

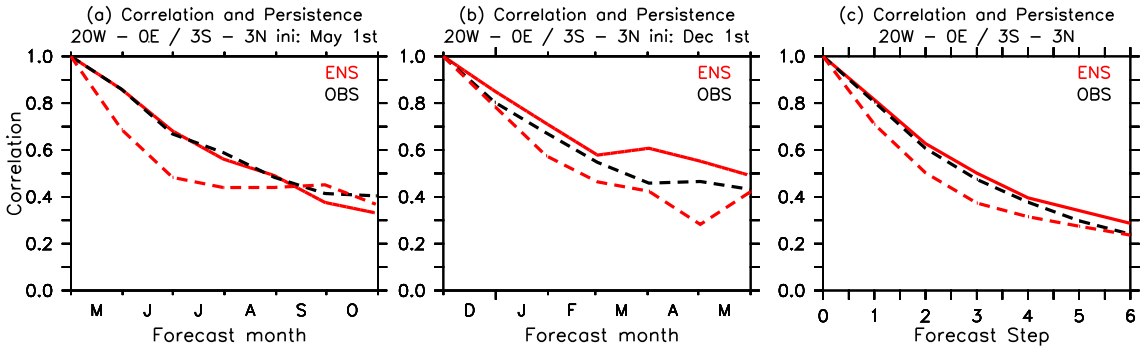

Figure 6.5: *Forecast skill using the ensemble mean (red solid line), model persistence (red dashed line) and observed persistence (black dashed line) for all runs initialized on May 1st (a) and Dec 1st (b). Forecast skill, model persistence and observed persistence for all hindcasts are shown in (c). Model persistence is defined in the same way as observed persistence except that it is calculated from model data.*

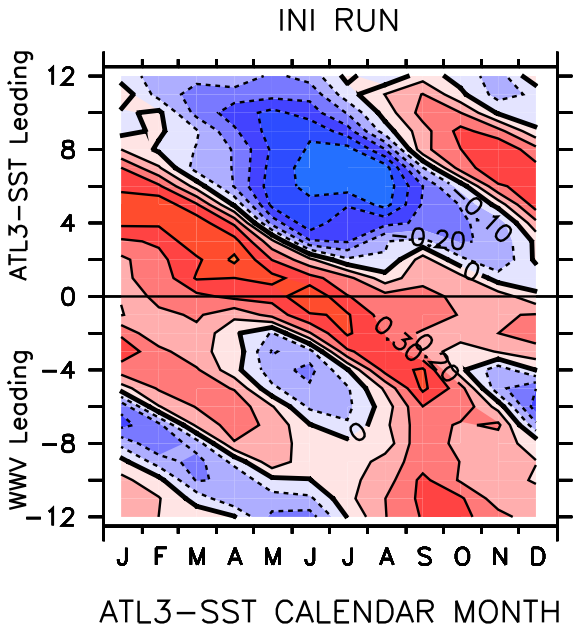

Figure 6.6: *Seasonally resolved cross-correlations (1970-2004) between ATL3 SST and Atlantic WWV in the initialization run with REF atmosphere configuration.*

May 1st forecast skill that matches observed persistence is found, but skill is well above persistence calculated from the ensemble average itself. Again, this result shows that none of the corrections applied to the mean state (FLX and Wano type experiments) or the modifications in the model physics (MOD type experiments) are sufficient to achieve forecast skill during boreal summer that beats persistence. In the ensemble hindcasts starting at the beginning of boreal winter (December 1st, Figure 6.5b) forecast skill that slightly beats persistence is found at all lead times. The overall skill (i.e. all forecasts independent of initialization month) is slightly above persistence (Figure 6.5c).

To understand the reason for the low skill in the different model configurations, both the components of the Bjerknes feedback and the relation between WWV and ATL3 SST anomalies have been carefully checked in all model configurations (The Bjerknes feedback in FLX and Wano is shown in Figure 5.4 and Figure 5.5, respectively; the cross-correlations between WWV and ATL3 SST anomalies in the FLX experiment are shown in Figure 5.6; all other figures are not shown), but no link between the forecast skill and those mechanisms could be found. One explanation might be that those mechanisms are not properly initialized (e.g. Figure 6.6) using the simple initialization technique of Keenlyside et al. (2008). Therefore, significant subsurface errors in the ocean as well as errors in the atmospheric circulation are present in the initialization run. These errors are most likely to increase once the model is run in forecast mode and reduce forecast skill. Additionally, the relative importance of the feedback mechanisms discussed here might be low. The small number of ensemble members possibly further contributes to the low skill. Both errors in the initial fields in the ocean and in the atmosphere (only SST is restored to observations in the initialization run) as well as systematic errors in the mean state and variability contribute to the large error in the hindcasts. The different configurations tested here attempt to improve the ocean mean state and the variability in the ocean in the equatorial Atlantic as predictability on long timescales (long timescales in the current sense means timescales which are beyond the scope of weather prediction) derives from the memory in the ocean due to its slower timescale. Except for the MOD configuration of KCM, which is an attempt to improve the atmospheric mean state and

variability (but still contains large errors), all model configurations used in this study still contain large errors in the atmospheric circulation. These errors and possible sources for these errors have been discussed in the previous chapters as well as earlier studies (e.g. Richter and Xie, 2008, DeWitt, 2005, Huang et al., 2007) and certainly contribute to the low predictive skill in the equatorial Atlantic. The very low resolution especially in the atmosphere (3.75° by 3.75°) poses another source of error.

A recent study that explicitly addresses predictability in the ATL3 region has been published by Stockdale et al. (2006). They use the high resolution (compared to KCM) coupled operational ECMWF model (Anderson et al., 2003) to study hindcast skill between 1959 and 2001. Compared to KCM a more elaborate initialization technique is used including nine ensemble members, but only 4 restart date per year are used (February, May, August, November). In forecast mode no flux corrections are applied. The impact of flux-corrections and surface stress corrections has been tested by Stockdale et al. (2006) but no improvement in ATL3 SST forecast skill was found. Using the setup just described, the ECMWF model is not able to produce forecast skill that significantly differs from the results shown in Figure 6.5c. As both setups are quite different, it is difficult to compare the results. Nevertheless it is encouraging that the ensemble mean of various configurations of KCM, which actually is a low resolution model designed for longterm climate studies, produces skill that is comparable to the skill from an operational model, especially in light of the very simple initialization scheme used.

7 Conclusion

In this work the Kiel Climate Model (KCM) was used to study the biases in the Tropical Atlantic mean state, the mean seasonal cycle and variability. The mean state in the standard configuration of KCM, which was used in previous studies (Park et al., 2009, Park and Latif, 2008, Latif et al., 2009), was shown to contain a large warm bias in eastern equatorial Atlantic SST. The bias peaks during boreal summer and is common to all state-of-the-art coupled climate models.

Different configurations of the Kiel Climate Model (KCM) are used to bring together various aspects which have been claimed to be responsible for the strong warm bias in the eastern Tropical Atlantic. All previous studies discuss possible explanations for the evolution of the eastern Tropical Atlantic warm bias by comparing their erroneous (coupled) models to observations and/or the respective uncoupled model versions. By comparing sensitivity experiments and an (with respect to the warm bias) improved version of KCM with the standard version this work highlights the major problems in coupled Tropical Atlantic climate modeling from a different perspective.

It turns out that the eastern Atlantic warm bias and the error in the zonal SST gradient along the equator are related to two mechanisms:

1) For the wrong zonal gradient and the equatorial warm bias, the error in the spring and early summer zonal winds associated with erroneous zonal precipitation distribution as discussed by e.g. Richter and Xie (2008) seems to be the key mechanism. Improved winds in boreal spring cause the summer cooling in the eastern Tropical Atlantic via shoaling of

the thermocline and increased upwelling. Reduced SSTs in the summer suppress convection and favor the development of low cloud cover in the ETA region through stabilization of the lower troposphere. Outgoing longwave radiation is largely increased through the reduction of high cloud due to cirrus spreading from convective towers. In the ocean the development of erroneous barrier layers (Breugem et al., 2008) and weakened southerly winds (Okumura and Xie, 2004) may significantly contribute to the rapid strengthening of the bias in boreal summer as well as the large errors in thermocline structure.

2) The strong warmbias along the southeastern coastline is related to underestimation of low cloud cover and the associated overestimation of surface SW radiation in the same area which has also been mentioned by Huang et al. (2007). Especially south of the equator along the African coastline low cloud cover increases in the MOD experiment. The largest differences are found from summer to fall and contribute to SST cooling. It coincides with the largest reduction of SST in that area and the timeperiod where low cloud cover and SST show the strongest correlation indicating that the amount of low cloud is also forced by SST. So in addition to the primarily wind forced response at the equator both changes in surface shortwave radiation and OLR contribute significantly to reduction of the warm bias from summer to fall. Supported by the WIND4, WIND10 and RAD sensitivity experiments it has been shown that both mechanisms need to be present to effectively reduce the eastern Atlantic warmbias. Weaker-than-observed southerly winds along the southeastern coast in the REF and MOD experiment are believed to be responsible for the local bias which is still present in both experiments.

A limitation of our results could be the low model resolution used, and therefore processes that can contribute to the reduction of the bias might be missing. However, similar bias patterns in the Tropical Atlantic are also present in higher resolution coupled models.

To successfully model Tropical Atlantic climate and to achieve a realistic representation of the seasonal cycle in e.g. SST or the wind field, convection over northeastern Brazil seems to be one key parameter as it is located at the beginning feedback chain discussed in this paper. The modifications applied in the model improve the east west difference in precipitation, but fail to correctly place convective activity. They key issue of future

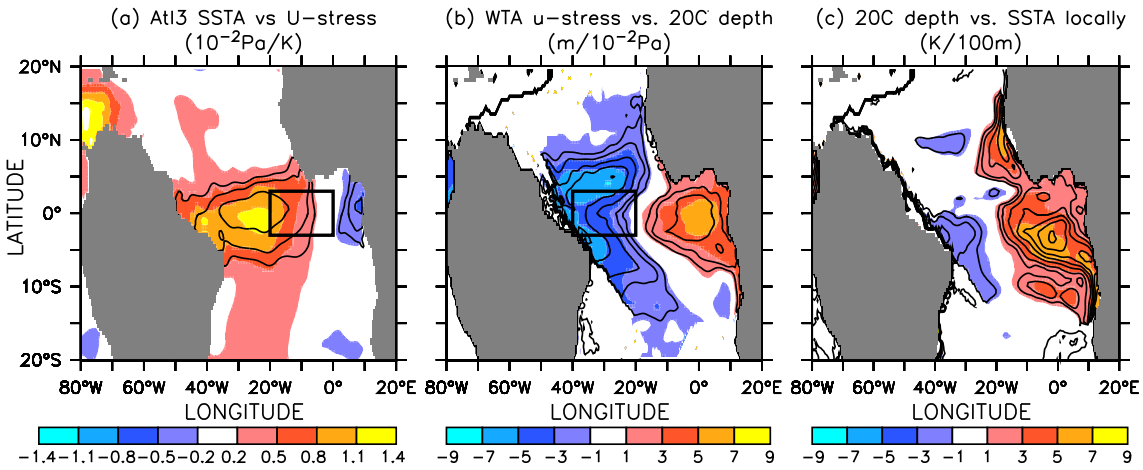

Figure 7.1: *The three components of the Bjerknes feedback in the Atlantic in the OCE05 experiment: regression of ATL3 SST anomalies on zonal wind stress anomalies (a), regression of WTA zonal wind stress anomalies onto 20C depth (b) and regression of 20C depth anomalies on to SST anomalies locally (c); Explained variance is overlayed on all figures with contour levels at 0.05, 0.1, 0.2, ...*

model development with respect to the tropical climate in the model should therefore be the improved representation of land convection over northeastern Brazil without destroying the quite realistic representation of other important climate features such as ENSO (e.g. Park et al., 2009) in the model.

The second part of this work focused on variability in response to an improved representation of the mean state in the equatorial Atlantic. In chapter 5 it was found that a better mean state leads to improved variability in the equatorial Atlantic. Especially the third step of the Bjerknes feedback, the thermocline feedback onto eastern Atlantic SST, is largely improved if the bias is reduced. Although improved, the individual steps of the Bjerknes feedback tend to be too strong compared to the ocean reanalysis dataset (SODA) used. Increasing the horizontal and vertical resolution in the ocean further improves the equatorial Atlantic variability in the ocean component of KCM, as indicated on Figure 7.1. The horizontal resolution in the OCE05 run is 0.5° in latitudinal and longitudinal

direction compared to 2° by 2° - up to 0.5° in latitudinal direction directly at the equator - in the previous experiments, and 46 instead of 31 vertical levels are used. The forcing dataset is the same as the one used for the OCE run.
In a coupled model the realistic representation of the ocean variability directly depends on realistic variability in the corresponding atmospheric fields. Therefore, as stated above, improvements in the atmospheric component of the model are essential. As higher resolution global coupled and uncoupled models (e.g. CFS/GFS used by Huang et al., 2007) share similar problems in reproducing the Tropical Atlantic mean state and variability, simply increasing the horizontal and vertical resolution does not provide a solution either.

In the last part of this work it was shown that the improvements in the mean state and variability in the FLX and MOD configuration with respect to the REF configuration result in larger potential predictability. As better potential predictability is only found in those forecasts starting in boreal spring and the increase in potential predictability is attributed to the improved representation of Atlantic equatorial variability in boreal spring and summer.
A set of six different versions of KCM, which use flux and/or surface wind stress corrections in the equatorial Atlantic as well as modifications in atmospheric parameters to account for the systematic errors in those parameters, was set up to test the ability of KCM to hindcast ATL3 SST. Using a simple initialization technique, forecast skill significantly above persistence could not be achieved in any of the configurations of KCM. Using and ensemble mean of all configurations resulted in forecast skill that is only slightly above persistence. Although this result is discouraging, the low forecast skill in KCM is comparable to state-of-the-art coupled forecast systems (Stockdale et al., 2006).

Overall this work, which is based on the output of a coarse resolution coupled climate model, showed that the mean annual cycle and variability in the Tropical Atlantic are tightly coupled, and a good representation of the annual cycle of both atmosphere and ocean parameters is the basis for modeling realistic variability in the equatorial Atlantic.

List of Figures

List of Tables

Bibliography

Anderson, D., T. Stockdale, M. Balmaseda, L. Ferranti, F. Vitart, P. Doblas-Reyes, R. Hagedorn, T. Jung, A. Vidard, A. Troccoli, and T. Palmer, 2003: Comparison of the ECMWF seasonal forecast Systems 1 and 2, including the relative performance for the 1997/8 El Nino. Technical report, ECMWF. Available online at `http://www.ecmwf.int/publications`. 86

Andersson, A., S. Bakan, K. Fennig, H. Grassl, C.-P. Klepp, and J. Schulz, 2007: Hamburg Ocean Atmosphere Parameters and Fluxes from Satellite Data - HOAPS-3 - monthly mean. Technical report, World Data Center for Climate. 23

Arakawa, A. and V. Lamb, 1977: Computational Design of the Basic Dynamical Processeses of the UCLA General Circulation Model. *Methods in Computational Physics: Advances in Research and Applications*, **17**, 173–265. San Francisco, Academic Press. 18

Barreiro, M., P. Chang, L. Ji, R. Saravanan, and A. Giannini, 2005: Dynamical elements of predicting boreal spring tropical Atlantic sea-surface temperatures. *Dynamics of Atmospheres and Oceans*, **39**(1-2), 61–85. 11

Bengtsson, L., S. Hagemann, and K. I. Hodges, 2004: Can climate trends be calculated from reanalysis data. *Journal of Geophysical Research*, **109**, D11111. 63

Bjerknes, J., 1969: Atmospheric Teleconnections from Equatorial Pacific. *Monthly Weather Review*, **97**(3), 163–172. 10

Boer, G., 2000: A studiy of ocean-atmosphere predictability on long time scales. *Climate Dynamics*, **16**, 469–477. 73, 75

Breugem, W.-P., P. Chang, C. J. Jang, J. Mignot, and W. Hazeleger, 2008: Barrier layers and tropical Atlantic SST biases in coupled GCMs. *Tellus A*, **60**(5), 885–897. 15, 16, 29, 30, 50, 55, 56, 69, 88

Burgers, G., F.-F. Jin, and G. J. van Oldenburg, 2005: The simplest ENSO recharge oscillator. *Geophysical Research Letters*, **32**, L13706. 12

Carton, J. A., X. Cao, B. S. Giese, and A. M. da Silva, 1996: Decadal and interannual SST variability in the tropical Atlantic Ocean. *Journal of Physical Oceanography*, **26**, 1165–1175. 8, 9

Carton, J. A. and B. S. Giese, 2008: A Reanalysis of Ocean Climate Using Simple Ocean Data Assimilation (SODA). *Monthly Weather Review*, **136**(8), 2999–3017. 23, 50

Carton, J. A. and B. Huang, 1994: Warm Events in the Tropical Atlantic. *Journal of Physical Oceanography*, **24**, 888–903. 9

Chang, C.-Y., J. A. Carton, S. A. Grodsky, and S. Nigam, 2007: Seasonal climate of the tropical Atlantic sector in the NCAR Community Climate System Model 3: Error structure and probable causes of errors. *Journal of Climate*, **20**, 1053–1070. 5, 6, 13, 16, 42

Chang, C.-Y., S. Nigam, and J. A. Carton, 2008: Origin of the Springtime Westerly Bias in Equatorial Atlantic Surface Winds in the Community Atmosphere Model Version 3 (CAM3) Simulation. *Journal of Climate*, **21**(18), 4766–4778. 14, 21

Chang, P., L. Ji, and H. Li, 1997: A decadal climate variation in the tropcial Atlantic Ocean from thermodynamic air-sea Interactions. *Nature*, **385**, 516–518. 8, 10, 11, 71

Chang, P., L. Ji, H. Li, C. Penland, and L. Matrosova, 1998: Prediction of Tropical Atlantic sea surface temperature. *Geophysical Research Letters*, **25**(8), 1193–1196. 11

Chang, P., R. Saravanan, and L. Ji, 2003: Atlantic seasonal predictability: The roles of El Nino remote influence and thermodynamic air-sea feedback. *Geophysical Research Letters*, **30**(10), 1501. 11

Chang, P., R. Saravanan, L. Ji, and G. Hegerl, 2000: The effect of local sea surface temperature on atmospheric circulation over the tropical Atlantic sector. *Journal of Climate*, **13**, 2195–2216. 9, 10

Collins, W., C. Bitz, M. Blackmon, G. Bonan, C. Bretherton, J. Carton, P. Chang, S. Doney, J. Hack, T. Henderson, J. Kiehl, W. Large, D. McKenna, B. Santer, and R. Smith, 2006: The Community Climate System Model Version 3 (CCSM3). *Journal of Climate*, **19**, 2122–2143. 14

Davey, M. K., M. Huddleston, K. Sperber, P. Braconnot, F. Bryan, D. Chen, R. Colman, C. Cooper, U. Cubasch, P. Delecluse, D. DeWitt, L. Fairhead, G. Flato, C. Gordon, T. Hogan, M. Ji, M. Kimoto, A. Kitoh, T. Knutson, M. Latif, H. L. Treut, T. Li, S. Manabe, C. Mechoso, G. Meehl, S. Power, E. Roeckner, L. Terray, A. Vintzileos, R. Voss, B. Wang, W. Washington, I. Yoshikawa, J. Yu, S. Yukimoto, and S. Zebiak, 2002: STOIC: a study of coupled model climatology and variability in tropcial ocean regions. *Climate Dynamics*, **18**, 403–420. 11, 13, 38

Deser, C., A. Capotondi, R. Saravanan, and A. Philips, 2006: Tropical Pacific and Atlantic Climate Variability in CCSM3. *Journal of Climate*, **19**, 2451–2481. 9

DeWitt, D. G., 2005: Diagnosis of the tropcial Atlantic near-equatorial SST bias in a directly coupled atmosphere-ocean general circulation mode. *Geophysical Research Letters*, **32**, L01703. 13, 40, 86

Ding, H., N. Keenlyside, and M. Latif, 2009: Seasonal cycle in the upper Equatorial Atlantic Ocean. *Journal of Geophysical Research*, **114**(C9), C09016. 7, 31

Dommenget, D. and M. Latif, 2000: Interannual to Decadal Variability in the Tropical Atlantic. *Journal of Climate*, **13**(4), 777–792. 8

Dommenget, D. and M. Latif, 2002: A Cautionary Note on the Interpretation of EOF. *Journal of Climate*, **15**(2), 216–225. 8

Enfield, D. B., 1996: Relationships of inter-American rainfall to tropical Atlantic and Pacific SST variability. *Geophysical Research Letters*, **23**, 3305–3308. 7

Fichefet, T. and M. Morales Maqueda, 1997: Sensitivity of a global sea ice mode to the treatment of ice thermodynamics and dynamics. *Journal of Geophysical Research*, **102**(C6), 12609–12646. 19

Florenchie, P., J. R. E. Lutjeharms, C. J. C. Reason, S. Masson, and M. Rouault, 2003: The source of Benguela Niños in the South Atlantic Ocean. *Geophysical Research Letters*, **30**(10), 1505. 6, 12, 32

Foltz, G. R., S. A. Grodsky, J. A. Carton, and M. J. McPhaden, 2003: Seasonal mixed layer heat budget of the tropical Atlantic Ocean. *Journal of Geophysical Research*, **108**(C5), 3146. 5

Fouquart, Y. and B. Bonnel, 1980: Computations of solar heating of the earth's atmosphere: A new parameterization. *Contributions to Atmospheric Physics*, **53**(1), 35–62. 17

Fu, R., A. D. Genio, and W. B. Rossow, 1994: Influence of Ocean Surface Conditions on Atmospheric Vertical Thermodynamic Structure and Deep Convection. *Journal of Climate*, **7**, 1092–1108. 42

Gates, W. L., 1992: AMIP: The Atmospheric Model Intercomparison Project. *Bulletin of the American Meteorological Society*, **73**(12), 1962–1970. 13

Giannini, A. R., R. Saravanan, and P. Chang, 2004: The preconditioning role of Tropical Atlantic Variability in the development of the ENSO teleconnection: implications for the prediction of Nordeste rainfall. *Climate Dynamics*, **22**, 839–855. 8

Gill, A., 1982: *Atmosphere-Ocean Dynamics*. International Geophysics Series. Academic Press. 50

Goddard, L. and J. Mason, 2002: Sensitivity of seasonal climate forecasts to persisted SST anomalies. *Climate Dynamics*, **19**, 619–631. 9

Goose, H., J.-M. Campin, E. Deleersnijder, T. Fichefet, M. P.-P., M. A. M. Maqueda, and B. Tartinville, 1999: Description of the CLIO model version 3.0. Technical report, Institut d'Astronomie et de Géophysique Georges Lemaître, Belgique. 19

Gordon, C. T., A. Rosati, and R. Gudgel, 2000: Tropical Sensitivity of a Coupled Model to Specified ISCCP Low Clouds. *Journal of Climate*, **13**, 2239–2260. 14

Graf, J., C. Sasaki, C. Winn, W. T. Liu, and W. Tsai, 1998: NASA Scatterometer Experiment. *Acta Astronautica*, **7-8**, 397–407. 23

Hagos, M. H. and K. H. Cook, 2009: Development of a Coupled Regional Model and Its Application to the Study of Interactions between the West African Monsoon and the Eastern Tropical Atlantic Ocean. *Journal of Climate*, **22**, 2591–2604. 6

Halley, E., 1686: A historical account of the trade winds, and monsoons, observable in the seas between and near the Tropicks, with an attempt to assign the phisical cause of the said winds. *Royal Society of London Philosophical Transactions Series I*, **16**, 153–168. 1

Harzallah, A. and R. Sadourny, 1995: Internal Versus SST-Forced Atmospheric Variability as Simulated by an Atmospheric General Circulation Model. *Journal of Climate*, **8**, 474–495. 73

Hastenrath, S., 1978: On Modes of Tropical Circulation and Climate Anomalies. *Journal of the Atmospheric Sciences*, **35**, 2222–2231. 7

Hastenrath, S. and L. Heller, 1977: Dynamics of climate in Northeast Brazil. *Quarterly Journal Royal Meteorological Society*, **103**(435), 77–92. 7

Hazeleger, W. and R. Haarsma, 2005: Sensitivity of tropical Atlantic climate to mixing in a coupled ocean-atmosphere model. *Climate Dynamics*, **25**(4), 387–399. 15, 68

Hirst, A. C. and S. Hastenrath, 1983: Atmosphere-Ocean Mechanisms of Climate Anomalies in the Angola-Tropical Atlantic Sector. *Journal of Physical Oceanography*, **13**(7), 1146–1157. 9

Houghton, R. W. and Y. M. Tourre, 1992: Characteristics of lowfrequency sea surface temperature fluctuations in the tropical Atlantic. *Journal of Climate*, **5**, 765–771. 8

Hu, Z. and B. Huang, 2007a: Physical Processes Associated with the Tropical Atlantic SST Gradient during the Anomalous Evolution in the Southeastern Ocean. *Journal of Climate*, **20**, 3366–3378. 9

Hu, Z.-Z. and B. Huang, 2007b: The predictive skill and the most predictable pattern in the tropical Atlantic: The effect of ENSO. *Monthly Weather Review*, **135**(5), 1786–1806. 12, 16

Hu, Z.-Z., B. Huang, and K. Pegion, 2008: Low Cloud Error over the Southeastern Atlantic in the NCEP CFS and their Association with Lower-Tropospheric Stability and Air-Sea Interaction. *Journal of Geophysical Research*, **113**, D12114. 12, 14, 19

Huang, B., J. A. Carton, and J. Shukla, 1995: A Numerical Simulation of the Variability in the Tropical Atlantic Ocean, 1980-88. *Journal of Physical Oceanography*, **25**, 835–854. 9

Huang, B. and Z.-Z. Hu, 2007: Cloud-SST feedback in southeastern tropical Atlantic anomalous events. *Journal of Geophysical Research*, **112**(C3), C03015. 9

Huang, B., Z.-Z. Hu, and B. Jha, 2007: Evolution of model systematic errors in the Tropical Atlantic Basin from coupled climate hindcasts. *Climate Dynamics*, **28**(7-8), 661–682. 7, 14, 30, 34, 37, 86, 88, 90

Huang, H.-P., A. W. Robertson, Y. Kushnir, and S. Peng, 2009: Hindcasts of tropical Atlantic SST gradient and South American precipitation: the influences of the ENSO forcing and the Atlantic preconditioning. *Journal of Climate*, **22**(9), 2405–2421. 12

Hulme, M., R. Doherty, T. Ngara, M. New, and D. Lister, 2001: African Climate Change: 1900-2100. *Climate Research*, **17**, 145–168. 3

Jansen, M., D. Dommenget, and N. Keenlyside, 2009: Tropical Atmosphere-Ocean Interactions in a Conceptual Framework. *Journal of Climate*, **22**, 550–567. 12, 65, 70, 71

Kalnay, M., E. Kanamitsu, R. Kistler, and Coauthors, 1996: The NCEP/NCAR 40-year reanalysis project. *Bulletin of the American Meteorological Society*, **77**, 437–470. 23

Kara, A. B., P. A. Rochford, and H. E. Hurlburt, 2000: Efficient and Accurate Bulk Parameterizations of Air–Sea Fluxes for Use in General Circulation Models. *Journal of Atmospheric and Oceanic Technology*, **17**(10), 1421–1438. 22

Keenlyside, N. and M. Latif, 2007: Understanding equatorial Atlantic interannual variability. *Journal of Climate*, **20**(1), 131–142. 10, 11, 62, 63, 65, 66

Keenlyside, N., M. Latif, J. Jungclaus, L. Kornblueh, and E. Roeckner, 2008: Advancing Decadal-Scale Climate Prediction in the North Atlantic Sector. *Nature*, **453**, 84–88. 81, 85

Klein, S. A. and D. L. Hartmann, 1993: The Seasonal Cycle of Low Stratiform Clouds. *Journal of Climate*, **6**, 1587–1606. 7, 37

Kumar, A. and M. P. Hoerling, 1995: Prospects and Limitations of Seasonal Atmospheric GCM Predictions. *Bulletin of the American Meteorological Society*, **76**, 335–345. 73

Lamb, P., 1978: Large scale tropical Atlantic surface circulation patterns associated with Sub-Saharan weather anomalies. *Tellus*, **36A**, 240–251. 7

Large, W. G. and G. Danabasoglu, 2006: Attribution and impacts of upper-ocean biases in CCSM3. *Journal of Climate*, **19**, 2325–2346. 15

Large, W. G. and S. G. Yeager, 2004: Diurnal to decadal global forcing for ocean and sea-ice models: the data sets and flux climatologies. Technical report, NCAR. 22

Latif, M. and A. Grötzner, 2000: The equatorial Atlantic oscillation and its response to ENSO. *Climate Dynamics*, **16**, 213–218. 8

Latif, M., W. Park, H. Ding, and N. Keenlyside, 2009: Internal and External North Atlantic Sector Variability in the Kiel Climate Model. *Meteorologische Zeitschrift*, **18**, 433–443. 19, 87

Lau, N.-C., 1985: Modeling the seasonal dependence of the atmospheric response to observed El Niño in 1962-1976. *Monthly Weather Review*, **113**, 1970–1996. 73

Lee, S.-K. and C. Wang, 2008: Tropical Atlantic Decadal Oscillation and Its Potential Impact on the Equatorial Atmosphere-Ocean Dynamics: A Simple Model Study. *Journal of Physical Oceanography*, **38**(1), 192–212. 15

Lohmann, U. and E. Roeckner, 1996: Design and performance of a new cloud microphysics scheme developed for the ECHAM general circulation model. *Climate Dynamics*, **12**, 557–572. 17

Ma, C., C. Mechoso, A. Robertson, and A. Arakawa, 1996: Peruvian Stratus Clouds and the Tropical Pacific Circulation: A Coupled Ocean-Atmosphere GCM Study. *Journal of Climate*, **9**, 1635–1645. 14

Madden, R., 1976: Estimates of natural variability of time-averaged sea level pressure. *Monthly Weather Review*, **104**, 942–952. 73

Madden, R. A. and P. R. Julian, 1971: Detection of a 40-50 day oscillation in the zonal wind in the tropical Pacific. *Journal of the Atmospheric Sciences*, **28**, 702–708. 1

Madden, R. A. and P. R. Julian, 1994: Observations of the 40–50-Day Tropical Oscillation—A Review. *Monthly Weather Review*, **122**, 814–837. 1

Madec, G., 2008: NEMO ocean engine. *Note du Pole de modelisation, Institut Pierre-Simon Laplace (IPSL)*, **No 27**. ISSN No 1288-1619. 18, 19

Madec, G., P. Delecluse, M. Imbard, and C. Levy, 1998: OPA 8.1, Ocean General Circulation Model Reference Manual. *Note du Pole de modelisation, Institut Pierre-Simon Laplace (IPSL)*, **No 11**, 97pp. 19

Marsland, S., H. Haak, J. Jungclaus, M. Latif, and F. Röske, 2003: The Max-Planck-Institute global ocean/sea ice model with orthogonal curvilinear coordinates. *Ocean Modelling*, **5**, 91–127. 65

Mehta, M., 1998: Variability of the tropical ocean surface temperatures at decadal-multidecadal time scales. Part I: The Atlantic Ocean. *Journal of Climate*, **11**, 2351–2375. 8

Mehta, V. M. and T. Delworth, 1995: Decadal Variability of the Tropical Atlantic Ocean Surface Temperature in Shipboard Measurements and in a Global Ocean-Atmosphere Model. *Journal of Climate*, **8**, 172–190. 8

Meinen, C. S. and M. J. McPhaden, 2000: Observations of warm water volume changes in the equatorial Pacific and their relationship to El Nino and La Nina. *Journal of Climate*, **13**, 3551–3559. 70, 77

Merle, J., M. Fieux, and P. Hisard, 1980: Annual Signal and interannual anomalies of sea surface temperature in the eastern equatorial Atlantic ocean. *Deep-Sea Research I*, **26, GATE suppl.**, 77–101. 9

Miller, M., A. Beljaars, and T. Palmer, 1992: The sensitivitiy of the ECMWF Model to Parameterization of Evaporation from the Tropical Oceans. *Journal of Climate*, **5**, 418–434. 22

Mlawer, E., S. J. Taubmann, P. D. Brown, M. J. Iacono, and S. A. Clough, 1997: Radiative transfer for inhomogeneous atmospheres: RRTM, a validated correlated-k model for the longwave. *Journal of Geophysical Research*, **102**(D14), 16663–16682. 17

Moura, A. D. and J. Shukla, 1981: On the Dynamics of Droughts in Northeast Brazil: Observations, Theory and Numerical Experiments with a General Circulation Model. *Journal of the Atmospheric Sciences*, **38**, 2653–2675. 7, 8

Murtugudde, R., J. Ballabrera-Poy, J. Beauchamp, and A. Busalacchi, 2001: Relationship between zonal and meridional modes in the tropical Atlantic. *Geophysical Research Letters*, **28**(23), 4463–4466. 10

Nigam, S., 1997: The Annual Warm to Cold Phase Transition in the Eastern Equatorial Pacific: Diagnosis of the Role of Stratus Cloud-Top Cooling. *Journal of Climate*, **10**, 2447–2467. 7, 14

Nobre, P. and J. Shukla, 1996: Variations of Surface Temperature, Windstress, and Rainfall over the Tropical Atlantic and South America. *Journal of Climate*, **9**, 2464–2479. 8

Nordeng, T. E., 1994: Extended versions of the convective parameterization scheme at ECMWF and their impact on the mean and transient activity of the model in the tropics. Technical Memorandum 206, ECMWF, Reading, UK. 17

Okumura, Y. and S.-P. Xie, 2004: Interaction of the Atlantic Equatorial Cold Tongue and the African Monsoon. *Journal of Climate*, **17**, 3589–3602. 6, 13, 88

Palmer, T. N., F. J. Doblas-Reyes, R. Hagedorn, and Coauthors, 2004: Development of a European multi-model ensemble system for seasonal to inter-annual prediction (DEMETER). *Bulletin of the American Meteorological Society*, **85**, 853–872. 12

Park, W., N. Keenlyside, M. Latif, A. Stroeh, R. Redler, E. Roeckner, and G. Madec, 2009: Tropical Pacific climate and its response to global warming in the Kiel Climate Model. *Journal of Climate*, **22**, 71–92. 3, 17, 18, 19, 20, 25, 60, 81, 87, 89, 91

Park, W. and M. Latif, 2008: Multidecadal and multicentennial variability of the meridional overturning circulation. *Geophysical Research Letters*, **35**, L22703. 19, 87

Penland, C. and L. Matrosova, 1998: Prediction of Tropical Atlantic Sea Surface Temperatures Using Linear Inverse Modeling. *Journal of Climate*, **11**, 483–496. 9, 11

Philander, S., D. Gu, G. Lambert, T. Li, D. Halpern, N.-C. Lau, and R. Pacanowski, 1996: Why the ITCZ Is Mostly North of the Equator. *Journal of Climate*, **9**(12), 2958–2972. 7

Philander, S. G. H. and R. C. Pacanowski, 1981: The oceanic response to cross-equatorial winds (with application to coastal upwelling in low latitudes). *Tellus*, **33**, 201–210. 6

Philander, S. G. H. and R. C. Pacanowski, 1986: A Model of the Seasonal Cycle in the Tropical Atlantic Ocean. *Journal of Geophysical Research*, **91**(C12), 14192–14206. 7

Pincus, R., H. W. Barker, and J.-J. Morcrette, 2003: A new radiative transfermodel for use in GCMs. *Journal of Geophysical Research*, **108**, 4376–4379. 17

Polo, I., A. Lazar, B. Rodriguez-Fonseca, and S. Arnault, 2008: Oceanic Kelvin waves and tropical Atlantic intraseasonal variability: 1. Kelvin wave characterization. *Journal of Geophysical Research*, **113**, C07009. 6, 32

Press, W. H., B. P. Flannery, S. A. Teukolsky, and W. T. Vetterling, 1992: *Numerical Recipes in FORTRAN: The Art of Scientific Computing*. Cambridge University Press, 2nd edition. 82

Randall, D., R. Wood, S. Bony, R. Colman, T. Fichefet, J. Fyfe, V. Kattsov, A. Pitman, J. Shukla, J. Srinivasan, R. Stouffer, A. Sumi, and K. Taylor, 2007: Climate Models and Their Evaluation. In: *Climate Change 2007: The Physical Science Basis. Contribution of Working Group I to the Fourth Assessment Report of the Intergovernmental Panel on Climate Change*, chapter 8, pp. 589–662. Cambridge University Press. 1, 2, 59, 91

Richter, I. and S.-P. Xie, 2008: On the origin of equatorial Atlantic biases in coupled general circulation models. *Climate Dynamics*, **31**(5), 587–598. 2, 13, 14, 21, 30, 40, 47, 52, 86, 87, 91

Roeckner, E., R. Brokopf, M. Esch, M. Girogetta, S. Hagemann, L. Kornblueh, E. Manzini, U. Schlese, and U. Schulzweida, 2004: Sensitivity of Simulated Climate to Horizontal and Vertical Resolution. *MPI Report*, **354**, 56p. 17

Roeckner, E., G. Bäuml, L. Bonaventura, R. Brokopf, M. Esch, M. Girogetta, S. Hagemann, I. Kirchner, L. Kornblueh, E. Manzini, A. Rhodin, U. Schlese, U. Schulzweida, and A. Tompkins, 2003: The atmospheric general circulation model ECHAM 5, Part I. *MPI Report*, **349**, 137p. Max-Planck-Institut für Meteorologie, Hamburg, Germany. 17, 18, 21, 22

Rossow, W. B. and R. A. Schiffer, 1991: ISCCP Cloud Data Products. *Bulletin of the American Meteorological Society*, **72**(1), 2–20. 23

Rowell, D. P., 1998: Assessing Potential Seasonal Predictability with an Ensemble of Multidecadal GCM Simulations. *Journal of Climate*, **11**, 109–120. 73

Rowell, D. P., C. K. Folland, K. Maskell, and M. N. Ward, 1995: Variability of summer rainfall over tropical North Africa. *Quarterly Journal of the Royal Meteorological Society*, **121**, 669–704. 73

Ruiz-Barradas, A., J. A. Carton, and S. Nigam, 2000: Structure of Interannual-to-Decadal Variability in the Tropical Atlantic Sector. *Journal of Climate*, **13**, 3286–3297. 8

Räisänen, P., S. Järvenoja, H. Järvinen, M. Giorgetta, E. Roeckner, K. Jylhä, , and K. Ruosteenoja, 2007: Tests of Monte Carlo Independent Column Approximation in the ECHAM5 Atmospheric GCM. *Journal of Climate*, **20**, 4995–5011. 17

Saha, S., S. Nadiga, C. Thiaw, J. Wang, W. Wang, Q. Zhang, H. M. Van den Dool, H. L. Pan, S. Moorthi, D. Behringer, D. Stokes, M. Pena, S. Lord, G. White, W. Ebisuzaki,

P. Peng, and P. Xie, 2006: The NCEP Climate Forecast System. *Journal of Climate*, **19**(15), 3483–3517. 14, 74

Scheinert, M., 2008: *Causes and Impacts of northern North Atlantic Freshening*. Ph.D. thesis, Christian-Albrechts-Universität, Kiel. 19

Schouten, M. W., R. P. Matano, and T. P. Strub, 2005: A description of the seasonal cycle of the equatorial Atlantic from altimeter data. *Deep-Sea Research I*, **52**, 477–493. 31

Seo, H., M. Jochum, R. Murtugudde, and A. Miller, 2006: Effect of ocean mesoscale variability on the mean state of tropical Atlantic climate. *Geophysical Research Letters*, **33**, L0960. 15

Servain, J., 1991: Simple Climatic Indices for the Tropical Atlantic Ocean and Some Applications. *Journal of Geophysical Research*, **96**(C8), 15137–15146. 8

Servain, J., A. J. Busalacchi, M. J. McPhaden, A. D. Moura, G. Reverdin, M. Vianna, and S. E. Zebiak, 1998: A Pilot Research Moored Array in the Tropical Atlantic (PIRATA). *Bulletin of the American Meteorological Society*, **79**, 2019–2031. 5

Servain, J., I. Wainer, J. P. McCreary, and A. Dessier, 1999: Relationship between the equatorial and meridional modes of climatic variability in the tropical atlantic. *Geophysical Research Letters*, **26**(4), 485–488. 8, 10

Stockdale, T. N., M. Balmaseda, and A. Vidard, 2006: Tropical Atlantic SST Prediction with Coupled Ocean-Atmosphere GCMs. *Journal of Climate*, **19**, 6047–6061. 12, 14, 16, 63, 86, 90

Sutton, R. T., S. P. Jewson, and D. P. Rowell, 2000: The Elements of Climate Variability in the Tropical Atlantic Region. *Journal of Climate*, **13**, 3261–3284. 11

Tanimoto, Y. and S.-P. Xie, 2002: Inter-hemispheric Decadal Variations in SST, Surface Wind, Heat Flux and Cloud Cover over the Atlantic Ocean. *Journal of the Meteorological Society of Japan*, **80**(5), 1199–1219. 11

Tiedtke, M., 1989: A comprehensive mass flux scheme for cumulus parameterization in large-scale models. *Monthly Weather Review*, **117**, 1779–1800. 17

Tompkins, A. M., 2002: A prognostic parameterization for the subgrid-scale variability of water vapor and clouds in large-scale models and its use to diagnose cloud cover. *Journal of the Atmospheric Sciences*, **59**(12), 1917–1942. 17

Tourre, Y. M., B. Rajagopalan, and Y. Kushnir, 1999: Dominant Patterns of Climate Variability in the Atlantic Ocean during the Last 136 Years. *Journal of Climate*, **12**(8), 2285–2299. 8, 65

Valcke, S., E. Guilyardi, and C. Larsson, 2006: PRISM and ENES: A European approach to Earth system modelling. *Concurrency Computat.: Pract. Exper.*, **18**(2), 231–245. 19

Weare, B. C., 1977: Empirical orthogonal analysis of Atlantic Ocean surface temperatures. *Quarterly Journal Royal Meteorological Society*, **103**, 467–478. 7, 8

Xie, P. and P. Arkin, 1997: Global precipitation: A 17-year monthly analysis based on gauge observations, satellite estimates, and numerical model outputs. *Bulletin of the American Meteorological Society*, **78**(11), 2539–2558. 23

Xie, P. and S. G. H. Philander, 1994: A coupled ocean-atmosphere model of relevance to the ITCZ in the eastern Pacific. *Tellus*, **46A**, 340–350. 8

Xie, S.-P. and J. A. Carton, 2004: Tropical Atlantic Variability: Patterns, Mechanisms, and Impacts. *Geophysical Monographs*, **147**, 121–142. 7, 9

Yu, J.-Y. and C. R. Mechoso, 1999: A discussion on the errors in the surface heat fluxes simulated by a coupled GCMs. *Journal of Climate*, **12**, 416–426. 14

Zebiak, S. E., 1993: Air-sea interaction in the equatorial Atlantic region. *Journal of Climate*, **6**, 1567–1586. 10

Zwiers, F., 1987: A Potential Predictability Study Conducted with an Atmospheric General Circulation Model. *Monthly Weather Review*, **115**, 2957–2974. 73

Abbreviations

AMIP	Atmospheric Model Intercomparison Project
ATL3	Atlantic 3 region (20°W-0°E, 3°S-3°N
CCSM3	Community Climate System Model, version 3
CFS	NCEP coupled forecast system
CMIP	Coupled Model Intercomparison Project
(C)GCM	(Coupled) general circulation model
DEMETER	Development of a European Multi-Model Ensemble Prediction System for Seasonal to Interannual Prediction
DJF	December, January, February
ECHAM5	Hamburg version of the ECMWF atmospheric model
ECMWF	European Center for Medium Range Weather Forecast
ENSO	El Niño Southern Oscillation
EOF	Empirical orthogonal function
ETA	Eastern Tropical Atlantic 0°E-8°E, 2°S-2°N
HOAPS	Hamburg Ocean–Atmosphere Parameters and Fluxes from Satellite Data
IES80	UNESCO International Equation of State
IPCC	Intergovernmental Panel on Climate Change
ILD	Isothermal layer depth
ISCCP	International Satellite Cloud Climatology Project
ITCZ	Intertropical Convergence Zone

JJA	June, July, August
KCM	Kiel Climate Model
LIM	Louvain-la-Neuve sea ice model
MAM	March, April, May
MLD	Mixed layer depth
MPIOM	Max-Planck Institute for Meteorology ocean model
NCEP	National Centers for Environmental Prediction
NEMO	Nucleus for European Modeling of the Ocean
NTA	Northern Tropical Atlantic (NTA)
OASIS3	Ocean Atmosphere Sea Ice Soil version 3
PIRATA	Prediction and Research Moored Array in the Tropical Atlantic
RRTM	Rapid Radiative Transfer Model
SODA	Simple Ocean Data Assimilation
SON	September, October, November
SST	Sea surface temperature
WES	Wind-evaporation-SST

Danksagung

Ganz herzlich möchte ich mich bei Herrn Prof. Dr. Mojib Latif für die Vergabe und die Betreuung des Themas bedanken. Besonderer Dank gebührt Dr. Wonsun Park für die technische Einweisung in KCM und viele weitere Tipps zu jeder Zeit. Dr. Noel Keenlyside danke ich für die wertvollen Hinweise und Ideen, die diese Arbeit massgeblich beeinflusst und verbessert haben. Die ungekoppelten Ozeanmodellläufe (OCE und OCE05) wurden freundlicherweise von Dr. Arne Biastoch zur Verfügung gestellt.

Danken möchte ich auch allen die mich während der Arbeit begleitet und unterstützt haben.

Ein Dank gebührt auch meinen Eltern, die alle meine bisherigen Entscheidungen finanziell und ideell unterstützt haben.

Erklärung

Hiermit bestätige ich, dass ich diese Doktorarbeit selbstständig verfasst und keine anderen als die angegebenen Quellen und Hilfsmittel verwendet habe.
Ich versichere, dass diese Arbeit zur Erlangung eines Doktorgrades noch nicht an anderer Stelle eingereicht worden ist.
Ich erkläre, dass die vorliegende Arbeit gemäß der Grundsätze zur Sicherung guter wissenschaftlicher Praxis der Deutschen Forschungsgemeinschaft erstellt wurde.

Kiel, 7. Dezember 2009

(Sebastian Wahl)